High Field Strength Element systematics and Lu-Hf & Sm-Nd garnet geochronology of orogenic eclogites

Dissertation

zur Erlangung des Doktorgrades

der Naturwissenschaften

Vorgelegt beim Fachbereich Geowissenschaften/Geographie

der Johann Wolfgang Goethe-Universität

in Frankfurt am Main

von

Alexander Schmidt

aus Gütersloh

Frankfurt (Januar, 2008)

Von Fachbereich Geowissenschaften/Geographie

der Johann Wolfgang Goethe-Universität als Dissertation angenommen.

Dekan:	Prof. Dr. G.P. Brey
Gutachter:	Jun.-Prof. Dr. Stefan Weyer
	Prof. Dr. G.P. Brey
Datum der Disputation:	09. Mai 2008

Acknowledgements

First and foremost I´d like to thank my supervisor Jun.-Prof. Dr. Stefan Weyer for his support and guidance. He has been an excellent tutor in both practical and theoretical means, in the laboratory and at the mass spectrometers, and always advised me to be a good scientist. He was never reluctant to send me to national and international conferences and helped me getting a good experience at presenting my data and also made sure I get in contact with other scientists.

I also like to thank Prof. Dr. Gerhard Brey, Dr. Axel Gerdes and Dr. Heidi Höfer for a lot of fruitful discussions about different topics, and Heidi Höfer especially for her introductions to the electron microprobe. Anna Neuman, Dr. Yann Lahaye and Jan Heliosh are thanked for the help in the laboratory, at the mass spectrometers and with sample preparations.

I thank all my colleagues at the Institute of Mineralogy for maintaining the perfect climate for my work and that we always had a good time.

Special thanks go to Prof. Dr. Klaus Mezger at the University of Münster and Dr. Timm John at the University of Oslo. They were very helpful at discussing different topics concerning geochronology, high field strength elements and eclogites in general.

Thanks go to Prof. Jochen Hoefs and Dr. Yilin Xiao at the University of Göttingen for providing some very interesting eclogites from the Dabie-Sulu UHP terrane in China, aswell as to Dr. Timm John and Dr. Thomas Zack who also provided eclogites from different localities.

Table of contents:

Deutsche Zusammenfassung

Einführung und Fragestellungen:

Die kontinentale Kruste und der Mantel sind die beiden wichtigsten geochemischen Reservoire der Silikaterde (Bulk Silicate Earth, BSE). Dementsprechend verhalten sie sich bezüglich ihrer Gehalte an refraktären lithophilen Elementen relativ zu Chondrit in der Regel komplementär. Dies gilt z.B. für viele Seltene Erden (REE) und Sr-Nd Isotope (HOFMANN, 1988; HOFMANN, 1997). Die High Field Strength Elemente (HFSE) Zr, Nb, Hf und Ta werden weitgehend ebenfalls als Spurenelemente betrachtet, die in chondritischer Häufigkeit in der Silikaterde vertreten sind und ebensolche Elementverhältnisse aufzeigen. Es zeigt sich allerdings, dass sowohl die Nb/Ta Verhältnisse der kontinentalen Kruste und des verarmten Mantels, als auch die gesamte Silikaterde, subchondritisch sind, ein Phänomen, das als „Nb-Paradox" bekannt ist (BARTH et al., 2000; KAMBER and COLLERSON, 2000; RUDNICK et al., 2000; MÜNKER et al., 2003; RAPP et al., 2003). Nb und Ta sind zwei HFSE mit sehr ähnlichen geochemischen Eigenschaften und wurden lange Zeit als „geochemische Zwillinge" betrachtet, die sich während der Entwicklung des Kruste-Mantel Systems identisch verhalten.

Erste Ideen um die Massenbilanz der Silikaterde auszugleichen legen ein superchondritisches Reservoir nahe, welches im Mantel zurückgehalten wird, und somit zu der heutigen Fraktionierung der Nb/Ta Verhältnisse zwischen BSE und dem chondritischen Wert geführt hat. Ein solches Reservoir kann in Form subduzierter ozeanischer Kruste vorliegen, deren Restit als Eklogit in den Mantel absinkt (MCDONOUGH, 1991; RUDNICK et al., 2000). Diese Betrachtungen basieren auf einem chondritischen Nb/Ta Verhältnis von 17.6, welches aus Analysen von Chondriten (Allende und Murchison) und Eukriten (Vesta) hergeleitet wurde (WEYER et al., 2002). MÜNKER et al. (2003) dagegen haben zur Berechnung des chondritischen Nb/Ta einen deutlich größeren Datensatz zugrundegelegt und kommen auf ein höheres Verhältnis von 19.9. Es wurden zudem von diesen Autoren einige kohlige Chondrite der CV-Gruppe (z.B. Allende) aussortiert, da diese eine ungewöhnliche Anreicherung von Nb-verarmten Einschlüssen zeigten. Dieser neue und höhere Wert für das

chondritische Nb/Ta Verhältnis wird in dieser Arbeit verwendet, da er diesen durch den größeren Datensatz besser repräsentiert.

Im Gegensatz zu den Nb/Ta Verhältnissen in den silikatischen Reservoiren, zeigen die anderen beiden HFSE Zr und Hf kaum Fraktionierung an und Zr/Hf Verhältnisse ± dem chondritischen Wert von 34.2 (WEYER et al., 2002).

Eine andere Lösung für das Nb Defizit der Silikaterde zeigen WADE and WOOD (2001) auf. Sie argumentieren, dass das normalerweise lithophile Element Nb unter sehr hohem Druck siderophile Eigenschaften annimmt, und sich somit ein Teil des Nb im Erdkern befinden könnte. Dies würde dann zu dem niedrigen Nb/Ta der Silikaterde führen.

Anhand der Elementverhältnisse Nb/Ta und Zr/Hf, aber auch anderer Spurenelemente, in Eklogiten wurde folgender Fragestellungen nachgegangen: (1) werden die in der kontinentalen Kruste verarmten HFSE durch akzessorische Mineralphasen oder durch ihre Fluidimmobilität in der subduzierten ozeanischen Kruste zurückgehalten und (2) ist ein langzeitstabiles Eklogitreservoir im Mantel wahrscheinlich und für die unterschiedlichen Nb/Ta Verhältnisse in Kruste, Mantel und Chondriten verantwortlich. Ein besonderes Augenmerk lag dabei auf der akzessorischen Mineralphase Rutil, von der bereits im Vorfeld zu erwarten war, dass sie zum Großteil die beiden Elemente Nb und Ta enthält. Für die Betrachtung dieser Fragestellungen wurden Gehalte und hochpräzise Verhältnisse der HFSE (insbesondere Nb/Ta) und anderer Spurenelemente in Eklogiten bestimmt. Zusammen mit bereits vorhandenen Hochpräzisionsdaten für HFSE in Mantel und kontinentaler Kruste tragen die Ergebnisse an den untersuchten Eklogiten zu der Frage bei, ob diese in einer Massenbilanz die bezüglich Nb/Ta subchondritische Silikaterde ausgleichen können. Die meisten Spurenelementgehalte der Mineralphasen (Rutil, Granat und Klinopyroxen) wurden in-situ mit Laser Ablation ICP-MS gemessen. Hochpräzise Nb/Ta Verhältnisse der Gesamtgesteine wurden indes aus der Lösung (zusammen mit Zr und Hf) mit einer Multi-Isotopenverdünnungsmethode bestimmt.

Aus dem vorhandenen Probensatz an Eklogiten ergab sich zudem ein Teilprojekt, das sich mit der Datierung von eklogitfaziellen Mineralparagenesen (Granat und Klinopyroxen) mit Hilfe des Lu-Hf Systems befasst. Das Lu-Hf System ist sehr geeignet um (hoch-)metamorphe Mineralparagenesen (mit Granat) zu datieren (SCHERER et al., 1997; DUCHÊNE et al., 1997; BLICHERT-TOFT and FREI, 2001; LAPEN, 2002; SCHERER et al., 2003; SKORA et al., 2006; ANCZKIEWICZ et al., 2007). Die untersuchten Proben stammen aus der Region des Qinling-Tongbai-Dabi-Sulu Orogengürtels in Ost-China, eines der weltweit größten Vorkommnisse von extrem hochdruckfaziellen Gesteinen (im Folgenden abgekürzt als UHP – ultrahigh-pressure). Im Bereich des Gürtels kam es während der Trias zur Kollision des Yangtze Kratons mit dem Sino-Koreanischen Kraton. Funde von Coesit und Diamant deuten darauf hin, dass hier kontinentales Material bis in Manteltiefen von über 100km subduziert wurde. Mit Hilfe verschiedenster Chronometer (U-Pb, Sm-Nd) wird der Zeitpunkt der Kollision und das UHP Ereignis auf einen Zeitraum von 240 bis 200 Ma datiert. Verschiedene U-Pb Alter von Zirkonen werden dabei häufig als mögliche Zeitabschnitte für verschiedene Metamorphoseereignisse interpretiert, zB. gehen LIU et al. (2006a) von 3 separaten eklogitfaziellen Metamorphosen bei 242.1 ± 0.4 Ma, 227.2 ± 0.8 Ma und 219.8 ± 0.8 Ma aus. Im Gegensatz dazu gliederten HACKER et al. (2006) anhand eigener U-Pb Alter von Zirkonen und Daten aus der Literatur die metamorphe Geschichte in 2 UHP Metamorphosen [1.) eine initiale UHP-Metamorphose zwischen 244 Ma und 236 Ma und 2.) das UHP-„Haupt“-Ereignis zwischen 230 Ma und 220 Ma] sowie eine anschließende amphibolitfazielle Überprägung zwischen 220 Ma und 205 Ma.

Abgesehen von einer möglichst präzisen Datierung des Hochdruckereignisses mit dem Lu-Hf System war auch ein Vergleich mit den Sm-Nd Altersdaten aus der Literatur (und eigenen Sm-Nd Daten an ausgewählten Proben) von Interesse. Es wurde der Frage nachgegangen, ob sich die mit dem Lu-Hf System gewonnenen Alter systematisch von den Sm-Nd Altern unterscheiden. Höhere Lu-Hf Alter könnten aufgrund der wahrscheinlich höheren Schließungstemperatur für Lu und Hf im Vergleich zu Sm-Nd im Granat erwartet werden (SCHERER et al., 2000; ANCZKIEWICZ et al., 2007). Eine geringe Differenz in der Schließungstemperatur beider Isotopensysteme kann zu großen Altersunterschieden führen, wenn das Sm-Nd Alter bei einer späteren amphibolitfaziellen Metamorphose resettet wurde, während das Lu-Hf System ungestört blieb. Desweiteren kann das Lu-Hf System in

Granaten, aufgrund der häufig vorkommenden Anreicherung von Lu im Kern, mit größerer Gewichtung die Granatkerne und damit das Granatwachstum datieren (LAPEN et al., 2003; SKORA et al., 2006; ANCZKIEWICZ et al., 2007). Bei weiteren Vergleichen mit z.B. U-Pb Altern von Zirkonen sollte u.a. auch festgestellt werden, ob mit Lu-Hf das tatsächliche UHP Ereignis erfasst werden kann oder ob beide Systeme unterschiedliche Metamorphosestadien datieren.

Die Anwendung des Lu-Hf Isotopensystem zur Datierung von Granaten hat sich in den letzten Jahren zu einer verlässlichen Methode entwickelt um z.B. eklogit- oder granulitfazielle Mineralparagenesen und deren metamorphe Entwicklung zeitlich zu erfassen (DUCHÊNE et al., 1997; SCHERER et al., 1997; SCHERER et al., 2000; BLICHERT-TOFT and FREI, 2001; SCHERER et al., 2001; LAPEN, 2002; SCHERER et al., 2003; MAHLEN et al., 2005; ANCZKIEWICZ et al., 2007). Besonders im Zusammenspiel mit Sm-Nd Daten an den gleichen Granaten können gelegentlich einzelne Metmorphoseereignisse unterschieden werden. Als Beispiel zeigen ANCZKIEWICZ et al. (2007) einen Unterschied von fast 20 Ma zwischen Lu-Hf und Sm-Nd Altern in Granuliten auf, die durch deutlich höhere Schließungstemperaturen des Lu-Hf Systems und einen späteren Reset des Sm-Nd Systems erklärt werden können. Für Eklogite aus dem Dabie-Sulu Terrain ist die Lu-Hf Datierung bisher nicht zur Anwendung gekommen und konnte hier neue Erkenntnisse über den Zeitrahmen des (U)HP-Ereignisses liefern.

Ergebnisse

High Field Strength Elemente in Eklogiten und Rutil:

In Abbildung 0·1 sind die Ergebnisse der Gesamtgesteinsanalysen dargestellt. Das Diagramm zeigt die zwei wichtigen Elementverhältnisse Nb/Ta und Zr/Hf gegeneinander aufgetragen, verglichen mit Bereichen für heutige MORB und OIB Gesteine (BÜCHL et al., 2002; PFÄNDER et al., 2007), sowie Bereichen für die kontinentale Kruste, kontinentale Basalte, Archaische Grünsteine und dem verarmten Mantel (BARTH et al., 2000; MÜNKER et al., 2003; WEYER et al., 2003). Die untersuchten Eklogite zeigen bis auf eine Ausnahme subchondritische Nb/Ta Verhältnisse, von denen die meisten relativ gut mit MORB und OIB

übereinstimmen. Die Zr/Hf Verhältnisse der meisten untersuchten Eklogite überlappen am besten mit denen eines MORB Protolithen, welcher auch den größten Teil der subduzierten Ozeankruste ausmacht. Die Nb und Zr Konzentrationen der Eklogite liegen ebenfalls im Bereich von MORB, d.h. es zu keiner Anreicherung im Eklogit zu kommen scheint. Somit ist es naheliegend, dass die Eklogite das Nb/Ta und Zr/Hf ihres Protolithen behalten haben und keine Fraktionierung während der Subduktion stattfand. Im Gegensatz zu den Eklogiten zeigen MORBs und OIBs einen positiven Trend zu höheren Nb/Ta Verhältnissen mit steigender Nb-Konzentration. Während MORB einen verarmten Mantel als Quelle hat, ist die Mantelquelle der OIBs etwas angereichert. Diese Anreicherung führt offensichtlich nicht nur zu höheren Nb und Ta Gehalten, sondern auch zu etwas höheren Nb/Ta Verhältnissen. Da jedoch Eklogite im Wesentlichen nicht im Nb/Ta gegenüber MORB erhöht sind, kommt subduzierte Ozeankruste nicht als Quelle der OIBs in Frage (PFÄNDER et al., 2007). Vermutlich hängt das niedrigere Nb/Ta von MORB im Vergleich zu OIB mit der verarmten Mantelquelle von MORB zusammen, welche aufgrund der Fraktionierung von Nb/Ta bei der partiellen Schmelzbildung ebenfalls ein niedrigeres Nb/Ta hat (WEYER et al., 2003).

Der Datensatz an Eklogiten zeigt, dass es zu keiner wesentlichen Nb/Ta Fraktionierung bei der Subduktion kommt, welche den Unterschied zwischen der Silikaterde und Chondriten erklären könnte. Hierzu wären durchschnittliche Nb/Ta Verhältnisse von >> 20 in Eklogiten notwendig. Eine geringere Nb/Ta Fraktionierung bei der Subduktion könnte für mögliche Unterschiede zwischen Kruste (≈ 12, BARTH et al., 2000, und Mantel (MORB-OIB ≈14-16, BÜCHL et al., 2002; PFÄNDER et al., 2007)) verantwortlich sein. Hierzu wären durchschnittliche Nb/Ta Verhältnisse in Eklogiten > 16 notwendig, was jedoch anhand der gemessenen Eklogite mit einem durchschnittlichen Nb/Ta von 14.9 nicht bestätigt wird.
Die LA-ICPMS Analysen der einzelnen Mineralphasen haben ergeben, das Rutil der Hauptträger der beiden Elemente Nb und Ta ist. Granate, Klinopyroxene und Zirkone haben allgemein nur einen sehr geringen Einfluss auf das Budget von Nb und Ta, wohl aber für die Elemente Zr und Hf, die weitgehend auf alle Phasen verteilt sind und eine Anreicherung in Zirkonen zeigen. Die Laser Ablations Untersuchungen von Rutilen ergaben außerdem, dass die meisten Rutilkörner eine Zonierung im Nb/Ta aufzeigen, mit höheren Verhältnissen im Kern als in Randbereichen. Diese Beobachtung ist bisher nicht durch experimentelle Daten belegt. So zeigen z.B. Rutile im Gleichgewicht mit partiellen Schmelzen eine Fraktionierung

hin zu niedrigen Nb/Ta Verhältnissen im Rutil und hohen Verhältnissen in der koexistierenden Schmelze. Ähnliches gilt für Verteilungskoeffizienten zwischen Rutil und einem Fluid. In beiden Fällen bevorzugt Rutil Ta gegenüber Nb. Einen Ansatz zur Erklärung einer solchen Zonierung in Rutil geben JOHN et al. (2007, persönliche Kommunikation): Wenn Rutil während der Metamorphose wächst und dabei einen vorher vorhandenen Titanit konsumiert, kann der Rutil eine Zonierung ausbilden, die umgekehrt zu der in Titaniten beobachteten Zonierung ist. Dieses Mineral zeigt in der Studie von JOHN et al. häufig eine Nb/Ta Zonierung mit hohen Nb/Ta Verhältnissen in Titanit-Rändern, die sich als erstes auflösen und vom wachsenden Rutil aufgenommen werden. Dies könnte die hohen Nb/Ta-Verhältinsse der Rutilkerne erklären. Da die meisten Rutile nur im Kern analysiert wurden, weisen diese im Mittel superchondritische Nb/Ta Verhältnisse auf (17.6 ± 0.6, die Einzelwerte liegen zwischen 5 und 60). Unabhängig von dem Mechanismus, der zu der beobachteten Zonierung führt, müssen LA-ICPMS Rutil-Daten also kritisch bewertet werden, da Rutilkörnern bezüglich Nb/Ta heterogen sein können.

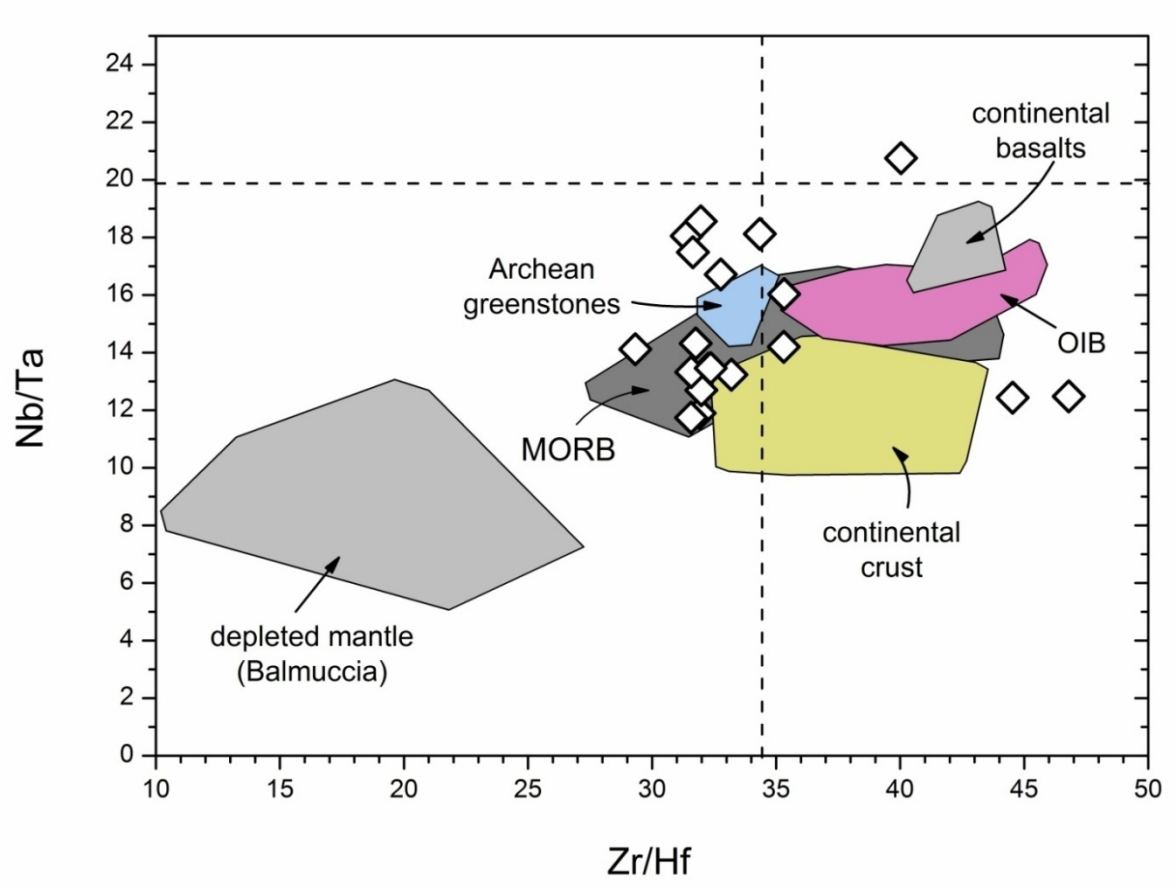

Abbildung 0·1: Zr/Hf gegen Nb/Ta Diagramm. Vergleich der untersuchten Eklogite mit verschiedenen Reservoiren der Silikaterde.

Lu-Hf & Sm-Nd Granat Geochronologie:

Die Ergebnisse der Lu-Hf und Sm-Nd Datierungen der ausgewählten Eklogitproben sind (vergleichend mit Daten aus der Literatur) in Abbildung 0·2 dargestellt. Sie umfassen ein Altersspektrum von 219.6 bis 224.1 Ma (siehe auch Fig. 2·10 in 2.6). Im Gegensatz zu vielen anderen Altersbestimmungen liegen die Lu-Hf Alter in einem sehr engen Zeitrahmen. Im Vergleich zu z.B. Sm-Nd Daten aus der Literatur, geben die Lu-Hf Daten ein wesentlich präziseres Alter wieder. Zwei Sm-Nd Alter aus dieser Studie sind mit den Lu-Hf Altern identisch, weisen aber einen deutlich höheren analytischen Fehler auf. Trotzdem spiegeln sie nicht das breite Spektrum der Sm-Nd Literaturdaten wieder. Die Granatalter dieser Studie geben ein scharf abgegrenztes Ereignis wieder, welches so z.B. durch die U-Pb Datierungen von Zirkonen nicht erkennbar ist.

Haupt- und Spurenelementanalysen zeigen, dass es sich bei den Protolithen der Proben zwar um voneinander unterscheidbare Basalte handelt, diese aber auf einem Differenziationstrend liegen, was u.a. auch für einen gemeinsamen bzw. chemisch ähnlichen Protolithen sprechen könnte. Mikrosondenanalysen ergaben eine relativ homogene Zusammensetzung von Granaten innerhalb einer Probe, jedoch deutlich unterscheidbare Granattypen zwischen den einzelnen Proben. Nur die Granate einer Probe zeigen deutliche Variationen in ihren Grossular- und Pyropanteilen. Diese Granate sind im Gegensatz zu denen aller anderen Proben zoniert. Mg und Ca sind im Randbereich dieser Granate an- bzw. abgereichert während Fe keinerlei Zonierung zeigt und das Mn nur sehr leicht zum Rand hin angereichert ist. Allerdings zeigen Granate aller Proben ähnliche Spurenelementmuster vom Kern zum Rand mit einer deutlichen Lu-Anreicherung im Kern.

Es existieren unterschiedliche Interpretationsansätze der verschiedenen U-Pb Altersspektren aus der Literatur. So gehen z.B. LIU et al. (2006a) aufgrund ihrer Daten von 3 zeitlich unterscheidbaren eklogitfaziellen Metamorphosen aus, während HACKER et al. (2006) nur von 2 verschiedenen (sog. „precursor“ und „main“) UHP Ereignissen ausgehen, auf die eine amphibolitfazielle Überprägung folgt.

Im Gegensatz zu den U-Pb Datierungen an Zirkonen deuten die Lu-Hf-Alter (an Granaten und Klinopyroxenen) auf Ereignisse hin, die einen relativ engen Zeitrahmen umspannen. Dies lässt maximal 2 verschiedene Interpretationsansätze zu: Entweder es wird direkt die Eklogitbildung, bzw. das Granatwachstum datiert, oder die Lu-Hf Alter spiegeln ein Abkühlalter wider. In beiden Fällen würde es sich um Ereignisse handeln, die großräumig mehr oder weniger gleichzeitig verschiedenste Proben beeinflusst haben. Diese würden dann in etwa mit dem von HACKER et al. (2006) postulierten Ende des UHP Ereignisses bei 220 Ma zusammenfallen. Sollte es sich hierbei um ein Abkühlalter handeln, so müsste sich die Abkühlung unmittelbar an das UHP Ereignis anschließen, was für einen schnellen „uplift" sprechen würde. Alternativ könnte das Lu-Hf System auch direkt die Eklogitisierung datieren. Als Auslöser für das Granatwachstum am Ende dieser UHP Phase könnte ein Fluid gedient haben, welches so vorher nicht zur Verfügung stand. Da das Lu deutlich in den Granatkernen angereichert ist, und damit das Lu-Hf Alter überwiegend ein Alter des Kernes wiederspiegelt, scheint die Interpretation eines Wachstumsalters am plausibelsten zu sein. Ebenfalls für ein schnelles Granatwachstumsereignis spricht die Homogenität der meisten Granate, aufgrund der langsamen Kationendiffusion in Granaten (z.B. RAIMBOURG et al., 2007, und dort enthaltene Referenzen). Auch scheint ein Abkühlereignis, welches großräumig alle Proben zur gleichen Zeit beeinflusst hat, aufgrund der Tatsache, dass Granate verschiedenster Chemismen deutlich unterschiedliche Schließungstemperaturen haben können, eher unwahrscheinlich. Es müsste sich dann um eine regional gleichzeitig sehr schnelle Abkühlung gehandelt haben. Eine spätere amphibolitfazielle Überprägung hatte offensichtlich die Lu-Hf Isotopie der Granate nicht beeinflusst. Diese könnte sich möglicherweise in den z.T. etwas jüngeren Sm-Nd Altern (z.B. CHAVAGNAC and JAHN, 1996) wiederspiegeln. Somit könnte die große Streuung der Sm-Nd Alter (abgesehen vom größeren Fehler der Einzelanalysen) auch durch partielles „Resetting" während der amphibolitfaziellen Metamorphose verursacht worden sein, was allerdings durch die in dieser Studie gemessenen Sm-Nd Alter nicht bestätigt werden kann.

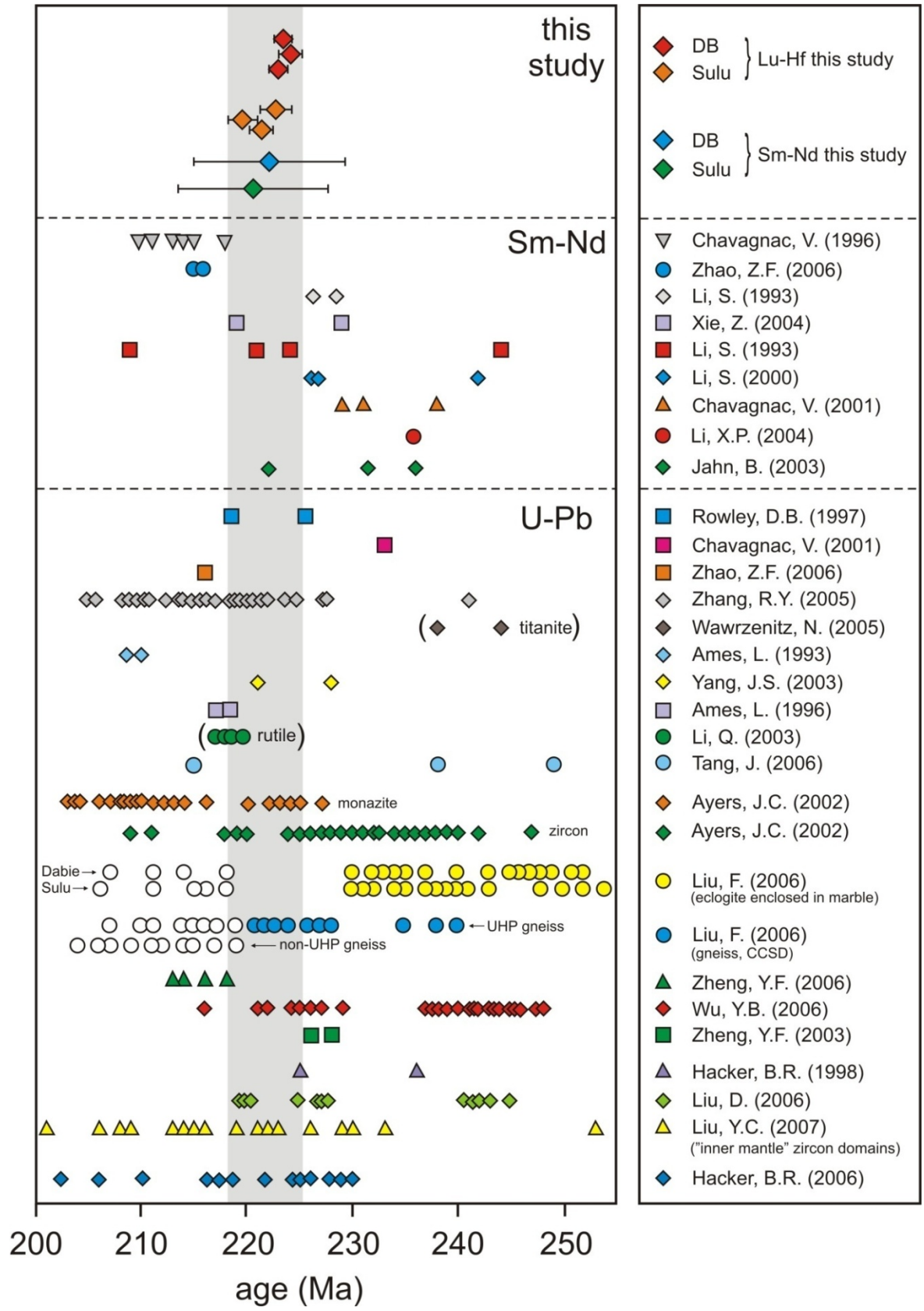

Abbildung 0·2: Lu-Hf & Sm-Nd Alter der Eklogite des Dabie-Sulu UHP Terranes im Vergleich mit Sm-Nd und U-Pb Literaturdaten.

1 CHAPTER I:

High Field Strength Element systematics of rutile-bearing, orogenic eclogites: Implications for crust-mantle evolution and the Nb-paradox

Abstract:

Concerning the Bulk Silicate Earth (BSE), the depleted mantle and the continental crust are thought to balance the budget of refractory and lithophile elements, resulting in complementary trace element patterns. However, the two high field strength elements (HFSE) Niob and Tantal appear to contradict this mass balance. All reservoirs of the silicate Earth exhibit subchondritic Nb/Ta ratios, possibly as a result of Nb depletion. The two HFSE Zr and Hf on the other hand seem not to be fractionated between the silicate reservoirs. They show more or less chondritic Zr/Hf ratios.

In this study a series of orogenic eclogites from different localities was analyzed to determine their HFSE concentrations and to contribute to the question if eclogites could form a hidden reservoir to account for the mass imbalance of the BSE.

The results show that the orogenic eclogites have subchondritic Nb/Ta ratios and near chondritic Zr/Hf ratios. The investigated eclogites show no fractionation of Nb/Ta ratios and no enrichment of Nb compared to e.g. MOR-basalts, the likely precursor of these rocks. With an average Nb/Ta ratio of 14.9 these eclogites could not balance the differences between BSE and chondrite. Additionally, with an average Nb/Ta ≈ MORB they also cannot balance the small differences in the Nb/Ta of the crust and the mantle.

LA-ICPMS analyses of rutiles in these eclogites reveal a zonation of Nb/Ta ratios in this mineral, with rutile cores having higher Nb/Ta than rutile rims. As a consequence, Laser Ablation data of rutiles have to be evaluated carefully and cannot necessarily reflect a bulk rock Nb and Ta composition, although over 90% of these elements reside in rutile.

1.1 Introduction:

The depleted mantle and the continental crust are thought to counter balance the bulk silicate Earth (BSE) composition with regards to most refractory lithophile elements. This relationship is valid for a number of trace elements and isotope ratios, such as the rare earth elements (REE) and Sr-Nd isotope systematics (HOFMANN, 1988; HOFMANN, 1997). High field strength elements (HFSE) are commonly considered as members of trace elements with chondritic BSE ratios; (e.g. HOFMANN et al., 1986) used Nb/U ratios to demonstrate the complementary relationship of the continental crust and the depleted mantle. However, all of the major silicate reservoirs on Earth appear to show subchondritic Nb/Ta ratios, a phenomenon commonly referred to as the "Nb paradox". The two high field strength elements (HFSE) niobium and tantalum are identical in charge and nearly of the same size and therefore show a similar geochemical behavior. They were long regarded as geochemical twins that show similar behavior during fractionation processes in the evolution of the crust-mantle system. However, due to analytical improvement (ICP-MS, ID-MC-ICPMS techniques) during the last decade it became possible to resolve small differences in the Nb/Ta ratios between the silicate Earth and chondritic reservoirs.

Early constraints on the behavior of Nb in the crust-mantle system were given by MCDONOUGH (1991), who proposed that residual eclogite can balance the continental crust and the depleted mantle. This assumption was based on Nb/La and Ti/Zr ratios. Later on the evaluations of the different reservoirs focused more on Nb/Ta and Zr/Hf ratios, since these elements show a more similar behavior than e.g. Nb and La. In earlier studies it was assumed that the mantle has a chondritic Nb/Ta ratio of around 17.5 and that only the crust displays subchondritic Nb/Ta ratios of ≈ 11 (TAYLOR and MCLENNAN, 1985; JOCHUM et al., 1986; JOCHUM et al., 2000; WEYER et al., 2002). Based on these values RUDNICK et al. (2000) proposed that refractory, rutile-bearing eclogite trapped in the lower mantle may be a hidden reservoir with superchondritic Nb/Ta that accounts for the low Nb/Ta and also for the Nb and Ta depletion (compared to La and U) of the continental crust. These authors analysed rutiles from eclogite xenoliths with on average superchondritic Nb/Ta, and reconfirmed the model of MCDONOUGH (1991), assuming a subchondritic Nb/Ta of both the depleted mantle and the crust. Rutile is generally thought to be the major carrier of Nb and Ta in eclogites.

As such it may hold back Nb and Ta in the subducted oceanic crust and thus account for the lower concentration of these elements in the continental crust (Foley et al., 2000; Kalfoun et al., 2002; Zack et al., 2002; Schmidt et al., 2004; Klemme et al., 2005; Xiong et al., 2005). Experimental data indicates that rutile in equilibrium with melt and fluid is also capable to fractionate Nb and Ta (Brenan et al., 1994; Stalder et al., 1998; Green and Adam, 2003; Schmidt et al., 2004; Xiong et al., 2005), but this fractionation is opposite to what would be necessary to create elevated Nb/Ta ratios in subducted oceanic crust.

In a later study, Münker et al. (2003) re-defined the chondritic Nb/Ta. These authors obtained a significantly higher value of 19.9 (compared to the old value of ≈ 17.5), based on analyses of various types of carbonaceous chondrites with the high precision (isotope dilution) technique described in Weyer et al. (2002). A range of samples from different geochemical reservoirs of the BSE were analysed meanwhile with this new technique and most of them display clearly subchondritic Nb/Ta ratios, e.g. MORB = 14.3 ± 0.8 (Münker et al., 2003; Büchl et al., 2002), OIB ≈ 15.8 (Pfänder et al., 2007). This implies that the Earth mantle is more significantly subchondritic in Nb/Ta as earlier assumed. Crustal Nb/Ta ratios (≈ 12) appear to be even slightly lower than those of the mantle (Barth et al., 2000) (the latter value is based on a common ICP-MS technique).

In the light of these new data, the interpretation for eclogite as a hidden reservoir has to be re-evaluated, as eclogites would need to display extreme Nb-Ta enrichment and Nb/Ta fractionation to account for the large difference in Nb/Ta between the BSE and chondrites. Alternatively, the subchondritic Nb/Ta of BSE may be produced by the incorporation of some Nb in the core, since experimental results of Wade and Wood (2001) showed a siderophile behavior of Nb under high pressures. In that case eclogites may be responsible for depletion of Nb and Ta in the crust and the fractionation of Nb/Ta between the mantle and the crust, however, would not counterbalance the chondritic and the BSE Nb/Ta.

To better constrain the role of eclogites in this interplay of reservoirs, orogenic eclogites were analysed in this study to determine their HFSE budget. High precision Nb/Ta and Zr/Hf ratios of bulk eclogites were performed as well as LA-ICPMS in situ analyses of single rutile grains to address this question. Zr/Hf ratios in the major silicate reservoirs appear not to be fractionated between crust and mantle. Most BSE reservoirs show near chondritic ratios (chondrite = 34.2, WEYER et al., 2002), although depleted mantle peridotites can have Zr/Hf ratios as low as 10 (WEYER et al., 2003). Thus, fractionated Zr/Hf appears to monitor fractionation during partial melting in oceanic mantle settings, while subduction appears not to fractionate Zr and Hf significantly. From these and other high precision data from the literature new mass balance constraints of HFSE distribution on Earth will be derived.

1.1.2 Sample description

The eclogite samples investigated in this study origin from different orogenic belts in Europe and Asia (table 1·1): four eclogites from Cabo Ortegal (Iberian Massif, Spain); two eclogites from the Zermatt-Saas-Fee ophiolite (Alps); four eclogites from the Vendée Region (Armorican Massif, France); five eclogites from the Western Gneiss Region ("WGR", Nordfjord and Stadtlandet area, Caledonides, Norway); and four samples from the Dabie ultrahigh-pressure terrane (eastern China). They were selected to cover a wide variety of eclogites from different large orogenic terranes. Most of the investigated eclogites are thought to represent remnants of subducted oceanic crust (Cabo Ortegal, Vendée and Zermatt), as evident from their trace element patterns or relicts of pillow structures. However, the Dabie UHP eclogites and eclogites from the Western Gneiss Region are probably of continental origin. Two eclogite localities, the Dabie terrane (OKAY et al., 1989) and the Nordfjord and Stadtlandet area of the WGR (WAIN, 1997), comprise ultrahigh-pressure eclogites (> 2.5 GPa), while all other localities rather are typical HP eclogites that experienced pressures of around ≈2.0 GPa. For the Zermatt ophiolite a maximum pressure of 2.5 - 3.0 GPa was reported by e.g. BUCHER et al. (2005), but coesite or coesite-pseudomorphs were not recognized in the eclogites sampled for this study (sample location near the Pfulwe Pass).

	Sample name	Locality
Cabo Ortegal, Iberian Massif, NW Spain	SCO16-1 SCO12-5 SCO13-1 SCO11-1 SCO15-1	massive SSW-NNE striking MORB eclogite unit in Cabo Ortegal
Vendée, Armorican Massif, Bretagne, France	SBE6-3 SBE6-1 SBE3-1 SBE7-5	St. Philbert de Bouaine, quarry "La Gerbaudière" (varrying pit levels)
Dabie UHP Terrane, East China	DB05 DB28 DB44 DB63	Bixiling eclogite complex Shuanghe Lidu Shima
Western Gneiss Region, Caledonides, Norway	WGR1 WGR2 WGR3 WGR4 WGR5	Verpeneset Verpeneset Kroken Årsheimneset Årsheimneset
Zermatt-Saas-Fee, Swiss Alps	ZM-Pf01 ZM-Pf05	Pfulwe pass Pfulwe pass

Table 1·1: Overview on the eclogite samples investigated in this study. Localities are named after the nearest cities/villages or landmarks.

The Cabo Ortegal eclogites consist of garnet + clinopyroxene + rutile + quartz, zircon is a very rare accessory phase and is difficult to detect within the thin sections. Most samples are relatively fresh, sample SCO12-5 has small amounts of chlorite minerals between the garnet and cpx grains. All samples have some amphibole minerals, which are mostly aligned along vein-like textures in the thin sections. Sample SCO11-1 shows a higher degree of alteration with abundant amphibole. Two samples (SCO12-5 and SCO13-1) also contain small amounts of Zoisite. Quartz occurs as large grains between garnet and cpx, but is also very abundant as small inclusions in garnet grains.

Eclogites from the Vendée area in the Armorican Massif consist of garnet + clinopyroxene + rutile + quartz. These samples show strong alterations of clinopyroxene grains where cpx was dissolved to form new smaller cpx grains accompanied by small quartz grains. The newly formed cpx + quartz minerals form textures, which show linear orientation in the thin section and resemble myrmecitic intergrowth structures. All four samples contain small amounts of amphibole. Quartz is also found as small inclusions in garnet, except for sample SBE6-1. Sample SBE6-3 also contains some chlorite between clinopyroxene grains.

The ultrahigh-pressure eclogites from the Dabie UHP terrane also consists of garnet + clinopyroxene + rutile + quartz. Zircon inclusions can be found in garnet grains. Samples DB05 and DB44 are "fresh" eclogites with minor alterations and occasional amphibolite minerals in oriented, vein-like textures within the thin sections. Sample DB63 differs from other eclogites, as it has more abundant garnet (70-80%) and rutile compared to all other investigated eclogites. Sample DB28 is a very unusual eclogite. It has the lowest abundances of rutile and quartz, but also contains abundant calcite and chlorite minerals. This is probably due to strong alterations after eclogitisation.

Ultrahigh-pressure eclogites of the Western Gneiss Region also mainly consist of garnet + clinopyroxene + rutile + quartz. Quartz mostly occurs as small inclusions in garnet and also quartz-pseudomorphs after coesite can be found in these samples. Samples WGR3 and WGR5 both contain biotite, while sample WGR4 shows occasional white mica. Samples WGR1 and WGR2 contain small amounts of chlorite. Sample WGR3 is strongly altered and shows similar dissolution of cpx similar to what is observed in some eclogites from the Armorican Massif. Sample WGR3 also contains ilmenite grains next to rutile.

The two investigated eclogites from the Zermatt-Saas-Fee ophiolite consist of garnet + clinopyroxene + glaucophane + rutile + quartz + zoisite. Likely, these samples represent eclogites with relicts of blueschist facies minerals. Rutile is quite abundant in these eclogites. Quartz occurs mainly as small inclusions in garnet grains. Phengite can also occasionally be found in these samples.

1.2 Analytical methods

1.2.1 Isotope dilution:

The eclogite samples were crushed in a jawcrusher and a fraction of the crushed material was used to produce fine bulk rock powders in a bor-carbide mortar. Small fractions were sieved and washed to separate e.g. rutiles for LA-ICP-MS (see section 1.4.2). For the determination of the high field strength elements (HFSE) concentrations the bulk rock powders were spiked with a ^{94}Zr - ^{180}Hf - ^{181}Ta mix-spike for isotope dilution analysis (ID). The sample/spike mix was dissolved in HF:HNO_3:$HClO_4$ acid using Parr© pressure-autoclaves for 24 hours at 180°C. The perchloric acid in the first dissolution step prevented that the silicates formed fluorides by reacting with HF. These fluorides could theoretically fractionate element ratios, such as Nb/Ta. After fuming of the acids at temperatures above 150°C, especially the $HClO_4$, 6M HCl was added to the sample, which was boyled for at least 1 hour on the hotplate at 120°C. Afterwards, the beaker was opened to check the liquid for any precipitates. If the solution was clear and transparent the sample had been fully dissolved and the HCl was dried down. For the separation of the HFSE we used a two-column chemistry after MÜNKER et al. (2001) on cation-exchange resins (Ln-spec + BIORAD AG1-X8). As Nb was the only unspiked element, its concentration was measured in a Zr-Nb aliquot from column 1, using Zr as an internal standard. The Zr concentration was precisely determined by isotope dilution, and a standard with a known Zr-Nb ratio was used for external standardisation, following the procedures described in WEYER et al. (2002). The Zr-Nb aliquot was measured on a Finnigan Neptune MC-ICP-MS. Mass bias has been exponentially corrected using a $^{91}Zr/^{90}Zr$ ratio of 0.21813. An influence of ^{90}Zr and ^{91}Zr from the spike on the natural $^{91}Zr/^{90}Zr$ of the sample is negligible for the precision of the isotope dilution measurement, as the spike abundances of these two isotopes are only 0.73% and 0.24% respectively. The Interferences of ^{92}Mo on ^{92}Zr and ^{94}Mo on ^{94}Zr were corrected using the mass bias corrected $^{95}Mo/^{92}Mo = 1.073$ and $^{95}Mo/^{94}Mo = 1.722$.

The Hafnium-ID and Tantal-ID analyses were also measured on a Finnigan Neptune MC-ICP-MS. Hafnium mass bias was exponentially corrected using the natural $^{179}Hf/^{177}Hf$ of 0.7325, also experiencing a negligible influence of spike ^{179}Hf and ^{177}Hf (spike abundances

0.77% and 0.31%). Interferences of ^{180}Ta and ^{180}W on ^{180}Hf were corrected using mass bias corrected ^{181}Ta/^{180}Ta and ^{183}W/^{180}W ratios. The Ta-fraction was doped with Re prior to measurement to calculate the mass bias on the measured Ta isotope ratio, since the mass bias for these two elements is very similar and Ta only consists of the two isotopes ^{180}Ta and ^{181}Ta. A ^{187}Re/^{185}Re ratio of 1.674 was used for this mass bias calculation.

External reproducibility for the concentrations of the measured HFSE is ≤ 1.5 % 2σ for Zr, Hf and Ta, and ≤ 5% 2σ for Nb. This yields propagated errors on the Nb/Ta and Zr/Hf ratios of ≤ 5% and ≤ 2% respectively.

1.2.2 LA-ICPMS:

The LA-ICPMS setup for this study consisted of a Finnigan Element-2 Single-Collector-ICPMS and a 213nm Nd-YAG UV-Laser (Merchantec). All concentration calculations were performed with the GLITTER program by Mcquarie Res. (2000).

Rutiles in this study were measured partly from thick sections. But, since rutiles often were scarce on these sections rutiles were also separated by hand from a sieve fraction of the crushed rocks, embedded in resin and polished. This procedure enabled for multiple rutile grain measurements on one sample holder. Spot sizes of the Laser Ablation ranged from 30-60µm with laser energies between 1.5 and 3.0 J/cm^2. For the rutile analyses and the calculation of their HFSE concentrations ^{47}Ti has been used for internal standardization and a natural rutile was used as an external standard. This rutile grain of ≈ 1cm in size is from an eclogite of the Zermatt-Saas-Fee ophiolite. It was calibrated with isotope dilution and additionally cross-calibrated with Laser Ablation using two other well known rutile-standards (provided by C. Münker and T. Zack). The cross calibration yielded an analytical uncertainty for the measured Nb/Ta and Zr/Hf ratios by LA-ICPMS of ±8.7% (2σ) and ±5.3% (2σ), respectively, for the new rutile-standard. Accordingly, an uncertainty of ≈ 9% can also be assigned to all measured Nb/Ta ratios of the rutile analyses.

Garnets and clinopyroxenes were always measured in-situ from thin sections. Since some HFSE concentrations, especially Nb and Ta, are very low in these minerals, large spot sizes (95-120µm) and a high laser energies of 4-8 J/cm^2 were used, to achieve a sufficiently high signal for most analysed elements. However, Nb and Ta were still measured near or below the detection limit of 10-20 ppb. Therefore,Nb/Ta ratios for these minerals suffer from very large analytical errors. Concerning the elements Nb and Ta, the Laser Ablation analyses of garnet and cpx additionally suffer by the contribution of very small inclusions of rutile (< 20µm), which are difficult to detect optically. Similar difficulties arise from inclusions of zircon. Therefore, the Ti and Zr signals were carefully monitored during Laser Ablation analyses to exclude analyses, which may suffer from such inclusions. For garnet and clinopyroxene analyses the BIR1-G basalt glass standard with the calibrated values of EGGINS et al. (1997) was used for external standardization.

For the determination of the trace element concentrations of the bulk eclogites, fused glasses were produced from fine rock powders, embedded and polished, and analysed by LA-ICPMS. Spot sizes ranged from 90 to 120 µm with laser energies of 3-5 J/cm^2. The BIR1-G basalt glass standard was used for external standardization. This procedure enabled a quick analyses of the eclogites bulk compositions, since the same fused glasses were already prepared for the major element analyses with the electron microprobe.

The major elements of all minerals (thin section) and the bulk rocks (fused glasses) were determined on a JEOL Superprobe JXA-8900 electron microprobe. The elements Si, Ca and Ti were used as the internal standard for the LA-ICPMS measurements of garnets, clinopyroxenes and rutile, Si was the internal standard in the analyses of the fused glasses (see also appendix table A·1 and A·2).

1.3 Results:

1.3.1 Bulk rock HFSE and trace element concentrations:

The results of the isotope dilution analyses of the HFSE and the trace element concentrations of the investigated eclogites are shown in table 1·2, Fig. 1·1 and Fig. 1·2. The diagram in Fig. 1·1 shows a plot of the Nb concentration vs. Nb/Ta, and the Zr concentration vs. Zr/Hf. Denoted errors are 5% for the Nb/Ta ratio and 2% for the Zr/Hf ratio, corresponding to a maximum error of the isotope dilution. The eclogites have Nb/Ta ratios between 11.7 and 20.8 and Zr/Hf ratios between 29.3 and 46.8. High Nb/Ta ratios are mainly observed for eclogites from the Dabie UHP terrane, two samples from the Western Gneiss Region and one sample from the Armorican Massif. Only one sample has a superchondritic Nb/Ta ratio of 20.8 (DB44). Figure 1-1 also shows two fields of reference for MORB and OIB (data of BÜCHL et al., 2002, and PFÄNDER et al., 2007). Most analysed eclogites lie in the field for MOR basalts. The average Nb/Ta and Zr/Hf ratios of all investigated eclogites are 14.9 and 34.2 respectively.

Table 1·2 and Fig. 1·2 show the results of the trace element analyses by LA-ICPMS of the bulk eclogites. The trace element patterns in Fig. 1·2 were normalized to the value of C1 (MCDONOUGH and SUN, 1995). Most patterns are flat without large differences compared to the reference NMORB (HOFMANN, 1988). Only Th and U are enriched compared to NMORB in most of the samples, and the Dabie UHP eclogites show the largest enrichment. All samples show a strong geochemical affinity to mid-ocean ridge basalts. The REE patterns of the samples are mostly parallel to the NMORB reference line. An oceanic basalt precursor is particularly evident for the eclogites from the Zermatt-Saas-Fee ophiolite, where relic pillow structures can be found in the outcrops (e.g. BUCHER et al., 2005, and own field observations). Most samples show a negative Sr anomaly, which is probably inherited from their MORB protoliths (which is also evident from the reference pattern for NMORB). In the case of the eclogites with a possible continental origin (WGR and Dabie UHP) their negative Sr anomaly could possibly be caused by plagioclase fractionation before their basalt protolith formed.

	Cabo Ortegal, Iberian Massif					Vendée, Armorican Massif				Dabie UHP Terrane				Western Gneiss Region, Caledonides					Zermatt-Saas-Fee, Alps	
	SCO 16-1	SCO 12-5	SCO 13-1	SCO 11-1	SCO 15-1	SBE 6-3	SBE 3-1	SBE 6-1	SBE 7-5	DB05	DB28	DB44	DB63	WGR 1	WGR 2	WGR 3	WGR 4	WGR 5	ZM Pf01	ZM Pf05
Ti **	7014	10894	7127	8108	6226	6708	6970	5536	7173	12501	7101	1904	12335	4005	7194	12081	7192	5738	12639	13790
Sr	73.4	40.4	110	64.8	60.4	84.7	80.5	141	176	107	80.3	97.8	125	102	85.2	105.0	81.9	104	183	143
Y	26.2	23.0	17.1	24.6	19.6	18.1	23.7	18.7	21.0	10.1	20.8	14.7	29.3	11.5	26.1	36.7	12.4	12.3	48.7	38.9
Zr *	65.5	63.0	66.7	128	58.6	56.6	79.0	58.4	69.5	23.5	144	125	41.0	38.5	72.4	135	72.7	64.1	264	259
Nb *	0.852	1.39	1.34	1.82	0.800	0.625	1.84	0.910	3.26	0.751	7.32	3.74	6.60	0.67	1.49	2.24	8.26	4.93	6.91	6.16
La	2.16	2.44	1.81	4.16	1.44	1.50	6.54	2.05	5.51	10.0	2.14	5.48	11.9	1.89	2.81	5.62	5.05	4.75	13.1	10.4
Ce	6.45	7.89	6.68	12.6	5.08	5.54	16.1	6.45	14.0	24.6	5.54	11.3	23.2	5.23	7.81	17.0	14.2	11.2	45.6	36.5
Pr	1.29	1.36	1.17	1.99	0.948	1.02	2.33	1.11	2.12	3.60	0.882	1.46	2.88	0.913	1.40	2.76	2.28	1.65	4.94	4.16
Nd	7.30	7.30	6.18	10.04	5.40	5.65	11.1	5.98	10.4	16.27	4.22	6.26	11.63	4.91	7.72	14.3	10.8	7.48	23.7	20.4
Sm	2.74	2.56	2.30	3.39	2.08	2.17	3.50	2.23	3.44	3.10	1.56	1.43	3.31	1.66	2.77	4.72	3.24	1.87	6.21	5.34
Eu	1.13	0.991	1.03	1.44	0.857	0.950	1.27	0.967	1.42	1.11	0.605	0.636	1.37	0.860	1.16	1.81	1.03	0.839	2.18	1.52
Gd	2.95	2.49	2.20	3.33	2.17	2.15	3.13	2.23	3.16	1.77	1.72	1.50	3.82	1.62	2.99	4.73	2.56	1.86	7.49	6.25
Tb	0.674	0.577	0.505	0.706	0.507	0.500	0.641	0.509	0.654	0.325	0.473	0.431	0.881	0.348	0.675	1.07	0.480	0.417	1.06	0.909
Dy	4.59	4.06	3.22	4.60	3.52	3.34	4.26	3.41	4.01	2.02	3.58	2.94	5.37	2.21	4.72	6.96	2.57	2.55	7.64	6.59
Ho	1.11	1.01	0.751	1.08	0.847	0.798	1.06	0.820	0.927	0.457	0.921	0.645	1.12	0.522	1.14	1.64	0.506	0.557	1.63	1.36
Er	2.92	2.69	1.94	2.78	2.20	2.10	2.77	2.13	2.42	1.15	2.57	1.56	2.52	1.33	3.01	4.21	1.18	1.35	4.65	3.81
Tm	0.421	0.383	0.283	0.404	0.317	0.306	0.403	0.308	0.355	0.161	0.390	0.208	0.301	0.186	0.433	0.600	0.160	0.190	0.559	0.464
Yb	2.85	2.65	1.97	2.78	2.18	2.12	2.77	2.16	2.44	1.02	2.66	1.37	1.75	1.20	2.81	4.01	1.01	1.23	4.13	3.42
Lu	0.438	0.390	0.291	0.424	0.339	0.320	0.413	0.323	0.371	0.156	0.401	0.216	0.249	0.191	0.450	0.605	0.150	0.197	0.633	0.547
Hf *	2.02	2.00	2.03	2.44	1.85	1.77	2.45	1.85	2.17	0.748	4.09	3.13	1.19	1.21	2.47	4.06	2.28	1.82	5.65	5.81
Ta *	0.063	0.119	0.080	0.109	0.046	0.049	0.137	0.068	0.176	0.042	0.457	0.180	0.364	0.047	0.106	0.169	0.694	0.347	0.554	0.495
Pb	0.59	0.365	0.468	0.480	0.692	0.618	1.88	1.99	1.94	2.93	1.69	3.20	5.16	0.370	0.453	1.34	14.8	3.21	0.841	1.20
Th	0.065	0.120	0.052	0.252	0.061	0.085	0.923	0.099	0.283	0.535	4.02	0.458	1.13	0.119	0.238	0.374	0.613	0.271	0.692	0.888
U	0.029	0.092	0.044	0.185	0.062	0.072	0.318	0.295	0.249	0.100	10.27	0.144	0.727	0.036	0.095	0.336	3.14	0.320	0.388	0.261
Nb/Ta	13.5	11.7	16.7	16.7	17.5	12.7	13.4	13.3	18.6	18.1	16.0	20.8	18.1	14.3	14.1	13.2	11.9	14.2	12.5	12.4
Zr/Hf	32.4	31.6	32.8	52.3	31.6	32.0	32.3	31.6	32.0	31.4	35.3	40.0	34.4	31.8	29.3	33.2	31.9	35.3	46.8	44.5
Nb/La	0.39	0.57	0.74	0.44	0.56	0.42	0.28	0.44	0.59	0.07	3.42	0.68	0.56	0.35	0.53	0.40	1.63	1.04	0.53	0.59

Table 1·2: Trace element concentrations of the eclogites in this study (values in ppm; * isotope dilution, ** electron microprobe)

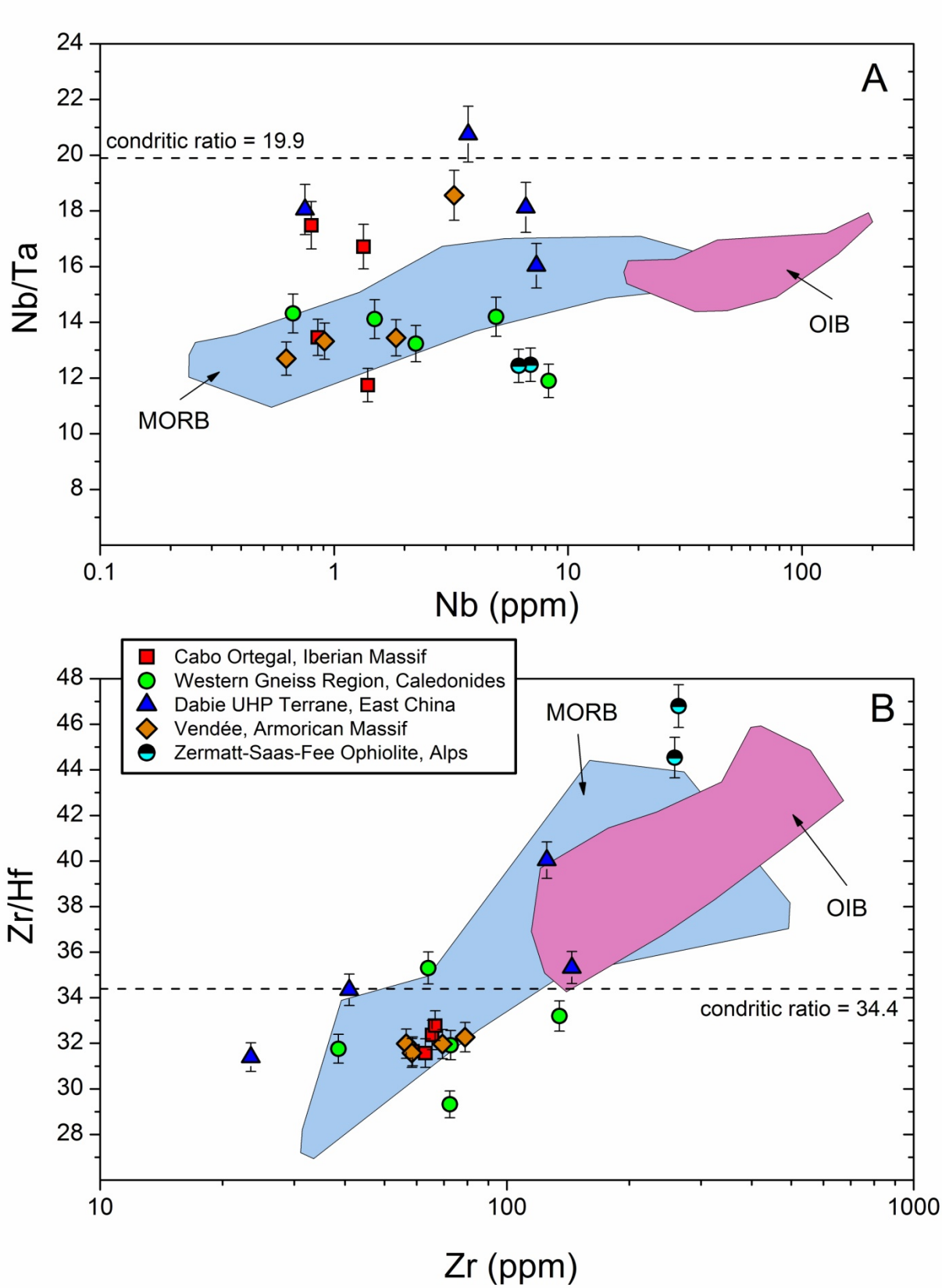

Fig. 1·1: Plots of Nb (ppm) versus Nb/Ta and Zr (ppm) versus Zr/Hf. Dashed lines represent the chondritic ratios. Fields of reference for MORB and OIB from BÜCHL et al. (2002) and PFÄNDER et al. (2007). Denoted errors are ±5% and ±2% for the Nb/Ta and Zr/Hf ratios, respectively.

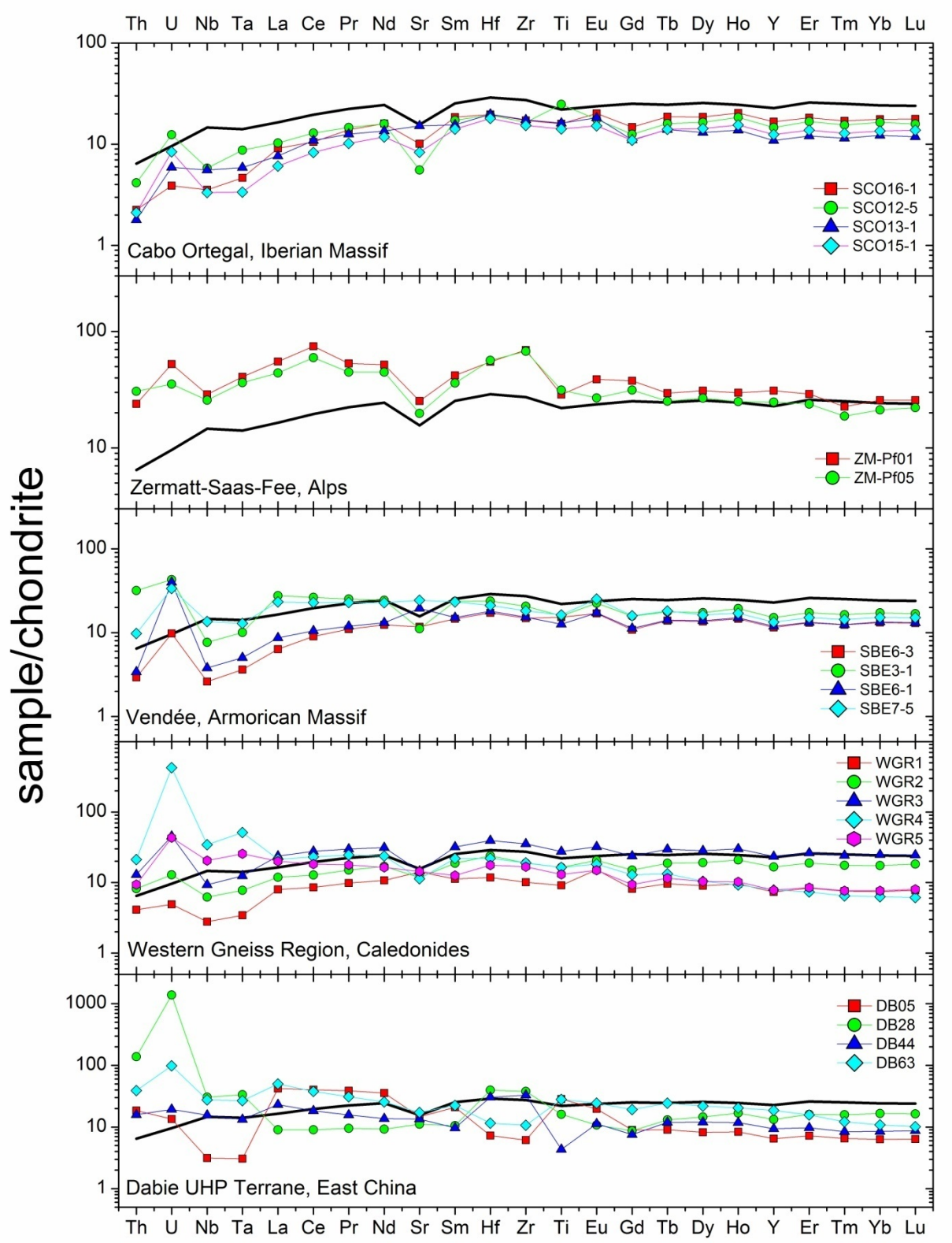

Fig. 1·2: Extended trace element spidergrams of eclogites from various locations (normalized to chondrite of McDonough and Sun (1995). Black line shows chondrite-normalized pattern of NMORB (Hofmann, 1988).

1.3.2 Rutiles, garnets and clinopyroxenes by LA-ICPMS:

The most important minerals for the HFSE budget of the investigated eclogites, rutiles, garnets and clinopyroxenes, have been analysed by Laser Ablation to determine their HFSE concentrations. Figure 1·3 shows the Nb/Ta and Zr/Hf ratios of rutiles and the Zr/Hf ratios of garnets and clinopyroxenes as histograms. In rutiles, Nb/Ta ratios range between 5 and 60 with an average of 17.9 ± 0.6 (2σ s.e.), and the Zr/Hf ratios vary between 8 and 50 with an average of 26.1 ± 0.6 (2σ s.e.). Both average ratios are subchondritic. Apart from single laser spots measurements of rutiles (Fig. 1·3a + 1·3b), "line scans" from rim to rim were performed for some grains. The results are shown in Fig. 1·4. Five representative patterns from three different eclogite samples are reported. In general, rutile grains show a zoning of their Nb/Ta ratio from core to rim, with high Nb/Ta in the core regions. Only rutiles from sample DB05 display flat patterns with no distinct Nb/Ta peaks. As most rutile grains were analysed in the centre (Fig. 1·3a+b), this zoning probably biased the measured Nb/Ta ratios towards higher values. Indeed when calculating average Nb/Ta ratios for bulk rutile of distinct samples the rutile yields higher Nb/Ta than the associated bulk rock ID measurement, although rutile contains ≈ 90% of Nb and Ta.

For garnets and clinopyroxenes only the Zr/Hf ratios are shown, since their Nb/Ta ratios suffer from large analytical error due to very low concentrations of Nb and Ta. Therefore the Nb/Ta ratios of these minerals also show a very large spread. However, the Nb and Ta concentrations of these minerals were used to calculate a maximum contribution of these minerals to the total Nb-Ta budget. Zr/Hf ratios in garnets range from 1 to 160 with an average of 64.0 ± 3.1 (2σ s.e.) and Zr/Hf ratios in clinopyroxenes range from 1 to 80 with an average of 22.7 ± 1.6 (2σ s.e.). In some samples amphiboles and mica (biotite and phengite) were also measured. These minerals have Nb and Ta concentrations below the detection limit of these elements by LA-ICPMS and therefore suffer from identical large uncertainties as for garnets and clinopyroxenes. From the mineral data and the available bulk rock concentrations the overall budget of the HFSE was calculated and is shown in summary in table 1·3. Modal abundances of garnet and clinopyroxene (and other minerals) were determined by counting in thin sections. The modal abundance of rutile was calculated assuming that it is the major host for Ti in the bulk rock. This can be assumed since Ti

concentrations are very low in garnet and clinopyroxene (ranging from 300 to 2000 ppm, determined by electron microprobe analyses). As no other Ti-phases are recognized in the investigated eclogites, the Ti budget must be dominated by rutile. Modal zircon has been determined similarly from Zr mass balance. However in this case, a significant amount of Zr was also in garnet, clinopyroxene and rutile. The Zr concentrations of the latter minerals were known from LA-ICPMS (≈ 1 - 12 ppm Zr and ≈ 0.1 - 1 ppm Hf in garnet and clinopyroxene; 200 - 500 ppm Zr and 2 - 20 ppm Hf in rutile). It was assumed that the remaining Zr resides in zircon. The HFSE concentrations of zircon were calculated based on the total mass balance of the bulk rock since this mineral was generally too small to analyze by Laser Ablation. However, zircon does not contribute significantly to the budget of Nb and Ta. Over 90% of the Nb and more than 86% of the Ta are found in rutile, making it the major contributing mineral for these elements.

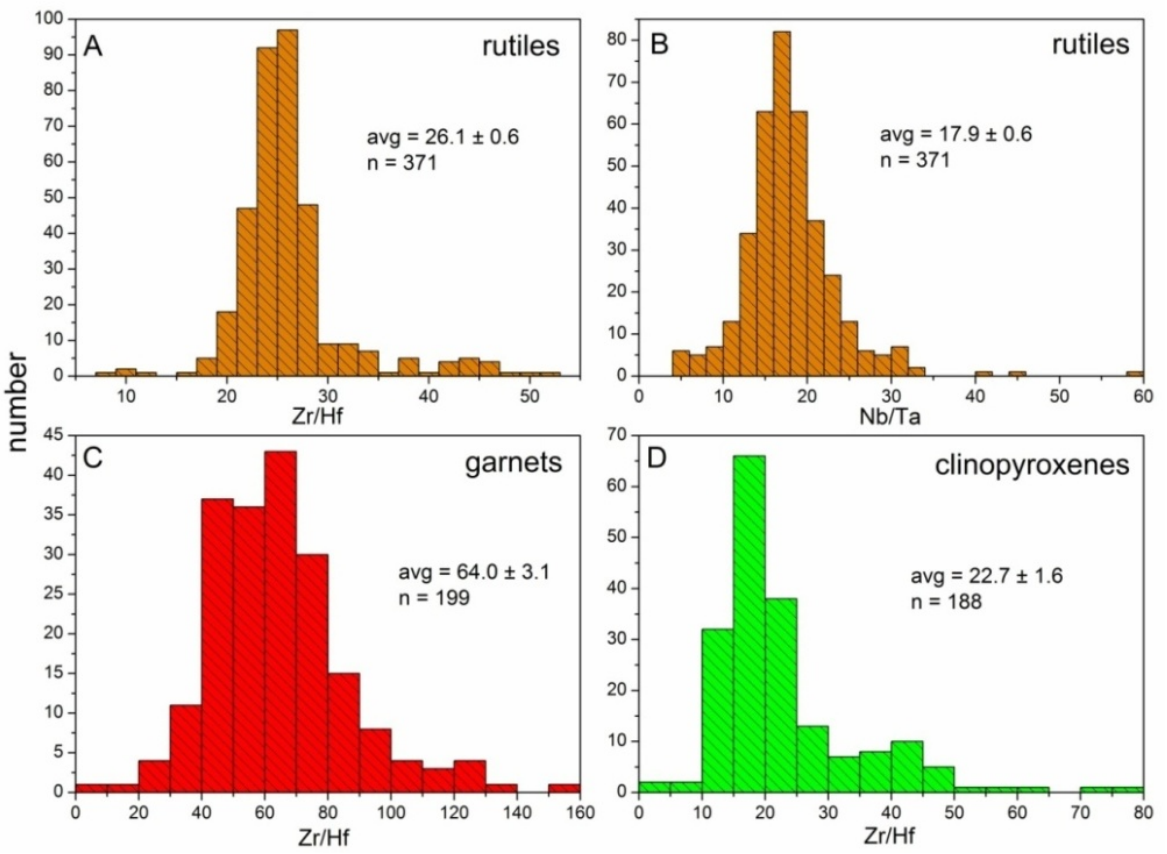

Fig. 1·3: Various mineral histograms showing the Nb/Ta and Zr/Hf ratios of rutiles, garnets and clinopyroxenes.

in %	garnet	cpx	rutile	zircon	other
Ti	0.8 - 10.5	1.4 - 13.5	81 - 97	--	1 - 3
Zr	0.3 - 8.7	1 - 14	1.7 - 8.8	69 - 96	2 - 3
Nb	0.04 - 6.5	0.05 - 2.6	92 - 100	--	< 1
Hf	0.3 - 9.1	2.8 - 34	2.9 - 16.6	43 - 93	1 - 3
Ta	0.5 - 6	0.3 - 6	88 - 99	--	1 - 6
Nb/Ta	1 - 30	1 - 20	5 - 60	--	1 - 20
Zr/Hf	1 - 160	1 - 80	8 - 50	30 - 50	10 - 40

Table 1·3: Proportions of the HFSE in the major and accessory mineral phases in eclogite (other = amphiboles + mica).

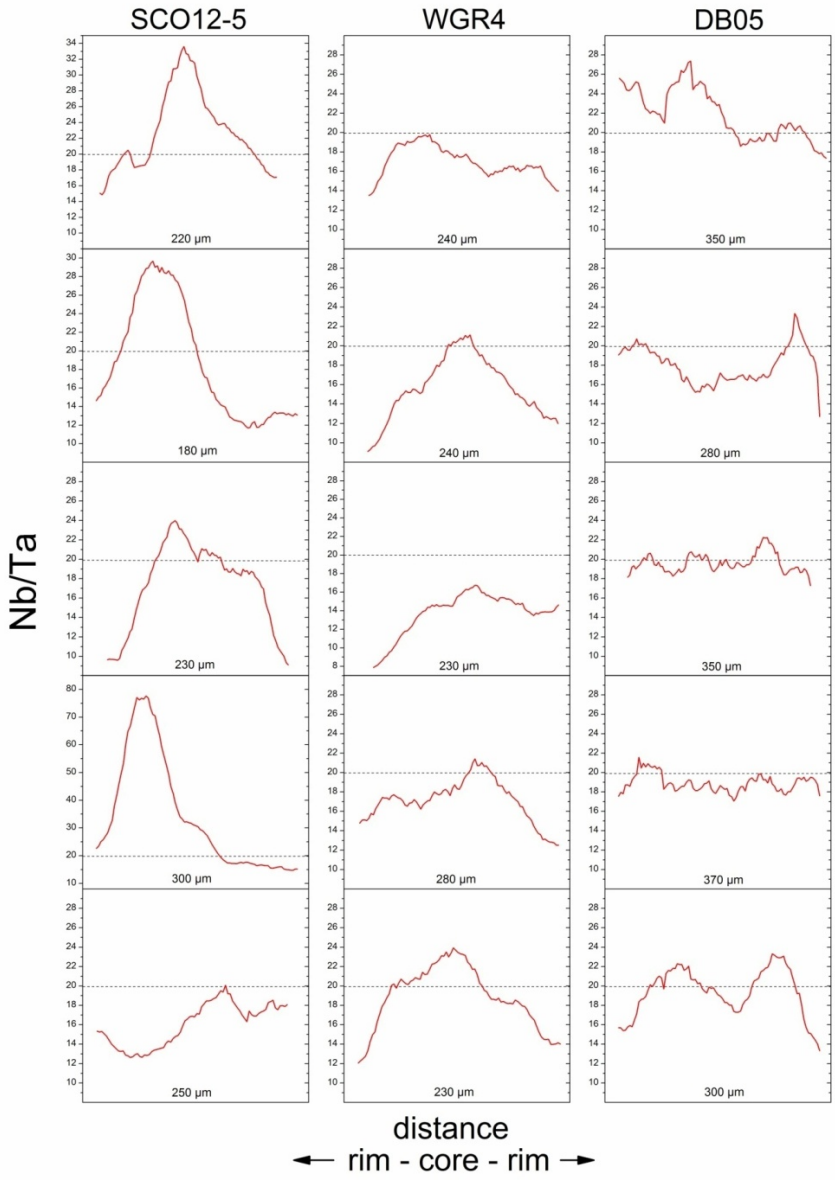

Fig. 1·4: Cross-grain line scans by LA-ICPMS of rutile grains. Scans follow a rim-core-rim pattern. Numbers indicate grain-size and length of line-scan in µm. Dashed line denotes chondritic Nb/Ta for reference.

1.4 Discussion:

1.4.1 Mineral HFSE systematics:

The mineral HFSE budget in table 1·3 shows that rutile is the dominant carrier for Nb and Ta, in agreement with (FOLEY et al., 2000; KALFOUN et al., 2002; ZACK et al., 2002; SCHMIDT et al., 2004; KLEMME et al., 2005; XIONG et al., 2005). If rutiles host most of the Nb and Ta, a bulk rutile average would also constrain the Nb/Ta ratio of the bulk rock. However, the bulk rutile Nb/Ta average of 17.9 is higher than the bulk eclogite Nb/Ta of 14.9. This offset is probably related to the fact that most rutiles display a zoning with high Nb/Ta in the core and lower values at the rim, resulting in a bias towards higher Nb/Ta, as most individual grains were only analysed in the core. The reason for the zoning of Nb/Ta ratios in rutile is not yet clear. XIONG et al. (2005) report experimental partition coefficients of Nb and Ta for rutile during melting of hydrous basalt, and also SCHMIDT et al. (2004) and KLEMME et al. (2005) conducted experiments for rutile-melt partitioning in subduction processes. Their experiments show that for any given rutile/melt pair D_{Nb} is lower than D_{Ta}. If rutile was produced in equilibrium with such a melt, this would result in low Nb/Ta ratios in the initially grown rutile. This is contrary to the rutile zoning that is observed in this study. Consequently, the rutiles of the investigated samples were probably not in equilibrium with such a melt. But, partial melting of subducted oceanic crust is not a common and expected feature of modern subduction zones, and rutile/melt partitioning is an unlikely mechanism for Nb/Ta fractionation. Partitioning data of BRENAN et al. (1993) and BRENAN et al. (1994) indicate that rutile/fluid partitioning may be opposite in direction to rutile/melt partitioning. In this case, rutile favors Nb over Ta, resulting in high Nb/Ta in rutile that grew or equilibrated in equilibrium with such a fluid. However, more recent data of GREEN and ADAM (2003) show $D_{Nb}/D_{Ta} < 1$ for rutile/fluid partitioning.

Recently, JOHN et al. (2007, pers. communication) suggested another mechanism for a similar Nb/Ta zoning these authors observed in rutile. They argued that such a zoning could be produced if rutile grows at the expense of titanite. Titanite, the lower pressure Ti-phase, has usually lower Nb/Ta than rutile and is frequently zoned with low Nb/Ta in the core and high Nb/Ta in the rim. If rutile grows at the expense of such zoned titanite, this

would generate rutile with an inverse zoning than that of the consumed titanite, i.e. rutile cores with high and rims with low Nb/Ta. Apart from the mechanism that produced the zoning of Nb/Ta in rutile, the results of this study demonstrate that in situ analyses of rutile grains by LA-ICPMS have to be taken with caution as zoning may produce artificial bias between rutile and bulk rock.

Garnets and clinopyroxenes both do not significantly contribute to the budget of Nb and Ta in eclogites. Their Nb/Ta ratios, although influenced by high analytical error, are on average between 8 and 12. However, these minerals do play a major role in controlling the budget of Zr and Hf. Although, zircon is the major carrier of these two elements in most cases, clinopyroxene can have up to 34%, garnet up to 9% and rutile up to 17% of the Hf content of the eclogite. The average Zr/Hf ratios of garnet and clinopyroxene are 64.0 and 22.7 respectively (Fig. 1·3c & Fig. 1·3d) while zircons have (modeled) Zr/Hf ratios between 30 and 50. Considering the modal abundances of these minerals, garnet and clinopyroxene are complementary in their Zr/Hf ratios. The same applies for the accessory phases rutile (average Zr/Hf = 26.1) and zircon (average Zr/Hf ≈40). These findings indicate that although Zr/Hf ratios are fractionated between the different eclogite minerals, the bulk eclogites remain close to that of their precursor rocks (± depleted basalts). Accordingly, the contrary fractionation behavior of Zr-Hf between their carriers in eclogite may explain the non-fractionated Zr/Hf ratio between crust and mantle, although this ratio can be highly fractionated during partial melting in other mantle settings, where the the Zr-Hf budget is only controlled by cpx (Weyer et al., 2003).

1.4.2 Bulk eclogite HFSE characteristics:

Most of the eclogites investigated during this study display Nb/Ta and Zr/Hf ratios which plot into the field for MORB samples, and their average Nb/Ta ratio of 14.9 ± 1.2 (2σ s.e.) is indistinguishable from the average MORB Nb/Ta of 14.3 ± 0.8 (2σ s.e.) (Fig. 1·1). Also Nb and Zr concentrations of the eclogites are well in the range of MORB and they display no enrichment or depletion relative to MORB. The behavior of the high field strength elements in the eclogites is illustrated in Fig. 1·5, which shows a log-log plot (Sims and DePaolo, 1997)

of Hf and Ta versus Zr and Nb, respectively. In this diagram, element pairs with a constant ratio and thus identical partition coefficients show a linear correlation with a slope of one. This is precisely the case for Nb/Ta. This indicates that for the element pair Nb and Ta no fractionation occurs in the sum of processes, including partial melting in the mantle, subduction and subsequent eclogitisation.

This identical behavior of Nb and Ta during the latter of these processes, eclogitisation, is also demonstrated by the trace element patterns of Fig. 1·2. Although LREE depletion relative to Nb-Ta have been occasionally described (e.g. for Zambian eclogites: JOHN et al. (2004) and BERNARD-GRIFFITHS et al. (1991)) most of the eclogites investigated in this study display no significant Nb/LREE fractionation (Fig. 1·6). Most eclogites have a subchondritic Nb/La and only two samples have slightly superchondritic Nb/La of 1.6 and 3.4. Concentrations of Nb and Ta generally range between 0.2 and 3 times the value of NMORB, which is well in the range of MORB samples (BÜCHL et al., 2002). These findings demonstrate that Nb and Ta are (1) not particularly enriched in eclogites, e.g. by accessory minerals, such as rutile and (2) that also no fractionation during eclogitisation occurs. This interpretation is confirmed by GAO et al. (2007) who recently showed for eclogites from Tianshan, that, even though Ti, Nb and Ta were mobilized by a fluid during transformation from blueschist to eclogite on a scale of several tenth of meters, no Nb/Ta fractionation occurred.

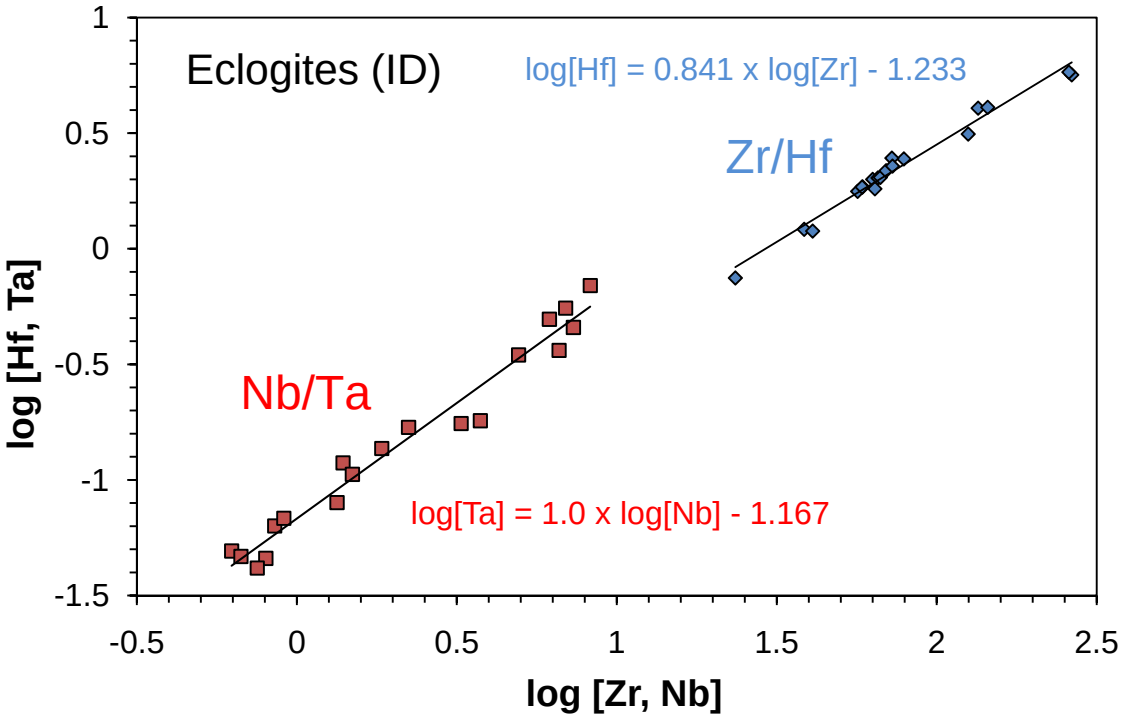

Fig. 1·5: Log-log plot after SIMS and DEPAOLO (1997) of log(Zr, Nb) vs. log(Hf, Ta). Elements with a uniform concentration ratio plot on a line with a slope of one.

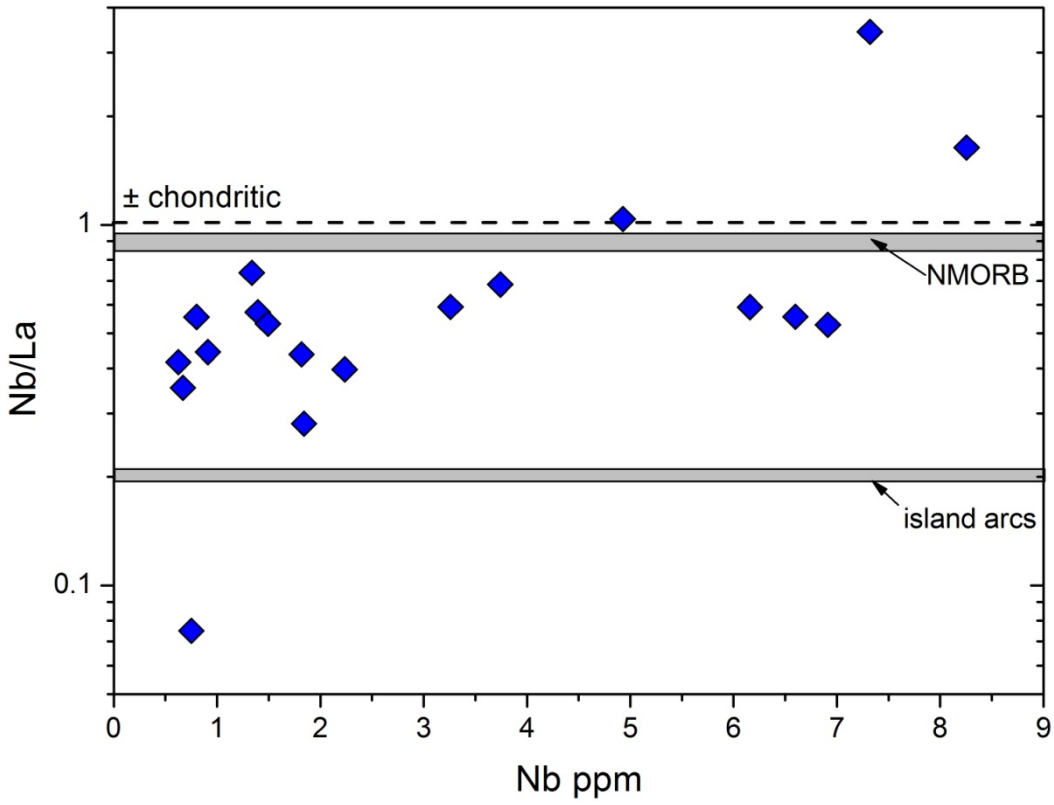

Fig. 1·6: Nb (ppm) versus Nb/La of eclogites (blue diamonds show the investigated eclogites, grey lines denote average Nb/La of NMORB and island arcs).

In contrast, the element pair Zr and Hf displays a correlation with a slope of 0.841 (Fig. 1·5), indicating a distinct fractionation of Zr/Hf. However, the agreement of Zr/Hf ratios and Zr concentrations with those of MORB indicates that this fractionation is likely inherited from the variably depleted mantle source of the MORB precursor rocks. This interpretation is supported by the positive correlation of Zr/Hf with the Zr concentrations (Fig. 1·1b), which indicates Zr/Hf fractionation during partial melting in the mantle source in the presence of clinopyroxene (WEYER et al., 2003) or during magma differentiation (PFÄNDER et al., 2007).

The results of this study provide some constraints on the mechanism of the Nb-Ta depletion (relative to LREE), which is commonly observed in island arc basalts. These rocks originate from partial melting of the mantle wedge overlying subducting slabs, induced by fluid migration from the slab into the wedge, and commonly show a negative "Nb-Ta trough" (RYERSON and WATSON, 1987; STOLPER and NEWMAN, 1994; GREEN, 1995; PLANK and WHITE, 1995; STOLZ et al., 1995; JOCHUM et al., 1996; MÜNKER, 1998; PROUTEAU et al., 2000).

Two principle mechanisms could produce the depleted patterns of subduction related basalts: (1) selective retention of these elements in the subducted oceanic crust by accessory minerals (e.g. rutile, SAUNDERS et al., 1980; GREEN, 1981; MORRIS and HART, 1983; BROPHY and MARSH, 1986), or (2) distinctly lower fluid mobility of Nb and Ta compared to LREE leading to a relative enrichment of LREE in the mantle wedge. Indeed many studies predict that Nb and Ta mobility in subduction-like fluids is low (e.g. BRENAN et al., 1993; BRENAN et al., 1994; BECKER et al., 2000; GREEN and ADAM, 2003), which may change to a certain degree if complex formers in the fluid are taken into account (ANTIGNANO and MANNING, 2005; GAO et al., 2007). Some experimental data in contrast show a high fluid mobility (STALDER et al., 1998), but also no fractionation of Nb/Ta. The findings of this study, showing that Nb and Ta are not enriched in eclogites and Nb/Ta ratios are not fractionated, imply that the second mechanism is more suitable to explain the Nb-Ta depleted patterns of island arc basalts. In contrast JOHN et al. (2004) argue that one group of their investigated eclogites shows complementary LREE patterns compared to typical arc tholeiites. They argue that the average trace element concentrations of the eclogites in question and the depletion of certain elements are a direct implication for fluid transport into the source of arc magmas, and responsible for their slab component. However, compared to an average arc tholeiite,

the average trace element pattern of the eclogites investigated in this study shows no complementary character regarding the LREE (Fig. 1·7, arc tholeiites data of PEATE et al. (1997)), as also shown for many other well equilibrated eclogites (e.g., SPANDLER et al., 2003; HERMANN et al., 2006; BEBOUT, 2007). The high U and Th of the average eclogite is mainly influenced by the high abundances of these elements in the Dabie UHP and WGR samples.

The results of this study imply that overall trace element transport through dehydration of the subducted oceanic crust into the source of arc magmas seems low. Transport might be more significant locally where fluid-rock ratios are high and fluid channelization into pathways with high fluid extraction rates occurs (HERMANN et al., 2006; JOHN et al., 2007; ZACK and JOHN, 2007), or processes at the slab wedge interface (BEBOUT, 2007; FEINEMAN et al., 2007). Compared to the trace element pattern of NMORB Th, U, La and Ce show some enrichment relative to Nb and Ta (Fig. 1·7). This might be attributed to alterations during tectonic overprint within the orogens and would also explain the overall low Nb/La (lower than MORB) ratios in most eclogites (Fig. 1·6).

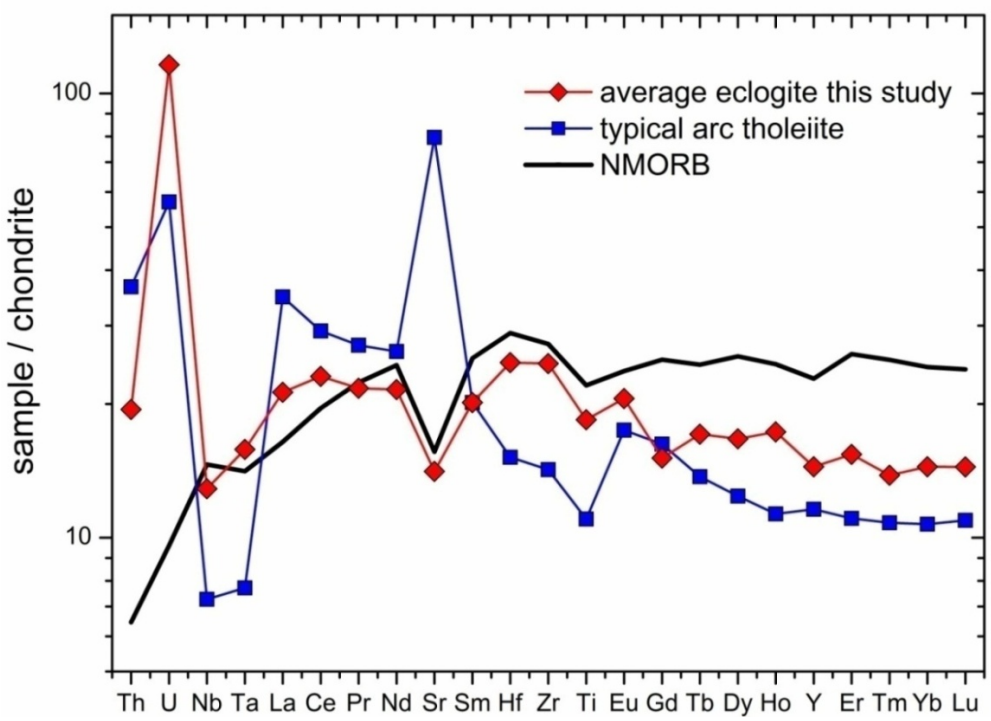

Fig. 1·7: Average eclogite of this study compared to a typical arc tholeiite (PEATE et al., 1997) and NMORB.

Accordingly, any fractionation of Nb/Ta between crust and mantle is more likely to be produced by the transport of these elements within the mantle wedge into the source region of partial melting (i.e. due to different fluid mobilities of Nb and Ta), rather than due to the retainment of Nb and Ta in an eclogite reservoir. Alternatively, the Nb/Ta of the crust may simply reflect that of the mantle wedge without any further fractionation. The average Nb/Ta of the mantle wedge might be lower than chondritic, due to previous depletion by partial melting (DIXON and BATIZA, 1979; HICKEY and FREY, 1982; RYERSON and WATSON, 1987; WEYER et al., 2003). Apparently, rutile, the major carrier of Nb and Ta in eclogites, does neither significantly fractionate Nb/Ta between crust and mantle, nor is it responsible for the Nb-Ta deficit in the continental crust.

1.4.3 Mass balance constraints:

Eclogites as remnants of subducted oceanic crust have been widely considered to be the missing link between the continental crust and the depleted mantle concerning refractory lithophile elements (e.g. MCDONOUGH, 1991; KAMBER and COLLERSON, 2000; RUDNICK et al., 2000) and to complete the mass balance between these reservoirs and the chondritic reservoir. Regarding Nb/Ta however, most of the previous studies are based on a chondritic value of 17.6. Compared to the revised chondritic Nb/Ta of 19.9 (MÜNKER et al., 2003) the eclogites of this study mostly exhibit subchondritic Nb/Ta ratios (with only one exception which displays a slightly superchondritic value of 20.8). This and the fact that most eclogites plot into the field of MORB with a mean Nb/Ta of 14.9 ± 1.2 makes them an unlikely candidate to balances the difference in Nb/Ta between BSE and the chondritic reservoir. Even if the second (older) chondritic Nb/Ta value of 17.6 is used, the eclogites remain widely subchondritic. Both Nb and Zr (Fig. 1·1) show the same abundance in eclogites as in MORBs, which is most likely inherited from the protolith of the orogenic eclogites.

There might be a small difference between Nb/Ta of the crust and that of basalts, representing the mantle (MORB, OIB), which could be balanced by a complementary reservoir, such as eclogites. This reservoir does not necessarily have to be superchondritic. However, the investigated eclogites display an average Nb/Ta ratio (14.9 ± 1.2) which is

indistinguishable within error with the BSE. Thus, they can barely be considered to balance a lower Nb/Ta of the continental crust.

The HFSE results of this study are summarized in Fig. 1·8 (Zr/Hf vs. Nb/Ta) together with other BSE reservoirs. It is evident that eclogites show the same shift to subchondritic Nb/Ta values than the continental crust, MORBs, OIBs, continental basalts, Archean greenstones and also mantle peridotites (data of BARTH et al., 2000; BÜCHL et al., 2002; PFÄNDER et al., 2007; MÜNKER et al., 2003; WEYER et al., 2003). The positive correlation of Nb/Ta ratios with increasing Zr/Hf ratios is likely produced by silicate fractionation (MÜNKER et al., 2003; WEYER et al., 2003; PFÄNDER et al., 2007). Beside the mantle peridotites with the lowest Nb/Ta and Zr/Hf values, all reservoirs, including eclogites, overlap in their range of Nb/Ta ratios (between 10 and 19). Additionally a reference field for Zambian MORB-type gabbros and eclogites of JOHN and SCHENK (2003) is shown. Although these eclogites formed along fluid pathways that reflect very high fluid-rock ratios in places, their Nb/Ta ratios also show no fractionation compared to MORB and are similar to the eclogites of this study. This confirms that eclogitisation, independent of the degree of fluid flow, does not fractionate Nb and Ta in the subducted oceanic crust.

The eclogites investigated in this study are of Phanerozoic ages. In contrast, eclogite xenoliths sampled from the lithospheric mantle under Archean cratons (as e.g. analysed by Rudnick et al.) are of Archean ages. Since subduction mechanisms were different and partial melting of the subducted crust was more frequent in the Archean, it cannot be excluded that some Nb/Ta fractionation in Archean eclogites occurred. Accordingly, Archean eclogite could be responsible for a fractionation between Archean crust and the depleted mantle, which is not evidenced by modern eclogites. If such Archean subducted oceanic crust with a superchondritic Nb/Ta is trapped in the mantle, it might influence the source region of ocean island basalt magmas. However, high Nb/Ta in OIB is not observed (PFÄNDER et al., 2007). Also, Archean crustal rocks do not display systematically lower Nb/Ta compared to modern continental crust (MÜNKER et al., 2007). Finally, such potentially superchondritic Archean eclogites could barely balance the difference of Nb/Ta between BSE and chondrite as proposed by RUDNICK et al. These circumstances, that obviously all silicate reservoirs on Earth have a subchondritic Nb/Ta value, support the idea of WADE and WOOD (2001) that some

30% of Nb may reside in a Ta-free Earth´s core, producing the observed bias of Nb/Ta of BSE compared to the chondritic reservoir.

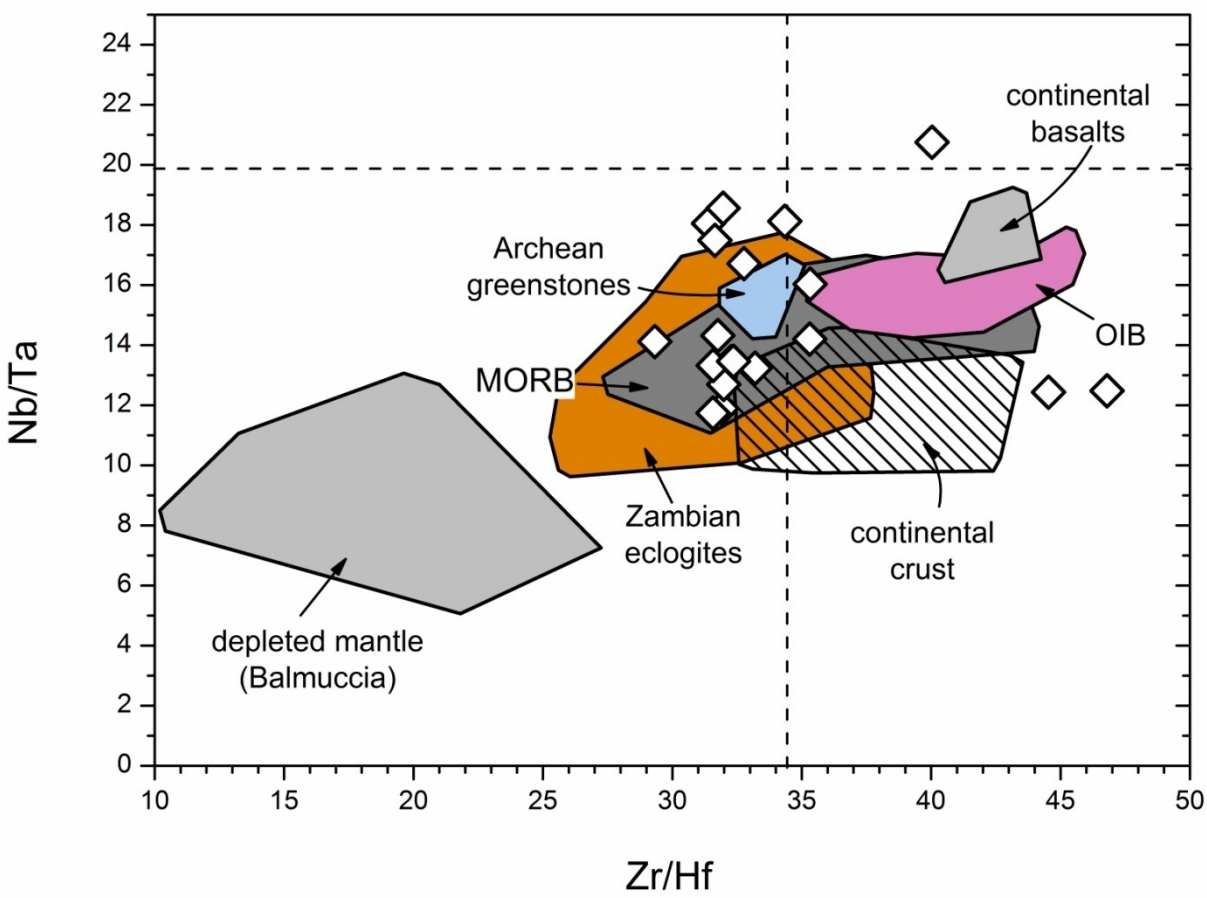

Fig. 1·8: Plot of the major silicate reservoirs on Earth and the eclogites of this study (white diamonds) in a Zr/Hf vs. Nb/Ta plot. Dashed lines denote chondritic values for Nb/Ta and Zr/Hf. All sampled silicate reservoirs as well as the investigated eclogites exhibit subchondritic Nb/Ta ratios.

2 CHAPTER II:

Lu-Hf & Sm-Nd garnet geochronology of ultrahigh-pressure eclogites

Abstract:

The Qinling-Tongbai-Dabie-Sulu collision zone in eastern China is one of the largest ultrahigh-pressure terrains worldwide. Samarium-Nd and zircon-U-Pb dating has been widely used to reveal the metamorphic history of this orogen. However, the exact timing of UHP metamorphic events is debated controversially within a range of 245 Ma and 220 Ma. We present high precision garnet-cpx Lu-Hf ages for six eclogites from the Dabie and Sulu areas. All ages fall in a range between 219.6 and 224.4 Ma. This very tight age range is particularly remarkable, considering the large regional distribution of sample localities (on the order of 100km at the time of metamorphism) and the very different chemical compositions of both garnets and eclogites. Two Sm-Nd isochrons yield ages that are indistinguishable from the Lu-Hf ages of the same samples, albeit with larger uncertainties.

The identical ages of eclogites from both the Dabie and the Sulu area emphasize their close genetic relationship and similar metamorphic history. The Lu-Hf results appear to date a punctuated event of garnet growth. Alternatively, the Lu-Hf garnet ages may represent the onset of contemporaneous fast uplift and subsequent cooling. However, trace element zoning of Lu and Hf is still preserved in garnets, even in those with a homogeneous major element distribution. Thus, complete re-equilibration of the Lu-Hf system during peak temperature conditions is unlikely. Combined with published zircon-U-Pb ages the garnet forming event can be placed toward the final stage of the UHP-metamorphism. A possible trigger for this episodic and widespread mineral growth episiode may have been a fluid that became available at that stage of the metamorphic history. Although, HREE-depleted patterns of older zircons indicate the presence of some garnet before, complete eclogitisation may have been hampered during the major part of the prograde P-T path due to dry conditions during most of the UHP metamorphism. The uniform Lu-Hf (and Sm-Nd) ages of all investigated Dabie and Sulu eclogites indicate mineral growth and thus possibly fluid availability only within a short time interval and contemporaneously over a remarkably large regional scale.

2.1 Introduction:

The collision between the Sino-Korean craton and the Yangtze block during the Triassic formed one of the most extensive ultrahigh-pressure metamorphic belts worldwide. Metamorphic rocks with minerals indicating extremely high pressure conditions are today exposed in the southern and eastern part of the Qinling-Tongbai-Dabie-Sulu collision zone (Fig. 2·1a). The Dabie and Sulu UHP terranes at the eastern margin of the belt contain large outcrops of high-pressure (HP) and ultrahigh-pressure (UHP) rocks. The Sulu UHP terrane is offset 500km to the NE by the Tan-Lu Fault, and there is an ongoing debate if both terranes experienced peak metamorphic conditions at the same time. Coesite and microdiamond were recognized as inclusions in garnet and other HP-minerals in eclogites and country rocks indicating deep subduction of continental material at mantle depth (Okay et al., 1989).

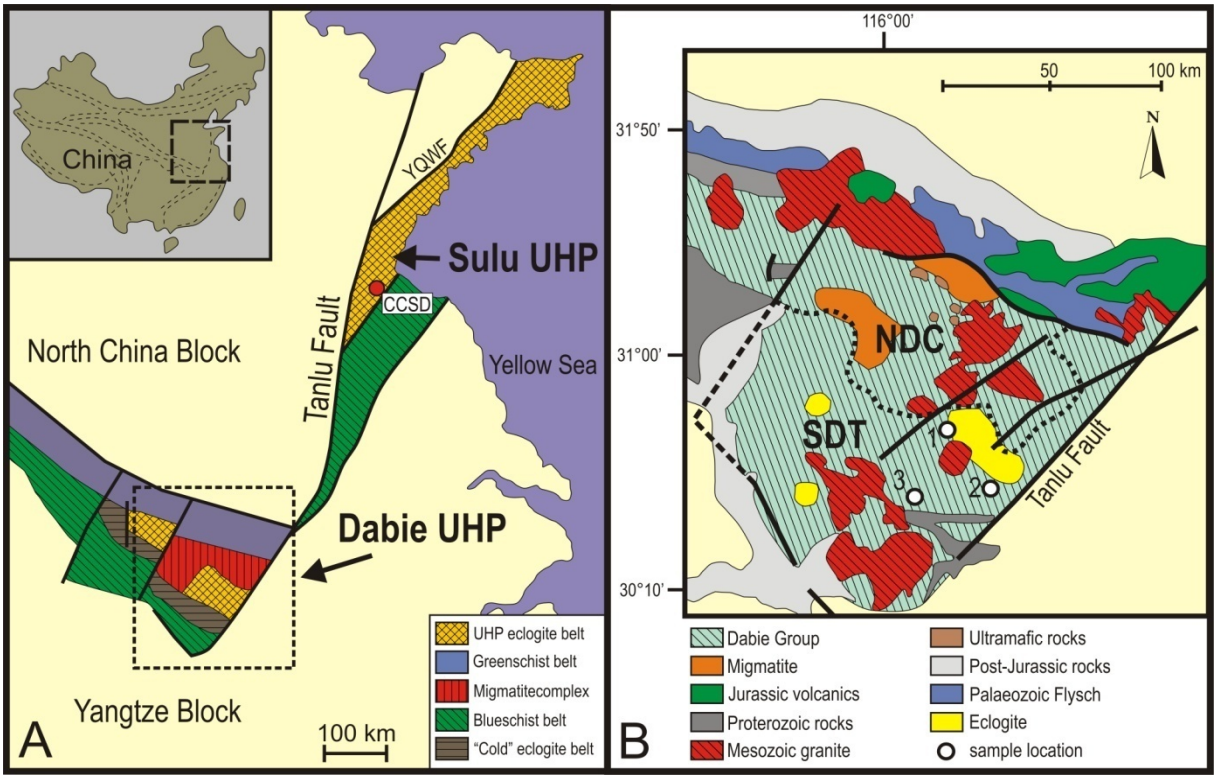

Fig. 2·1: A: Overview of the Dabie-Sulu terrane (with small inset showing outlines of China), and B: detailed map of the Dabie terrane with sample locations (1 = Bixiling, 2 = Shima, 3 = Lidu).

Based on petrologic observations, the metamorphic events that formed the Dabie-Sulu UHP terrane can be divided into three distinct stages (Cong et al., 1994; Ernst and Liou, 1999; Zheng et al., 2005): (1) a peak ultrahigh-pressure eclogite facies imprint at coesite/diamond conditions with temperatures of 800-700 °C at >2.8 GPa; (2) an episode of high-pressure quartz eclogite facies conditions that produced garnet and omphacite coexisting with quartz instead of coesite at temperatures of 750-600 °C and 2.4-1.2 GPa; and (3) a retrograde amphibolite facies overprint with replacement of omphacite by symplectites of amphibole + plagioclase at P-T conditions of 600-450 °C and 1.0-0.6 GPa.

The timing of peak metamorphism and the collision between the Sino-Korean craton and the Yangtze block are of key importance for the understanding of the geodynamic evolution of the Dabie and Sulu terrane. Li et al. (1993) first proposed a timing of (U)HP events between 240-200 Ma based on Sm-Nd analyses of eclogite minerals. A Triassic collision was supported by many subsequent studies using Sm-Nd isotope systematics on garnet bearing, mostly high pressure rocks or U-Pb isotopes on zircons and other accessory minerals. However, all these studies combined provide a wide range of ages for the metamorphism and the timing of highest pressure metamorphism is still controversial. For example Okay et al. (1993) reported Sm-Nd mineral isochron ages of 246 ± 8 Ma for eclogites exposed at Wumiao, while Chavagnac and Jahn (1996) obtained significantly younger Sm-Nd ages of 210 ± 9 Ma to 218 ± 4 Ma for eclogites from the Bixiling Complex, the largest coesite-bearing mafic-ultramafic body in the Dabie Mountains. A Late Triassic metamorphic event is also supported by Sm-Nd ages of e.g. Li et al., 2000; Jahn et al., 2003; Xie et al., 2004; Li et al., 2004. A Triassic collision between 210 Ma and 240 Ma is generally supported by U-Pb zircon ages obtained for various mafic and ultramafic rocks (e.g. Ames et al., 1993; Ames et al., 1996; Rowley et al., 1997; Hacker et al., 1998; Chavagnac et al., 2001; Ayers et al., 2002; Faure et al., 2003; Li et al., 2003; Yang et al., 2003; Li et al., 2004; Zhang et al., 2005). Recently some authors proposed an early Triassic UHP event >240 Ma based on U-Pb zircon ages (Liu et al., 2006a; Hacker et al., 2006), which they interpreted as the onset of UHP metamorphism.

Constraints on the cooling and uplift history of the Dabie complex are e.g. given by CHAVAGNAC and JAHN (1996) who report Rb-Sr phengite ages of 179-223 Ma and a mean phengite age of 212 ± 19 Ma. From their data these authors calculated high initial cooling rates of ~40°C/Ma and fast uplift (~10mm/yr) for the Bixiling eclogites. EIDE et al. (1994) dated the timing of initial exhumation of eclogite facies rocks in the Dabie Mountains at 230-195 Ma based on phengite $^{40}Ar/^{39}Ar$ ages and furthermore asserted cooling at 128-117 Ma based on $^{40}Ar/^{39}Ar$-ages for biotite + hornblende. These results either indicate that cooling was very slow or that Ar isotopes were reset by a later event. Earlier OKAY et al. (1993) acquired higher $^{40}Ar/^{39}Ar$ plateau ages of 244.3 ± 1.8 Ma on micas from eclogites at Wumiao and LI et al. (1993) determined K-Ar-ages for biotites of 231 ± 5 Ma. These Ar-ages are older than most U-Pb and Sm-Nd ages, which are supposed to date more closely peak metamorphism. However, as discussed by these authors, Early to Middle Triassic $^{40}Ar/^{39}Ar$ ages could be affected by excess Ar.

U-Pb zircon ages and Nd model ages give some constraints on the protolith age of the Dabie-Sulu eclogites. While HACKER et al. (1996) and HACKER et al. (1998) obtained Neoproterozoic Protolith ages between 727 Ma and 856 Ma based on concordant or upper intercept zircon ages, AYERS et al. (2002) obtained an early Proterozoic zircon-core upper intercept age of 1921±22 Ma for a jadeite quartzite at Shuanghe. This latter U-Pb age is more in agreement with Nd model ages, which span a large range between 1.6 and 3 Ga (OKAY et al., 1993; JAHN et al., 1996; CHAVAGNAC et al., 2001). All these ages combined attest to the great antiquity of the protoliths of the eclogites.

In this study, the Lu-Hf system was applied to three eclogites from the Dabie Mountains at Bixiling, Lidu and Shima and also to three subsurface eclogite samples from the Sulu terrane obtained during the Chinese Continental Scientific Drilling Program (CCSD). In addition, the Sm-Nd isotope system was used to date two eclogites from the Dabie and Sulu terrane. Lutetium-Hf geochronology has been widely used to date peak metamorphism in eclogites and eclogite facies assemblages (SCHERER et al., 1997; DUCHÊNE et al., 1997; BLICHERT-TOFT and FREI, 2001; LAPEN, 2002; SCHERER et al., 2003; SKORA et al., 2006; ANCZKIEWICZ et al., 2007) and has several advantages compared to Sm-Nd. In contrast to Sm-Nd, the Lu-Hf system preferentially dates initial garnet growth since Lu is commonly enriched in garnet

cores (LAPEN et al., 2003; SKORA et al., 2006). Thus differences in Sm-Nd and Lu-Hf ages may occur if initial garnet formation was followed by late stage garnet growth that formed younger garnet rims (e.g. LAPEN et al., 2003; ANCZKIEWICZ et al., 2007). Also the closure temperature (T_C) for Lu-Hf in garnet may be higher than that of Sm-Nd (SCHERER et al., 2000). An advantage of applying garnet geochronology to date peak metamorphic events is that petrology and mineral chemistry can be used to link the garnet growth history with the metamorphic evolution of the host rocks. In contrast, accessory phases like zircon are often difficult to tie to specific metamorphic conditions or events (e.g. WHITEHOUSE and PLATT, 2003). The major goal of this study was to test the suitability of the Lu-Hf system to date high pressure events by applying it to one of the world's best studied high pressure terranes. This investigation helps to critically compare the new Lu-Hf data with published Sm-Nd and U-Pb zircon data. Furthermore, the aim was to apply Lu-Hf systematics on samples from various eclogite bodies of both the Dabie and Sulu UHP terranes to investigate their temporal relations and contribute to a better geodynamical understanding of the eastern part of this large orogen.

2.2 Geological setting and sample description:

The Dabie and Sulu UHP terranes are located at the eastern margin of the E-W trending Qinling-Tongbai-Dabie-Sulu orogenic belt which forms the collision zone between the Sino-Korean craton (explicitly the North China Block as part of the craton) to the north and the Yangtze block to the south (see Fig. 2·1a). It preserves a record of late mid-Proterozoic to Cenozoic tectonism in Central China (RATSCHBACHER et al., 2003). HP and UHP rock assemblages can be found in the Tongbai, Hong'an and Dabie-Sulu segments of the belt which comprise coesite- and quartz-eclogite. For detailed descriptions of the tectonic evolution and lithologies see e.g. WANG et al. (1990) and RATSCHBACHER et al. (2003.

The Dabie terrane can be divided into four major units (LIOU et al., 1995): the North Huaiyung Flysch Belt, the North Dabie Complex (NDC), the South Dabie Collision Terrane (SDT), and the Susong Metamorphic Belt. The NDC mainly consist of orthogneisses, migmatites, metasediments, amphibolite and ultramafic rocks (OKAY et al., 1993; ZHANG et

al., 1996). The NDC was subjected to intense deformation during a Cretaceous granite intrusion event and is interpreted as a thermally overprinted subduction complex (WANG and LIOU, 1991; OKAY et al., 1993; MARUYAMA et al., 1994). The SDT consists mainly of quartzofeldspathic gneisses and eclogites. Marbles, ultramafic rocks and jadeite quartzites occur as lenses, blocks and layers interbedded with the gneisses. Inclusions of coesite and diamond have been found in eclogite minerals (e.g. OKAY et al., 1989). Pseudomorphs after coesite and relict high P/T metamorphic assemblages have also been found in gneisses indicating that they also underwent UHP metamorphism (WANG and LIOU, 1991; SCHERTL and OKAY, 1994; CONG et al., 1995). OKAY et al. (1993) divided the SDT into a northern "hot" eclogite zone, characterized by coesite-bearing eclogites and a marble-eclogite association, and a southern "cold" eclogite zone, characterized by sodic amphibole-bearing quartz-eclogites, where no coesite or micro-diamond inclusions were found, but peak metamorphism for both parts of the SDT was thought to be contemporaneous between 210-230 Ma (LI et al., 1993; AMES et al., 1993; FRANZ et al., 2001).

The Sulu UHP terrane is the northeastern extension of the Qinling-Tongbai-Dabie orogenic belt and is offset by ≈500km along the Tanlu Fault. It consist mainly of HP and UHP eclogitic rocks in the central part flanked by blueschist to amphibolite facies rocks to the south and a amphibolite-granulite-migmatite zone to the north, separated by the Yantai-Qingdao-Wulian-Fault (YQWF) (HIRAJIMA and NAKAMURA, 2003).

Eclogites from the SDT dated in the present study are (1) from the Bixiling Complex (sample DB05), the largest coesite-bearing eclogitic body in Dabie-Shan (described in detail by LIOU et al., 1995, and CHAVAGNAC and JAHN, 1996), (2) one sample from an eclogite outcrop near the village of Shima (DB63), and (3) one sample (DB44) from an outcrop near the village of Lidu near Huangzhen (Fig. 2·1b). All three samples are coarse grained coesite-bearing eclogites mainly consisting of garnet + omphacite and rutile as accessory phase (1-3%). Zircons are present as very small inclusions in garnet and omphacite. Minor amphibole can be found as symplectite between omphacite grains (e.g. in sample DB44). A detailed description of the Dabie samples can be found in XIAO et al. (2002). Eclogite sample DB05 is a "fresh eclogite" from the central part of the Bixiling complex with no signs of retrograde effects. Sample DB63 of the Shima area is strongly foliated and exhibits compositional bands

of garnet-rich layers interbedded with omphacite-rich layers. While the samples DB05 and DB63 originate from the ”hot eclogites” of the coesite eclogite zone in the SDT, sample DB44 represents a “cold eclogite” from the quartz eclogite zone (Okay et al., 1993). The samples from the SDT represent three different eclogite localities that are ≈40km apart from each other.

Samples PH04, PH10 and PH20 are eclogites from the main drill hole of the CCSD near Donghai in the Sulu orogen (location of the drill hole is marked “CCSD” in Fig. 2·1a). They originate from depths of 312m, 1066m and 1993m, respectively (Xiao et al., 2006).

2.3 Analytical methods:

Rock samples were processed in a jawcrusher and sieved. From the 250-355µm sieve fraction 100mg to 1g separates of garnet and clinopyroxene were carefully separated by hand, excluding grains with visible inclusions like rutile and zircon. The mineral separates were washed with Milli-Q H_2O to get clean dust-free mineral grains. A refined dissolution technique after Erik E. Scherer (personal communication, partially described in Lagos et al., 2007) was applied to dissolve garnet and clinopyroxene grains and leave inherited zircon and rutile inclusions behind, minerals, which could bias the ages obtained by the mineral isochrons (Scherer et al., 2000). The effect of zircon inclusions is demonstrated in Fig. 2·2. If zircon is present in both the analysed bulk rock and garnet, apparent isochron ages are too young; and, if zircon is dissolved with the whole rock only apparent isochron ages appear too old. Therefore, bulk rock powders were not used in this process because they inevitably influence the isochron ages if old zircon is present, which is the case for both the Dabie and Sulu rocks.

The dissolution of the garnets was achieved in closed Savillex™ vials in $HF:HNO_3:HClO_4$ on a hotplate at 120°C for 24h. The $HClO_4$ was added to break down fluoride complexes which develop from the breakdown of silicates in HF. After this first step the initial acids were dried down and afterwards 6M HCl was added to dissolve the sample. If this HCl solution was clear without visible precipitates, the 6M HCl was diluted to 3M HCl

and the sample was ready for Lu-Hf separation. The inclusions were clearly visible in this step at the bottom of the vials and have been removed by centrifuging prior to loading the sample onto the columns.

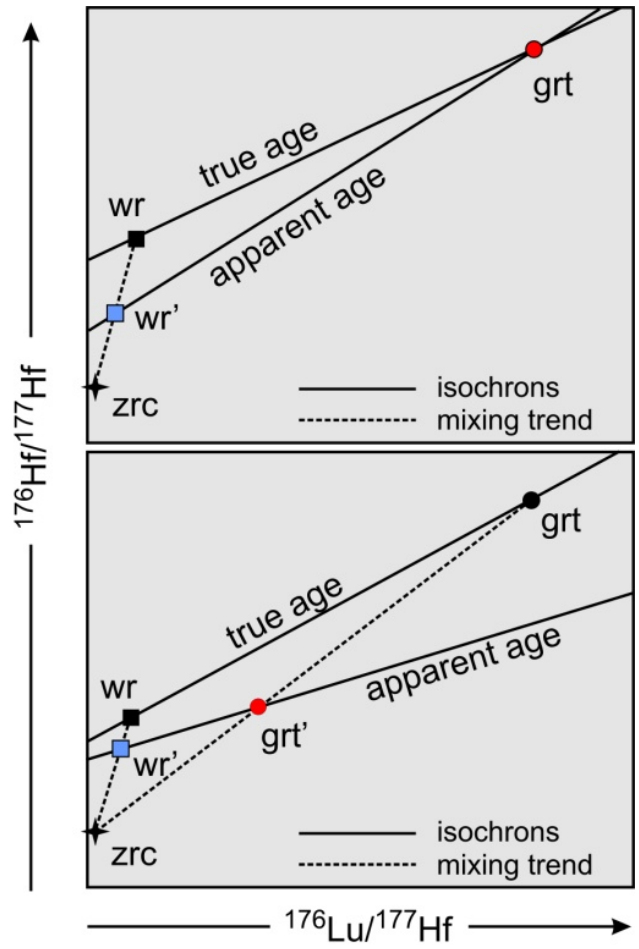

Fig. 2·2:
Effect of zircon inclusions on Lu-Hf geochronology. Top: zircon in matrix only. Bottom: zircon in both matrix and garnet. (grt = garnet, wr = whole rock, zrc = zircon). After SCHERER et al., 2000.

A ^{176}Lu - ^{180}Hf mixed tracer was added prior to final dissolution for the determination of Lu and Hf concentrations by isotope dilution (ID). Separation of Lu and Hf was achieved with a single column ion exchange purification procedure using Eichrom Ln-Spec resin (MÜNKER et al., 2001). The procedure described in there was slightly altered. The original recipe involved a separation step for zirconium, which has been removed because the MC-ICPMS used by MÜNKER et al. (2001) included a Hexapole collision cell that is prone to building up blank levels higher than acceptable if Zr isotopes had to be measured on the same machine. This time-consuming step has been skipped in the procedure as it was not necessary for the measurement on the Finnigan Neptune MC-ICPMS in Frankfurt. An additional purification step on cation exchange columns (PATCHETT and TATSUMOTO, 1980) was

applied to the Hf fraction (of column 1) for all garnet mineral separates to remove all remaining Lu. This yielded pure Hf fractions with no remaining Lu. Hafnium isotope compositions (IC) together with ID and Lu ID measurements were performed on a Finnigan Neptune MC-ICPMS combined with a Cetac ARIDUS™ sample introduction system at the University of Frankfurt. This instrumental set up ensured high sensitivity enabling us to measure precise Hf isotope compositions on amounts as low as 10 ng of Hf with a signal of ≈ 100mV on ^{176}Hf for a 10ppb Hf solution. High sensitivity is essential to minimize the effect of counting statistics and the amplifier noise on the precision of the measurement.

Since only 50-80% of the Yb were separated from Lu with this purification technique, a large correction was necessary for the mass interference of ^{176}Yb on ^{176}Lu (BLICHERT-TOFT et al., 1997). However, this was possible with high precision, by using an interference free Yb isotope ratio for instrumental mass bias correction, which was applied for precise interference correction of ^{176}Yb on ^{176}Lu. For this, the natural ^{173}Yb/^{171}Yb ratio of 1.129197 (VERVOORT et al., 2004) was used for online mass bias correction. Mass bias on the Hf-ratios was corrected using the natural ^{179}Hf/^{177}Hf = 0.7325 for online mass bias correction. However, the online mass bias correction with a natural ^{179}Hf/^{177}Hf produces an overcorrection that increases with the amount of spike that is added. Therefore, Hf mass bias was re-corrected offline to account for the spike influences on ^{179}Hf and ^{177}Hf. The Hafnium fraction was virtually clean of any Yb and Lu, but contained different amounts of Ta and W. All elemental interferences on Hf isotopes have been monitored and corrected using the mass bias corrected ^{173}Yb/^{176}Yb, ^{175}Lu/^{176}Yb, ^{180}Ta/^{181}Ta and ^{183}W/^{180}W ratios, respectively.

Long-term standard reproducibility for Lu is given with a ^{176}Lu/^{175}Lu of 0.026553±46 (2σ ~0.18%, n=23), and the Hf-Standard JMC475 is reproduced with a ^{176}Hf/^{177}Hf of 0.282151 ± 31 (2σ = 1.1ε, n=97, including 100ppb, 50ppb, 20ppb and 10ppb solutions). In-run statistic for ^{176}Hf/^{177}Hf is typically ≈ 0.3ε. For the calculation of the mineral isochrons the ISOPLOT program v3.41b from K.Ludwig was used with a λ^{176}Lu decay constant of 1.865 x 10^{-11} year^{-1} (SCHERER et al., 2001). Instead of using the in-run precision for each sample, uncertainties on ^{176}Hf/^{177}Hf were assumed to be ≤ 1.1ε (2σ), according to the long term reproducibility of the Hf-standard. Uncertainties on ^{176}Lu/^{177}Hf were calculated using the reproducibility of the Lu-

standard and the uncertainty in the spike calibration (0.15%), multiplied with an error magnification factor (calculated from the measured $^{176}Lu/^{175}Lu$) for each sample. Resulting uncertainties for the $^{176}Lu/^{177}Hf$ ratios are 0.25-0.35%. Repeated blank measurements yielded blank levels <15pg for both Lu and Hf.

The Sm-Nd analyses were performed on the same instrumental set up. For each eclogite sample approximately 100mg of garnet, clinopyroxene and bulk rock were used and a mixed $^{150}Nd/^{149}Sm$ spike was added. Sm and Nd were separated in a 2-column ion exchange purification procedure. A cation exchange resin (AG1-50Wx8) was used on column 1 to separate the bulk REE from the matrix. On a second column, filled with Eichrom Ln-Spec resin, Sm and Nd were separated from the other REEs (PIN and ZALDUEGUI, 1997). The mass bias on Nd isotope ratios was calculated online using the natural $^{146}Nd/^{144}Nd = 0.7219$, which was later re-corrected to account for spike influences on the Nd isotopes. For Sm, $^{147}Sm/^{152}Sm$ was used for mass bias correction. A $^{143}Nd/^{144}Nd = 0.511912 \pm 33$ ($2\sigma \sim 0.7\varepsilon$, n=8) was achieved for the Nd-isotope standard from AMES. Interferences of remaining Sm on Nd-isotopes were corrected using the mass bias corrected $^{147}Sm/^{144}Sm$, $^{147}Sm/^{150}Sm$ and $^{147}Sm/^{148}Sm$ ratios. In the Sm fraction, varying amounts of Gd were present whose influence on Sm-isotopes was also corrected using the mass bias corrected $^{155}Gd/^{152}Gd$ and $^{155}Gd/^{154}Gd$ ratios. The 2σ error for $^{143}Nd/^{144}Nd$ of replicate Ames standard measurements was used for the calculations of the Sm-Nd isochrons (ISOPLOT v3.41b). Errors on the $^{147}Sm/^{144}Nd$ ratios were estimated to 0.1% according to the maximum error in the reproducibility of the Sm-ratios of the samples.

All errors on the ages of the Lu-Hf and Sm-Nd isochrons in this study are reported as the 2σ error from a model 1 fit of the ISOPLOT program, which only takes into account the analytical error of the single measurement.

The major element composition of the bulk rocks was measured on a JEOL Superprobe JXA-8900 on fused glasses (with run parameters of 15keV, 20nA and 3µm spot size). The same setup was used for the major element analyses of garnets in thin sections. The fused glasses were produced by rapid heating (<30seconds) of ≈ 100mg of sample (without using a flux) on an Ir-strip, which was subsequently quenched. These glass pellets

were also used for the trace element analysis which were performed by Laser Ablation coupled with a Finnigan Element-2 single-collector ICPMS. Laser spot sizes ranged from 90-120µm and laser energies between 1.5-4.0 J/cm^2 were used (see also chapter 1.2.2)

2.4 Results

2.4.1 Bulk rock major and trace element chemistry

The major and trace element compositions of the bulk rocks are given in table 2·1. SiO_2 contents range from 45.6 to 51.3 wt-%. The results agree with analyses of the same samples by XIAO (2000). In the TAS-diagram (Fig. 2·3) 5 samples plot in the basalt field while sample DB63 plots in the picro-basalt field. Although the TAS diagram relies on alkali elements which can become mobile under metamorphic conditions, this traditional classification is still applicable since most eclogites in the Dabie-Sulu area appear to have remained closed systems during eclogite facies metamorphism as evident from stable isotope systematics (e.g. RUMBLE and YUI, 1998; ZHENG et al., 1998; XIAO et al., 2000; XIAO et al., 2001). Samples from the Dabie terrane (DB) have lower K_2O contents (0.03 - 0.11 wt%) than samples from the Sulu terrane (PH, 0.32 - 1.13 wt%). From the latter samples 2 out of 3 have K_2O >1 wt-%. In the AFM diagram (Fig. 2-4) most samples follow a tholeiitic differentiation trend. This finding is supported by the cation plot after JENSEN (1976) (Fig. 2·4).

All samples display a more or less evolved positive Eu anomaly and relatively flat REE patterns with only slightly elevated LREE (Fig. 2·5, samples normalized to C1 of MCDONOUGH and SUN (1995)). Samples PH04 and PH20 have a positive, while all other samples have a negative Sr anomaly or a rather flat pattern. All samples show pronounced negative Nb-Ta anomalies and positive and negative Ti, Hf and Zr anomalies. The compositional variety observed in all 6 eclogite samples can be attributed to both igneous (heterogeneous protoliths) and metamorphic processes. Recently, TANG et al. (2007) suggested that the eclogite protoliths originated from a basaltic magma that formed in a continental setting.

	DB05	DB44	DB63	PH04	PH10	PH20
(wt-%)						
SiO_2	45.6	51.3	43.5	48.6	48.2	47.4
K_2O	0.06	0.11	0.03	1.27	1.16	0.32
Na_2O	2.36	4.82	2.12	2.58	2.80	2.40
CaO	10.7	10.4	16.7	9.18	9.90	10.8
MnO	0.22	0.22	0.26	0.25	0.21	0.22
MgO	7.47	7.09	5.58	6.33	9.17	7.74
TiO_2	1.46	1.29	2.07	1.93	0.77	1.98
P_2O_5	0.07	0.18	0.15	0.54	0.21	0.12
FeO	16.4	9.43	13.4	11.1	10.1	13.8
Al_2O_3	15.6	14.9	16.2	18.2	17.4	15.1
Cr_2O_3	0.03	0.04	0.02	0.02	0.06	0.04
NiO	0.03	0.25	0.01	0.01	0.04	0.02
(ppm)						
Sr	107	97.8	125	143	60.4	244
Y	10.1	14.7	29.3	11.3	19.4	14.4
Zr	23.5	125	41.4	33.9	71.5	52.3
Nb	0.75	3.74	7.23	0.75	1.67	1.31
La	10.0	5.48	11.9	4.51	21.0	1.88
Ce	24.6	11.3	23.2	9.41	40.5	2.71
Pr	3.60	1.458	2.88	1.40	5.01	0.555
Nd	16.3	6.26	11.6	7.23	20.1	3.64
Sm	3.10	1.43	3.31	2.13	3.84	1.92
Eu	1.11	0.636	1.37	1.33	1.39	1.16
Gd	1.77	1.50	3.82	2.04	2.76	2.16
Tb	0.325	0.431	0.881	0.371	0.530	0.441
Dy	2.02	2.94	5.37	2.31	3.53	2.74
Ho	0.457	0.645	1.12	0.519	0.856	0.632
Er	1.150	1.56	2.52	1.30	2.28	1.61
Tm	0.161	0.208	0.301	0.180	0.341	0.228
Yb	1.021	1.37	1.75	1.18	2.35	1.49
Lu	0.156	0.216	0.249	0.187	0.380	0.231
Hf	0.748	3.13	1.20	4.20	1.32	1.14
Ta	0.04	0.18	0.36	0.06	0.07	0.06
Pb	2.93	3.20	5.16	3.25	5.18	4.21
Th	0.535	0.458	1.13	0.336	2.17	0.039
U	0.100	0.144	0.727	0.231	0.304	0.044

Table 2·1: Bulk rock major and trace element chemistry.

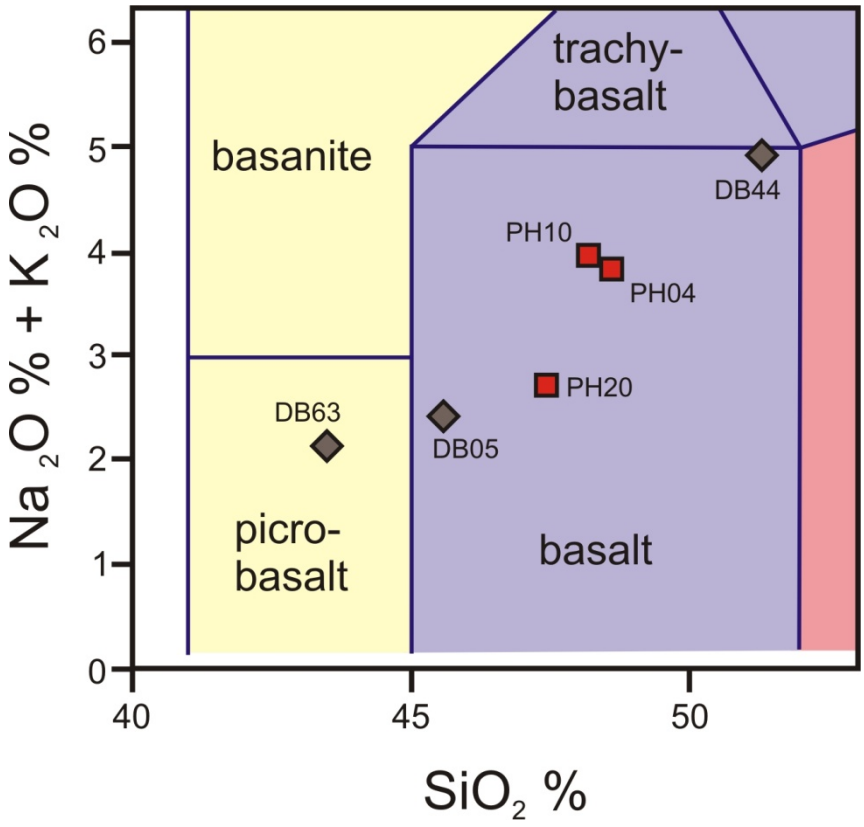

Fig. 2·3: Total-alkali-vs-silica (TAS) diagram showing the investigated eclogite samples.

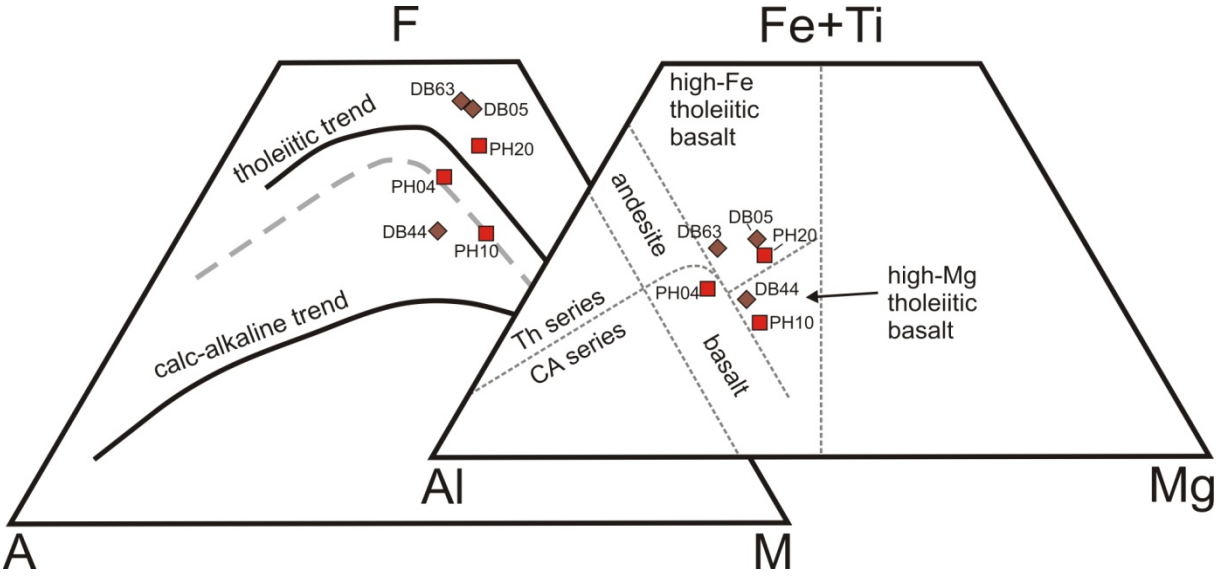

Fig. 2·4: Left: AFM plot showing the tholeiitic trend of the investigated samples. Right: Cation plot after JENSEN (1976).

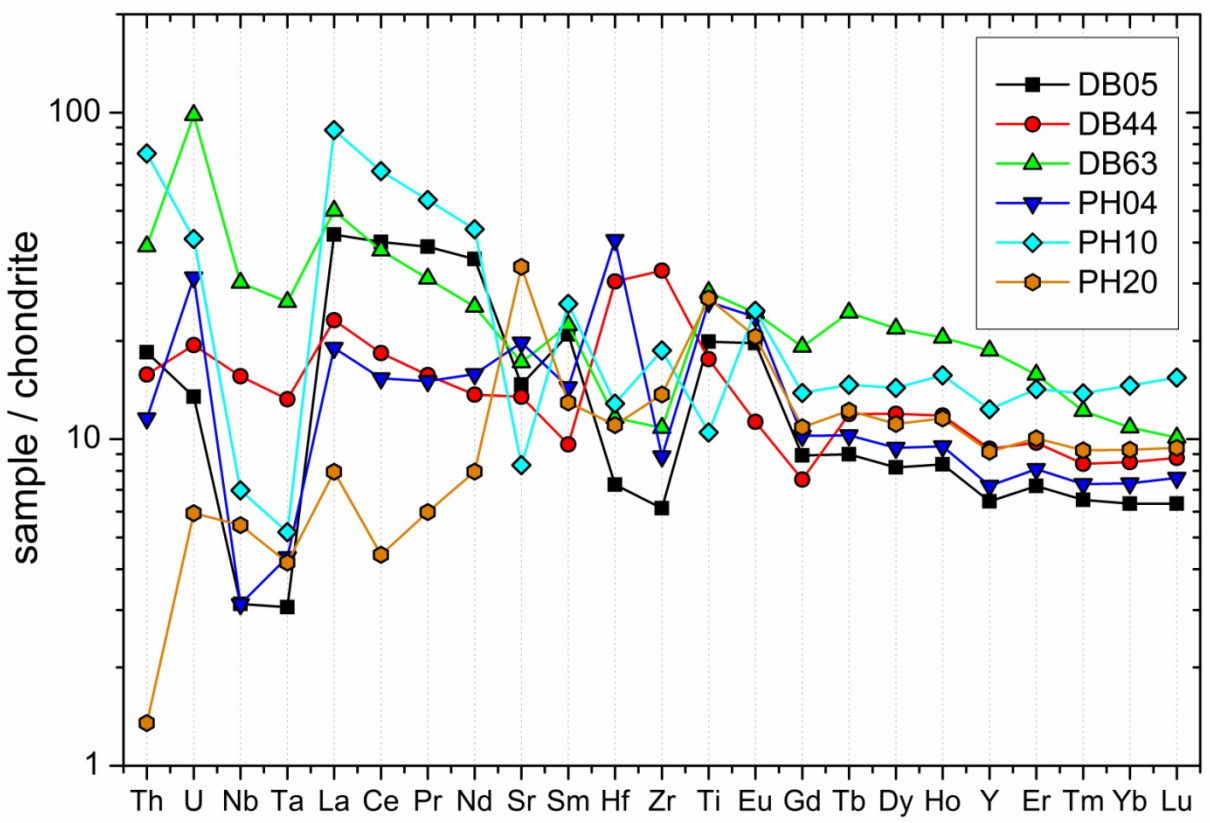

Fig. 2·5: Chondrite-normalized trace element spidergram for the investigated eclogites (normalized to C1 of McDonough and Sun (1995)).

2.4.2 Garnet major and trace element chemistry

The major element chemistry of the garnets in the investigated eclogites is shown in table 2·2 and Fig. 2·6. There are large variations between garnets from different samples. However, within each sample, most garnet grains are homogenous. They are almandine- + spessartine-rich with variable contents of pyrope and grossular. Figure 2·7 shows compositional maps of two garnet grains (samples PH20 and DB44) for the elements Mg, Fe, Ca and Mn. The grain in sample PH20 (Fig. 2·7a) is a typical garnet, representing all analysed samples, except for DB44, with respect to major element distribution and size. All mapped elements in this garnet are homogenously distributed and there is no compositional zoning in core- and rim-regions. In contrast, the garnet grains in sample DB44 are clearly zoned and show distinct core and rim regions (Fig. 2·7b, black areas in the grain is quartz, "drop-shaped" inner area of grain is clinopyroxene). Magnesium and Mn are enriched in the rim

and Ca is slightly enriched in the garnet core. Only Fe is homogeneously distributed in the whole grain. A small reaction rim is visible for all elements around the grain boundary. Also garnet grains in sample DB44 are euhedral and differ greatly in size compared to the other 5 samples (0.2 – 10 mm in DB44 and 50 - 500 µm in all other samples).

In order to investigate the trace element distribution of the garnets, several line scans were performed across individual garnet grains with LA-ICPMS. The line scans were placed to cut from rim to rim through the center of single garnet grains (performed on thick sections; as we do not know, if we sampled the real center of the garnet, any observed zoning represents a minimum zoning of respective garnets). Figure 2·8 shows a representative rim to rim scan for the elements Lu, Y, Zr, Hf, Sm and Nd in sample DB05. Since the Hf concentrations in the garnets are mostly near the detection limit of the LA-ICPMS, its geochemical twin Zr was used as a proxy for the distribution of Hf. Zirconium was also used as a tracer for zircon inclusions. However, in this case the Hf concentration was sufficient to record a meaningful profile. The scan shows the expected Lu enrichment in the garnet core region and also distinct peaks in the Y, Hf and Zr concentrations. An uncommon observation is the fact that the Lu + Y peaks are offset from each other, and also both peaks are offset from the Hf and Zr peaks. Sm shows irregular enrichment to the right, Nd shows no marked zoning.

Clinopyroxenes in all rocks are without exception omphacites with jadeite components ranging from 35 to 60% and a minor acmite component.

sample	SiO_2	K_2O	Na_2O	CaO	MnO	MgO	TiO_2	P_2O_5	FeO	Al_2O_3	Cr_2O_3	NiO
DB05 grt	39.31	0	0.05	7.55	0.39	6.46	0.04	0.02	25.4	21.4	0.02	0
DB44 grt	39.31	0	0.04	8.16	0.91	5.98	0.06	0.01	24.9	21.6	0.03	0
DB63 grt	39.31	0.01	0.07	16.4	0.41	3.39	0.15	0.02	19.3	20.9	0.02	0
PH04 grt	39.41	0	0.03	10.9	0.51	7.47	0.04	0.03	20.4	22.0	0	0.01
PH10 grt	40.25	0	0.03	9.32	0.44	11.7	0.01	0.02	16.5	22.3	0.001	0
PH20 grt	39.13	0	0.03	9.20	0.42	7.29	0.04	0.01	22.8	21.8	0	0.01

Table 2·2: Average garnet compositions (major elements, values in wt-%)

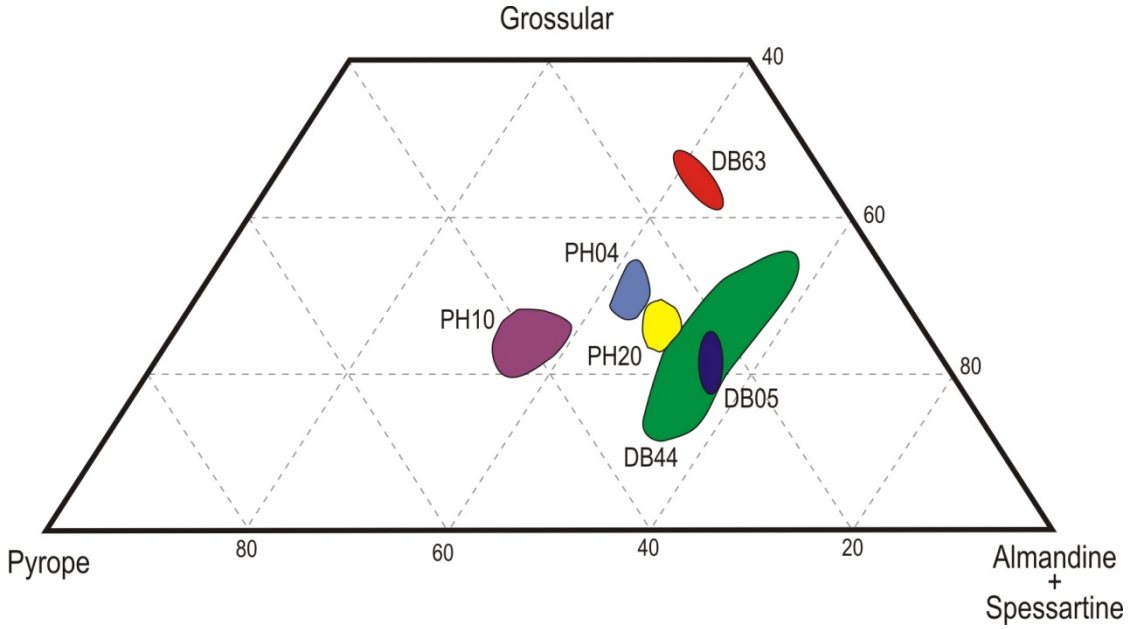

Fig. 2·6: Ternary plot of the cation percent of Mg, Ca and Fe+Mn in eclogite garnets.

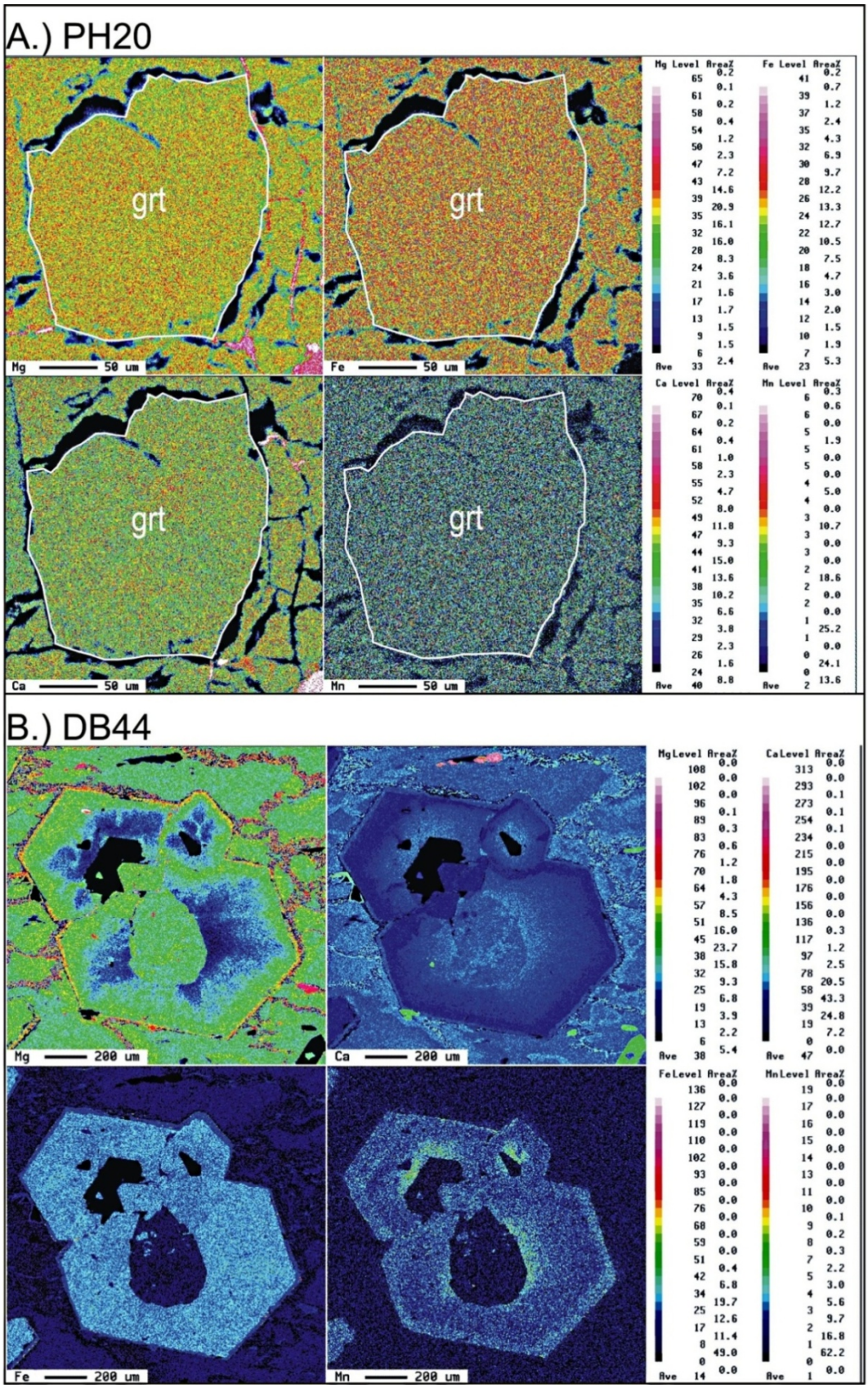

Fig. 2·7: Element composition maps of garnets for representative eclogite samples. Note: black areas within garnet in sample DB44 are quartz, “drop-shaped” center is clinopyroxene.

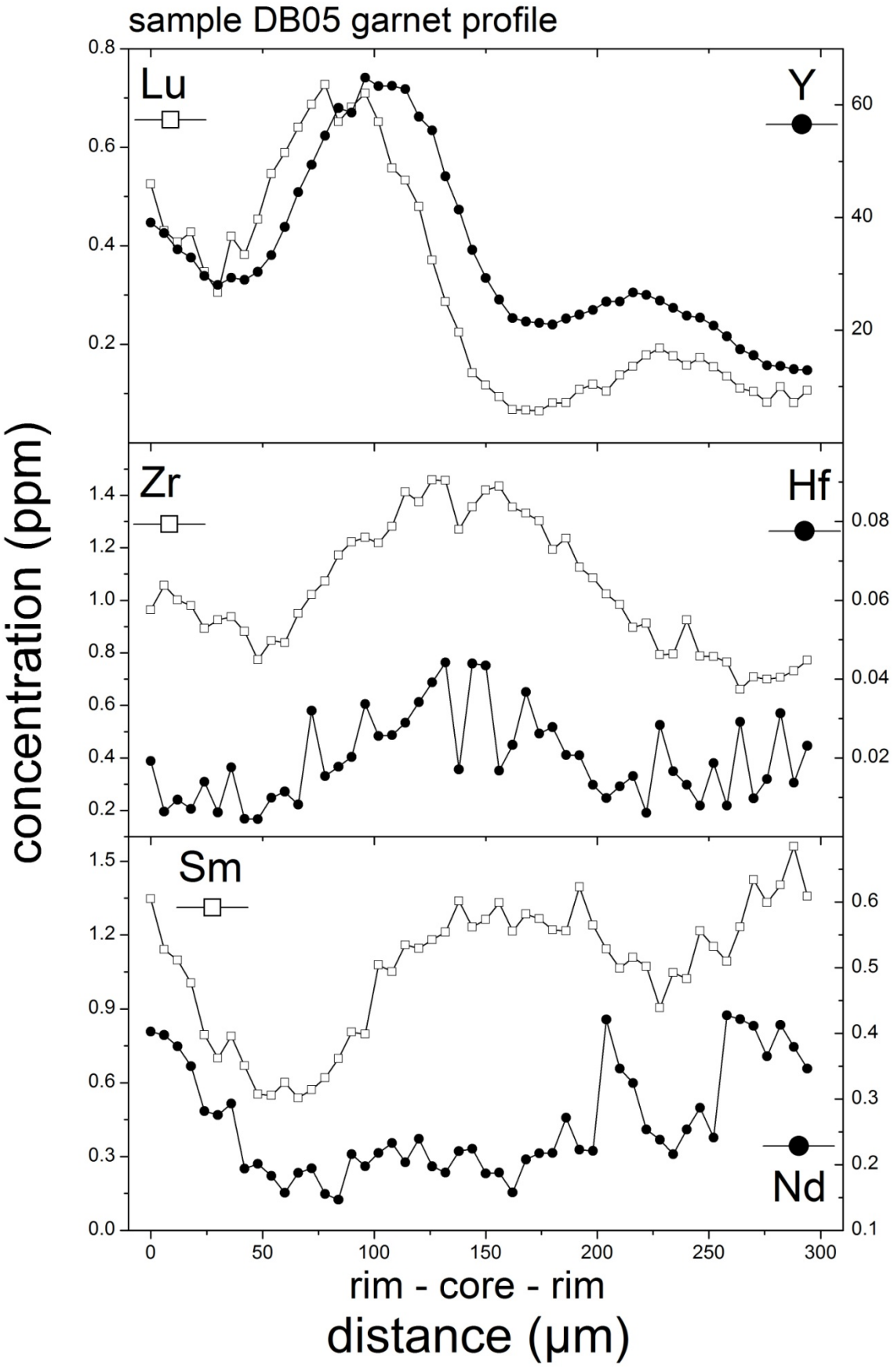

Fig.2·8: Lu, Y, Hf, Zr, Sm & Nd profiles of garnets in sample DB05 performed by LA-ICP-MS. Zr was used as a proxy for its chemical twin Hf, however, in this case the Hf concentration was sufficient to record a meaningful profile.

2.4.3 Lu-Hf and Sm-Nd ages:

The results of the Lu-Hf analyses are shown in table 2·3 and Fig. 2·9. The garnet + cpx isochrons yield a tight cluster of late Triassic ages between 219.6 Ma and 224.4 Ma. The average age of all 6 samples is 222.4 Ma. Isochron initial $^{176}Hf/^{177}Hf$ values range from 0.282394 to 0.282843, and their respective εHf values at the isochron ages are between +7.45 and -8.45.

No bulk rock data were used for the calculations of the Lu-Hf isochrons, because inherited accessory minerals, particularly zircon, can affect these ages. SCHERER et al. (2000) describe in detail the effect of inherited zircon in both bulk rock and garnet and bulk rock only, which leads to lower or higher apparent ages (see also section 2.2). Although zircon is not a common accessory mineral in basalts, it was observed in thin sections of the investigated eclogites and also in the residues of garnet dissolution.

All calculated ages rely on the garnet and omphacite data only since they can be expected to be contemporaneous. The variation of analytical points for garnets in the same sample is most likely due to contamination with traces of omphacite. Thus, all analyzed garnet fractions can be considered to lie on mixing lines between "pure" garnet and cpx (which are identical with the respective isochrons). Consequently, the isochrons with a range of garnet compositions are essentially 2-point isochrons. Nevertheless, the strict co-linearity of all mineral analyses confirms the precision of our method and supports the cogenetic formation of omphacite and garnet.

Results of the Sm-Nd analyses of two eclogites (DB05 + PH20) are shown in table 2·4 and Fig. 2·9. The garnet + clinopyroxene + whole rock isochrons provide ages of 221.1 ± 7.2 Ma and 220.6 ± 7.1 Ma which are indistinguishable from the Lu-Hf ages. However, the Sm-Nd garnet-cpx isochron ages exhibit distinctly larger uncertainties than corresponding Lu-Hf isochrons despite similar analytical uncertainties in the isotope and parent/daughter ratios. This is due to the significantly larger spread of $^{176}Lu/^{177}Hf$ compared to that of $^{147}Sm/^{144}Nd$ between garnet and clinopyroxene and the higher decay constant of ^{176}Lu compared to that of ^{147}Sm.

sample	fraction	$^{176}Lu/^{177}Hf$	$^{176}Hf/^{177}Hf$	Lu ppm	Hf ppm	isochron initial $^{176}Hf/^{177}Hf$	εHf	isochron age [Ma]
DB05	cpx1	0.01402	0.282900 ± 28	0.020	0.118	0.282843 ± 22	+7.45	223.43 ± 0.92
	cpx2	0.02430	0.282948 ± 35	0.020	0.118			
	grt1	2.162	0.291865 ± 38	0.337	0.022			
	grt2	2.694	0.294101 ± 35	0.348	0.018			
DB44	cpx	0.01483	0.282456 ± 14	0.012	0.119	0.282394 ± 31	-8.45	224.4 ± 1.2
	grt	2.893	0.294528 ± 28	1.165	0.057			
DB63	cpx	0.01318	0.282490 ± 28	0.007	0.079	0.282436 ± 30	-6.99	222.94 ± 0.95
	grt1	2.371	0.292284 ± 23	0.421	0.025			
	grt2	1.988	0.290734 ± 21	0.419	0.030			
	grt3	2.374	0.292360 ± 20	0.419	0.025			
PH04	cpx	0.01575	0.282846 ± 11	0.014	0.128	0.282779 ± 30	+5.14	222.7 ± 1.6
	grt1	0.9988	0.286928 ± 40	0.367	0.052			
	grt2	1.513	0.289081 ± 18	0.364	0.034			
PH10	cpx	0.03696	0.282673 ± 16	0.036	0.137	0.282522 ± 31	-4.02	219.6 ± 1.4
	grt	1.964	0.290584 ± 11	0.933	0.067			
PH20	cpx	0.02651	0.282712 ± 08	0.031	0.168	0.282603 ± 31	-1.12	221.4 ± 1.2
	grt1	1.733	0.289781 ± 20	0.479	0.039			
	grt2	2.051	0.291087 ± 22	0.477	0.033			

Table 2·3: Lu-Hf isotope results of the investigated eclogites. Errors on the isochron-ages are reported as the 2σ error from a model 1 fit of the ISOPLOT program. Shown εHf of isochron initial is at the respective isochron age.

sample	fraction	$^{147}Sm/^{144}Nd$	$^{143}Nd/^{144}Nd$	Sm ppm	Nd ppm	isochron initial $^{143}Nd/^{144}Nd$	isochron age [Ma]
DB05	grt	1.1227	0.513853 ± 41	0.7269	0.393	0.512220 ± 45	222.1 ± 7.2
	cpx	0.2759	0.512613 ± 21	0.5775	1.277		
	wr	0.1535	0.512451 ± 08	1.974	8.163		
PH20	grt	1.1571	0.513393 ± 27	1.751	0.926	0.511723 ± 46	220.6 ± 7.1
	cpx	0.2233	0.512025 ± 24	1.082	2.953		
	wr	0.2455	0.512098 ± 07	2.068	5.156		

Table 2·4: Sm-Nd isotope results of the investigated eclogites. Errors on the isochron-ages are reported as the 2σ error from a model 1 fit of the ISOPLOT program.

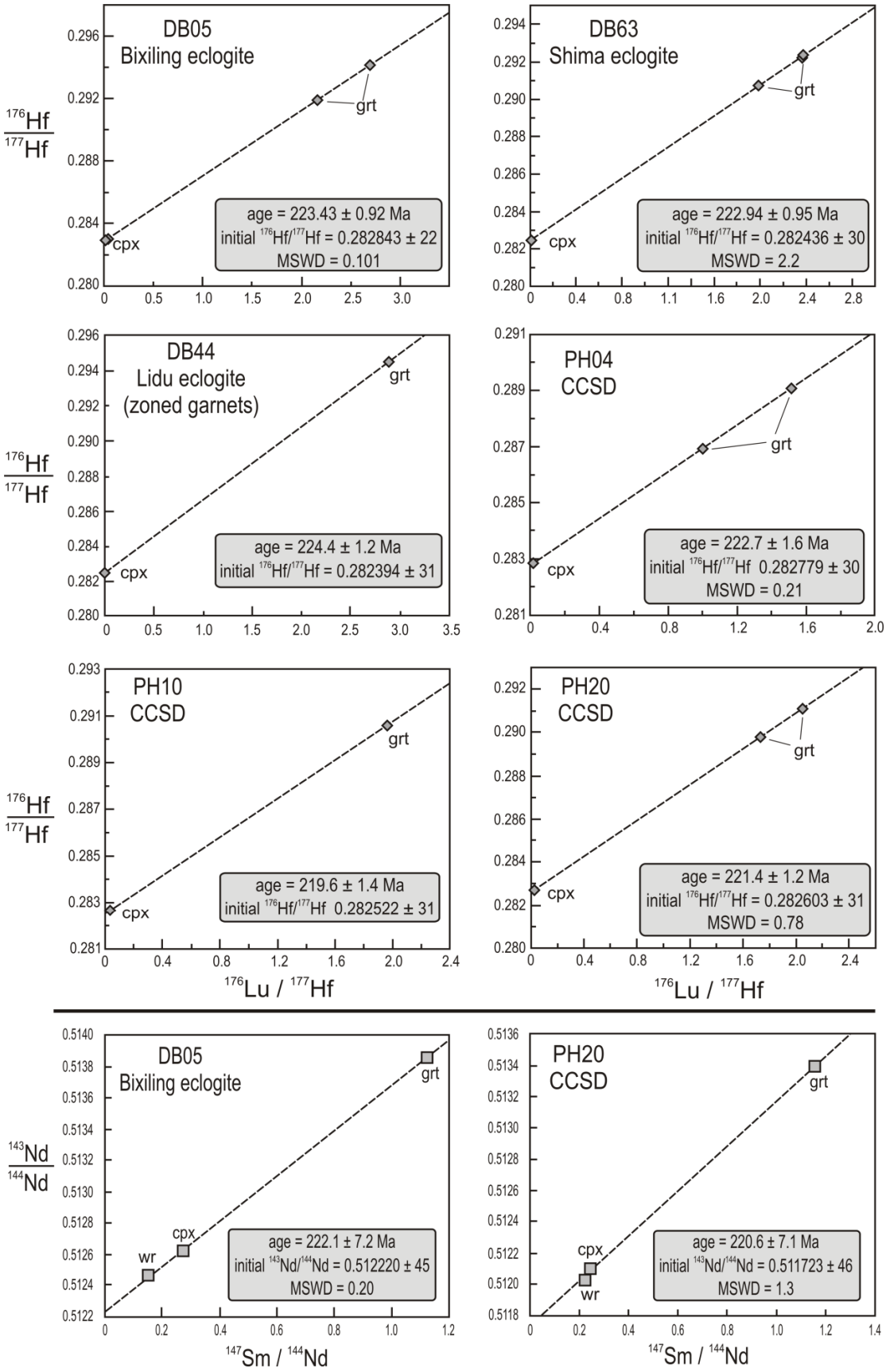

Fig. 2·9: Lu-Hf & Sm-Nd garnet + clinopyroxene isochrons of the eclogites. Age errors are reported as 2σ of a model 1 fit in the ISOPLOT program, individual errors are smaller than the icon size.

2.5 Discussion

All ages determined during this study for eclogites from both the Dabie and Sulu terrane range between 220 and 224 Ma. This tight age range, mainly defined by the Lu-Hf system, contrast dramatically with the numerous results of previous Sm-Nd and U-Pb studies on eclogites, gneisses and other metamorphic rocks from both the Dabie and Sulu terrane that are published in the literature (Fig. 2·10). Both isotope systems (U-Pb on zircon, monazite, titanite, rutile, and Sm-Nd on garnet, cpx and whole rock) display a large age range between 200 Ma and 255 Ma. The U-Pb data comprises both conventional (TIMS) and in-situ (SHRIMP, LA-ICPMS) measurements. Grouping of data and classification into metamorphic episodes provided by the authors is not shown, since applied classification systematics widely differ between individual studies and also depend on data interpretation. Only zircon rims that are attributed to amphibolite facies metamorphism are highlighted. The major aim of Fig. 2·10 is to show an overview of age ranges obtained by the individual studies for Dabie and Sulu UHP rocks. Compared to all applied methods of previous geochronological studies, the Lu-Hf garnet-cpx ages of this study are unique with respect to their precision and the tight age range they define. All Lu-Hf ages of this study overlap within their analytical uncertainties, show a narrow absolute range of only 4.8 Ma and yield a precise average age of 222.4 Ma. This finding is intriguing, as the investigated rocks differ widely in their bulk (and garnet) composition, and were regionally separated from each other by 50 to 100 km (although the actual position of the Sulu terrane next to the Dabie terrane at the timing of the collision is not fully constrained).

The comparison of the Lu-Hf data with previous results (Fig. 2·10) implies that either the Lu-Hf system is particularly suitable to date eclogite facies metamorphism (and the large spread of previous studies is due to analytical uncertainties) or that other isotope systems date (or are affected by) multiple events while Lu-Hf represents only one particular event within (U)HP metamorphism.

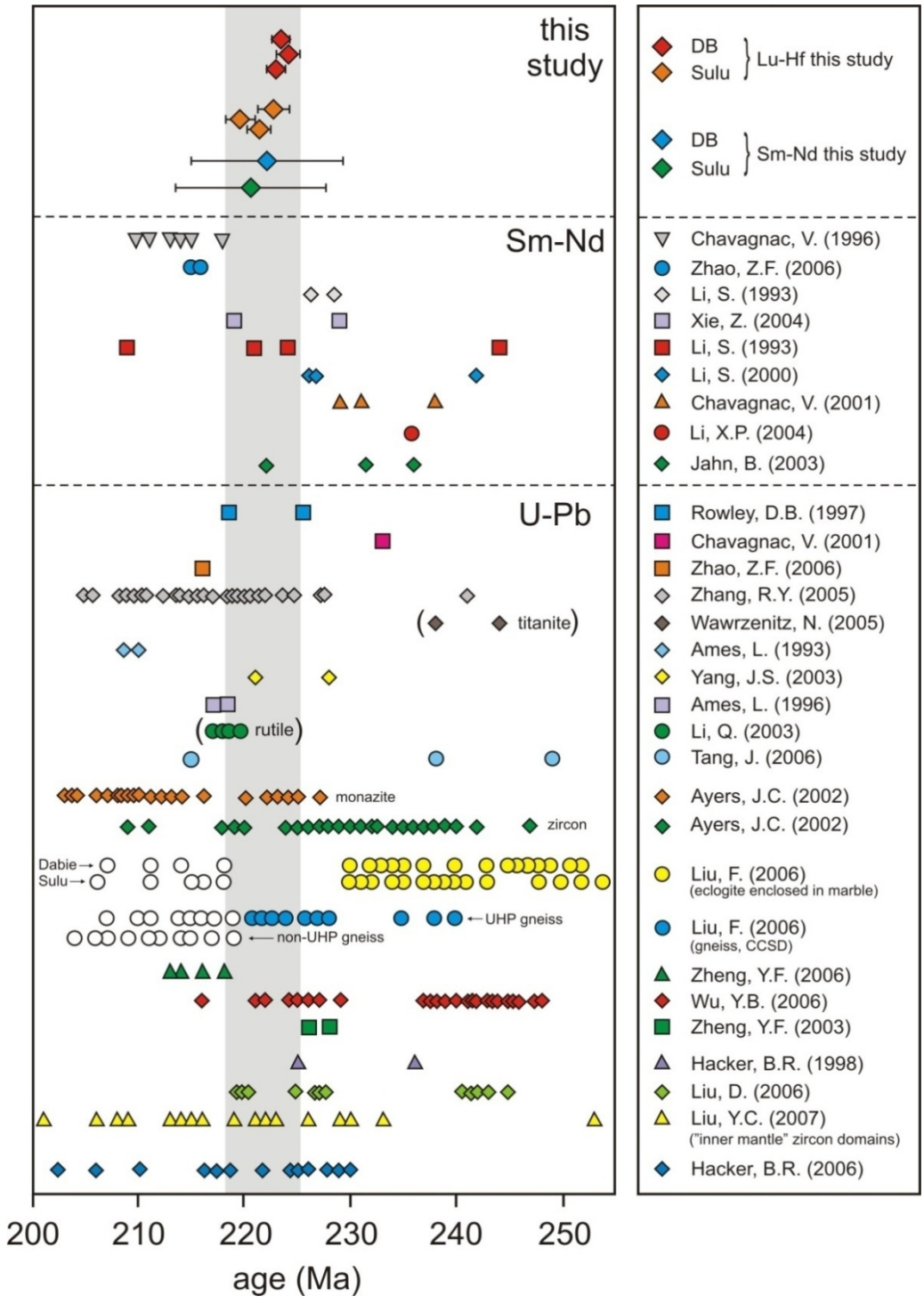

Fig. 2·10: Comparison of geochronological literature data with the results of this study. U-Pb zircon data comprises TIMS, SHRIMP and LA-ICPMS data. Individual errors are left out for convenience. Open symbols are zircon rims (data from AMES et al., 1993; LI et al., 1993; AMES et al., 1996; CHAVAGNAC and JAHN, 1996; ROWLEY et al., 1997; HACKER et al., 1998; LI et al., 2000; CHAVAGNAC et al., 2001; AYERS et al., 2002; JAHN et al., 2003; LI et al., 2003; YANG et al., 2003; ZHENG et al., 2003; LI et al., 2004; XIE et al., 2004; ZHANG et al., 2005; HACKER et al., 2006; WAWRZENITZ et al., 2006; TANG et al., 2006; ZHAO et al., 2006; LIU et al., 2006a; LIU et al., 2006b; LIU et al., 2006c; WU et al., 2006; LIU et al., 2007).

Indeed, compared to the Lu-Hf data, Sm-Nd mineral isochrons of previous and this study suffer from larger analytical uncertainties, which can be attributed to the smaller fractionation of Sm and Nd in garnet. Corresponding uncertainties for Sm-Nd ages are typically on the order of 5-10 Ma. Thus, most of the Sm-Nd ages for the Dabie-Sulu terrane (between 210 and 240 Ma) can barely be distinguished. Slightly younger Sm-Nd ages, like those from CHAVAGNAC and JAHN (1996), could be explained by a lower closure temperature of Sm-Nd, compared to Lu-Hf in garnet (SCHERER et al., 2000). Additionally, Lu is highly enriched in garnet cores (Fig. 2·8), even if the major elements are virtually unzoned. Thus, contrarily to Sm-Nd, Lu-Hf preferentially dates garnet cores. However, a systematic shift towards younger ages cannot be confirmed neither by this study nor by the average Sm-Nd ages for Dabie–Sulu rocks (Fig. 2·10). Instead, the identical Sm-Nd and Lu-Hf ages of our samples indicate that both isotope systems most likely date the same event.

The published U-Pb results on zircons and other accessory minerals define even a larger age range for UHPM in the Dabie-Sulu region (200 Ma to 255 Ma). Based on their U-Pb zircon ages LIU et al. (2006a) (green diamonds in Fig. 2·10) defined at least three distinct episodes of eclogite facies metamorphism for the Dabie terrane at 242.1 ± 0.4 Ma (UHPM onset >2.7 GPa), 227.2 ± 0.8 Ma (peak UHPM >4 GPa) and 219.8 ± 0.8 Ma (quartz stability ≈1.8 GPa before exhumation). These authors used multiphase mineral textures and index minerals enclosed in zircon to link their ages with distinct metamorphic events. However, such a correlation of mineral inclusions with U-Pb zircon ages can be ambiguous. The continuous range of zircon ages (Fig. 2·10) may point to continuous zircon growth over ≈ 40-50 Ma under variable metamorphic conditions possibly combined with partial Pb-loss. Based on their own U-Pb zircon and Th-Pb monazite ages in combination with U-Pb and Sm-Nd data from the literature HACKER et al. (2006) divided the history of the Dabie-Sulu terrane in two UHP and one retrograde stage: (1) a “precursor” UHP event at 244-236 Ma, (2) a second UHP “main” event between 230-220 Ma, and (3) a terminating amphibolite-facies overprint at 220-205 Ma. In the context of these interpretations the Lu-Hf and Sm-Nd ages presented here would date the second episode of eclogite (or UHP) facies metamorphism. However, most of the garnets used for Lu-Hf dating show a homogeneous major element distribution which is not expected for garnets affected by multiple metamorphic overprints. The only exceptions are garnets from sample DB44 which, however, still have a similar age as the

homogeneous garnets of the other samples. The Lu-Hf (and Sm-Nd) isotope systems provide no evidence for events before 225 Ma.

The Lu-Hf ages for the six samples analyzed range from 219.6 to 224.4 with an average age of 222.41 ± 1.26 Ma. Combining the five analytically indistinguishable samples and excluding the youngest sample PH10 yields a pooled age of 222.97 + 0.88 Ma. This tight clustering of the Lu-Hf ages is unexpected because the samples were collected over a distance of 50-100 km and were taken from eclogites with quite different bulk compositions. In addition the major element composition of the garnets, which reflects the bulk composition of the parent rock and the specific P-T conditions of garnet growth, are quite variable. If the garnets formed on the prograde metamorphic path during the subduction of the Dabie-Sulu terrane, it is expected that garnet growth depended on the bulk composition of the whole rock and the specific P-T regime of the given area. As a result it is to be expected that the garnets grew at different times in different samples, and should yield different ages. The narrow Lu-Hf age range appears to represent a distinct event, either the concomitant growth of garnets in all samples or the concomitant closure of Lu-Hf in all garnets. The εHf values of the measured isochron initials point to quite different protoliths and/or a substantially different genesis. Positive εHf values indicate MORB and OIB like protolith rocks, while negative εHf values indicate a more crustal origin or at least crustal contamination.

Sm-Nd ages obtained from two of the six samples agree with the Lu-Hf ages, although the Sm-Nd ages have significantly larger uncertainties due to the more limited fractionation of the parent and daughter elements during garnet formation. The coincidence of the Lu-Hf and Sm-Nd ages and the tight cluster of the Lu-Hf ages can be the result of a regional punctuated garnet growth event or be due to re-equilibration of Lu, Hf, Sm and Nd and all the major elements during peak-temperature conditions followed by rapid and regional identical uplift and cooling below the blocking temperature of these elements. In the latter case, the cooling rate had to be fast enough to ensure that the time interval between the blocking temperatures of the Lu-Hf (>800°C at 222.91 ± 0.80 Ma) and the Sm-Nd (ca. 650°C at 221.4 ± 1.5 Ma) systems cannot be resolved analytically.

The high temperatures, at least those of the hot eclogites (> 750 °C) may also imply that both the Lu-Hf and Sm-Nd isotope systems have been open continuously during peak temperature metamorphism. Published data indicate that closure temperatures for the Lu-Hf system in garnet are between 550°C and 800°C, depending on the size and chemical composition of the garnet, the cooling rate and fluid availability (SCHERER et al., 2000; ANCZKIEWICZ et al., 2007). Considering the observed chemical and morphologic differences of the investigated garnets (including the small homogeneous and large zoned garnets), differences in the blocking temperature of e.g. 100 °C can well be expected for the Lu-Hf system. The nearly identical age for these garnets would then indicate an exhumation rate of at least 3 mm/a (assuming a retrograde thermal gradient of ~10°C/km for subduction zones) in this short timeframe. This is reasonable compared to uplift rates of similar orogens (e.g. Dora Maira Massif in the Western Alps (SCHERTL et al., 1991) or Kokchetav Massif in Kasachstan (JAGOUTZ et al., 1990)). This estimate represents a minimum rate on a large regional scale and uplift rates probably were locally higher.

Although the homogenous major element distribution in the garnets favors the interpretation that they were homogenized during peak metamorphic conditions, the preserved zoning of trace element compositions in garnets (Fig. 2·8) strongly indicates that the Lu-Hf isotope system has not been homogenized completely during peak metamorphism. Most garnets including those with homogeneous major element compositions have preserved zoning of trace elements, including Lu and Hf. Lutetium is commonly enriched in the garnet cores, which strongly indicates the preservation of growth zoning. Also Zr (and most likely Hf as well) displays zoning in most garnets. Thus, complete homogenization of Hf isotope compositions during peak metamorphism is unlikely. Consequently, corresponding Lu-Hf ages are unlikely to represent cooling ages, but probably represent the age of garnet growth.

Since metamorphic zircons in the eclogites (including those with U-Pb ages older than the Lu-Hf ages) display HREE depletion (as e.g. described by LIU et al., 2006b, and LIU et al., 2006a) it is unlikely that no garnet was present before the time interval given by the Lu-Hf ages. However, new garnet growth could have been triggered on a regional scale. The phenomena, that anhydrous mafic rocks do not react during prograde metamorphism due to

kinetic inhibition is known from HP rocks if they had an anhydrous protolith, as in the case of the Bergen Arcs in Norway (AUSTRHEIM and GRIFFIN, 1985; FOUNTAIN et al., 1994). A similar situation may apply to the eclogites in the Dabie-Sulu area. As indicated by the major and trace element compositions of these eclogites their protolith was of basaltic composition and possibly an anhydrous gabbro in some cases. In the Bergen Arcs in Norway (AUSTRHEIM and GRIFFIN, 1985; FOUNTAIN et al., 1994) eclogitisation is restricted to shear zones, and thus arrested. The reaction was triggered by a fluid infiltration into the shear zone or by fluids enclosed within un-affected metamorphic rocks (AUSTRHEIM, 1986/1987; JOHN and SCHENK, 2003). It is likely that this same phenomenon applies to the Dabie-Sulu area, as indicated by the tight cluster of garnet growth ages, but here the reaction went to completion and did not leave any unreacted protoliths behind. The reaction may have been triggered by a fluid or by shearing or both. The fluid, which was most likely hydrous, must have become available instantaneously on a geologic timescale, possibly due to dehydration reactions in the hydrated subducting oceanic crust and/or a change in the overall geologic setting that changed the fluid paths during subduction. The small grain size of most samples and the layered structure of some of the eclogites may also indicate that the mineral reaction may have been initiated due to shearing well after the stability field of eclogite was reached. The shearing process then may have triggered rapid mineral growth, further enhanced by the release of thermal energy due to the reaction. The end result were eclogites that did not form by continuous prograde metamorphism (increasing P and T) but rather by a punctuated event that initiated reaction in a supercritical mineral assemblage after the reaction boundaries had been overstepped significantly.

Metasomatic overprint by a fluid may be indicated by the variable oxygen isotope composition of both Dabie and Sulu samples. The Dabie samples (DB05, DB44 and DB63) have $\delta^{18}O$ values of 3.7, -2.8 and 6.6 (XIAO, 2000), and the Sulu samples (PH04, PH10 and PH20) have $\delta^{18}O$ values of 2.6, -4.0 and 5.9 (XIAO et al., 2006). These authors interpreted the difference between ^{18}O-depleted rocks of the CCSD and adjoining rocks with positive $\delta^{18}O$ values as a result of different fluid histories. According to several authors (XIAO, 2000; XIAO et al., 2000; XIAO et al., 2001; XIAO et al., 2002; FU et al., 2001; FU et al., 2003) stable isotope analyses of fluid inclusions in the Dabie eclogites indicate the presence of at least five compositionally different fluids during different metamorphic stages.

The homogeneous major element composition of most garnets indicates that P-T-conditions have been rather constant during their growth, supporting garnet growth within a short time interval. Only the larger euhedral, zoned garnets in sample DB44 apparently have grown under variable P-T conditions. This sample belongs to the so-called "cold eclogites", a different eclogite type compared to the "hot eclogites" represented by the other samples. Temperatures for the hot eclogite zone are proposed at 800 ± 50 °C while the cold eclogite zone equilibrated at 635 ± 40 °C (OKAY et al., 1993). Potentially, these zoned garnets may have preserved remnants of an older garnet generation that may have produced the HREE depleted pattern of some older zircons. The age of these garnets is slightly older than the average of the other homogeneous garnets, but this difference is insignificant on the 2σ level.

2.6 Conclusions

Applying the Lu-Hf isotope system on garnet-cpx mineral pairs of the Dabie-Sulu orogen yields a very tight age range of 219.6 to 224.4 Ma with a mean age 222.4 Ma. The Lu-Hf ages agree with two Sm-Nd ages from the same samples, which however have larger analytical uncertainties. This close agreement of all isochron ages can be interpreted as (1) a garnet growth event within UHP metamorphism, or (2) re-equilibration during peak metamorphic conditions and closure of Lu-Hf and Sm-Nd during the onset of cooling and uplift. In either case, the event must have been relatively fast and contemporaneous over a large region. However, the preserved zoning of trace element compositions in garnets strongly indicates that the Lu-Hf isotope system has remained undisturbed during peak metamorphism. This implies that most garnets have been formed within a very limited timeframe of only a few Ma. Despite the fact that today the Dabie and Sulu terranes are offset by the Tan-Lu fault, our Lu-Hf results support their relationship and a contemporaneous metamorphic history of both terranes.

Intriguingly, most of the previously observed U-Pb zircon ages (LIU et al. 2006a) imply a substantially longer period of UHP metamorphism or even several HP and UHP events (HACKER et al., 2006). HP conditions during the growth of these zircons are indicated by e.g.

coesite inclusions. Although HREE-depleted patterns of some zircons also indicate the presence of garnet before 225 Ma, the uniform garnet growth ages imply that the major eclogitisation event occurred relatively late at the final stage of the proposed UHP metamorphic period. Maybe it was hampered before through the absence of fluids. The importance of such fluids is well known from eclogitisation, which is limited to shear zones, while surrounding metabasalts were not transformed to eclogites (JOHN and SCHENK, 2003). The young and uniform Lu-Hf ages of the Dabie and Sulu eclogites however indicate that eclogitisation generally occured during a relatively short period of fluid availability, while the entire (U)HP event may have lasted much longer.

3 References:

Ames L., Tilton G. R., and Zhou G. (1993) Timing of collision of the Sino-Korean and Yangtze cratons: U-Pb zircon dating of coesite-bearing eclogites. *Geology* **21**, 339-342.

Ames L., Zhou G., and Xiong B. (1996) Geochronology and isotopic character of ultrahigh-pressure metamorphism with implications for collision of the Sino-Korean and Yangtze cratons, central China. *Tectonics* **15**(2), 472-489.

Anczkiewicz R., Szczepanski J., Mazur S., Storey C., Crowley Q., Villa I. M., Thirlwall M. F., and Jeffries T. E. (2007) Lu-Hf geochronology and trace element distribution in garnet: Implications for uplift and exhumation of ultra-high pressure granulites in the Sudetes, SW Poland. *Lithos* **95**, 363-380.

Antignano J. and Manning C. E. (2005) Rutile solubility in H2O-NaAlSiO3 fluids at high T and P: implications from HFSE mobility in subduction zones. *EoS (Trans. Am. Geophy. Union)* **85 (52) Fall Meet. Suppl. (abstract)**, V31C-0620.

Austrheim H. (1986/1987) Eclogitization of lower crustal granulites by fluid migration through shear zones. *Earth and Planetary Science Letters* **81**, 221-232.

Austrheim H. and Griffin W. L. (1985) Shear deformation and eclogite formation within granulite-facies anorthosites of the Bergen Arcs, Western Norway. *Chemical Geology* **50**, 267-281.

Ayers J. C., Dunkle S., Gao S., and Miller C. F. (2002) Constraints on timing of peak retrograde metamorphism in the Dabie Shan Ultrahigh-Pressure Metamorphic Belt, east-central China, using U-Th-Pb dating of zircon and monazite. *Chemical Geology* **186**, 315-331.

Barth M. G., McDonough W. F., and Rudnick R. L. (2000) Tracking the budget of Nb and Ta in the continental crust. *Chemical Geology* **165**, 197-213.

Bebout G. E. (2007) Metamorphic chemical geodynamics of subduction zones. *Earth and Planetary Science Letters* **260**, 373-393.

Becker H., Jochum K. P., and Carlson R. W. (2000) Trace element fractionation during dehydration of eclogites from high-pressure terranes and the implications for element fluxes in subduction zones. *Chemical Geology* **163**, 65-99.

Bernard-Griffiths J., Peucat J. J., and Menot R. P. (1991) Isotopic (Rb-Sr, U-Pb and Sm-Nd) and trace element geochemistry of eclogites from the Pan-African Belt; a case study of REE fractionation during high-grade metamorphism. *Lithos* **27**, 43-57.

Blichert-Toft J., Chauvel C., and Albarède F. (1997) Separation of Hf and Lu for high-precision isotope analysis of rock samples by magnetic sector-multiple collector ICP-MS. *Contributions to Mineralogy and Petrology* **127**, 248-260.

Blichert-Toft J. and Frei R. (2001) Complex Sm-Nd and Lu-Hf isotope systematics in metamorphic garnets from the Isua supracrustal belt, West Greenland. *Geochimica et Cosmochimica Acta* **65**(18), 3177-3187.

Brenan J. M., Shaw H. F., Phinney D. L., and Ryerson F. J. (1993) Partitioning of trace elements between clinopyroxene, rutile and aquaeous fluids at high P and T: implications for the chemistry of subduction zone fluids. *EoS (Trans. Am. Geophy. Union)* **74: 340**.

Brenan J. M., Shaw H. F., Phinney D. L., and Ryerson F. J. (1994) Rutile-aquaeous fluid partitioning of Nb, Ta, Hf, Zr, U and Th: implications for high field strength elements depletions in island-arc basalts. *Earth and Planetary Science Letters* **128**, 327-339.

Brophy J. G. and Marsh B. D. (1986) On the origin of Hi-Alumina arc basalt and the mechanics of melt extraction. *Journal of Petrology* **27**, 763-790.

Bucher K., Fazis Y., De Capitani C., and Grapes R. (2005) Blueschists, eclogites and decompression assemblages of the Zermatt-Saas ophiolite: High-pressure metamorphism of subducted Tethys lithosphere. *American Mineralogist* **90**, 821-835.

Büchl A., Münker C., Mezger K., and Hofmann A. W. (2002) High precision Nb/Ta and Zr/Hf ratios in global MORB. *Geochimica et Cosmochimica Acta* **66 A108 (Spec. Suppl.)**.

Chavagnac V. and Jahn B. (1996) Coesite-bearing eclogites from the Bixiling Complex, Dabie Mountains, China: Sm-Nd ages, geochemical characteristics and tectonic implications. *Chemical Geology* **133**, 29-51.

Chavagnac V., Jahn B. M., Villa I. M., Whitehouse M. J., and Liu D. (2001) Multichronometric Evidence for an In Situ Origin of the Ultrahigh-Pressure Metamorphic Terrane of Dabieshan, China. *Journal of Geology* **109**, 633-646.

Cong B.-L., Wang Q. C., Zhai M., Zhang R. Y., Zhao Z. Y., and Ye K. (1994) Ultrahigh-Pressure Metamorphic Rocks in the Dabishan-Sulu Region of China. *The Island Arc* **3**, 135-150.

Cong B.-L., Zhai M. G., Carswell D. A., Wilson R. N., Wang Q. C., Zhao Z. Y., and Windley B. F. (1995) Petrogenesis of ultrahigh-pressure rocks and their country rocks at Shuanghe in Dabieshan, Central China. *Eur. J. Mineral.* **7**, 119-138.

Dixon T. H. and Batiza R. (1979) Petrology and chemistry of recent lavas in the Northern Marianas: Implications for the origin of island arc basalts. *Contributions to Mineralogy and Petrology* **70**, 167-181.

Duchêne S., Blichert-Toft J., Luais B., Télouk P., J.-M. L., and Albarède F. (1997) The Lu-Hf dating of garnets and the ages of the Alpine high-pressure metamorphism. *Nature* **387**, 586-589.

Eggins S. M., Woodhead J. D., Kinsley L. P. J., Mortimer G. E., Sylvester P., McCulloch M. T., Hergt J. M., and Handler M. R. (1997) A simple method for precise determination of > 40 trace elements in geological samples by ICPMS using enriched isotope internal standardisation. *Chemical Geology* **134**, 311-326.

Eide E. A., McWilliams M. O., and Liou J. G. (1994) $^{40}Ar/^{39}Ar$ geochronology and exhumation of high-pressure to ultrahigh-pressure metamorphic rocks in east-central China. *Geology* **22**, 601-604.

Ernst W. G. and Liou J. G. (1999) Overview of UHP metamorphism and tectonics in well-studied collisional orogens. *International Geology Review* **41**, 477-493.

Faure M., Lin W., Schärer U., Shu L., Sun Y., and Arnaud N. (2003) Continental subduction and exhumation of UHP rocks. Structural and geochronological insights from the Dabieshan (East China). *Lithos* **70**, 213-241.

Feineman M. D., Ryerson F. J., DePaolo D. J., and Plank T. (2007) Zoisite-aquaeous fluid trace element partitioning with implications for subduction zone fluid composition. *Chemical Geology* **239**, 250-265.

Foley S. F., Barth M. G., and Jenner G. A. (2000) Rutile/melt partition coefficients for trace elements and an assessment of the influence of rutile on the trace element characteristics of subduction zone magmas. *Geochimica et Cosmochimica Acta* **64**(5), 933-938.

Fountain D. M., Boundy T. M., Austrheim H., and Rey P. (1994) Eclogite-facies shear zones - deep crustal reflectors? *Tectonophysics* **232**, 411-424.

Franz L., Romer R., Klemd R., Schmid R., Oberhänsli R., Wagner T., and Shuwen D. (2001) Eclogite-facies quartz veins within metabasites of the Dabie Shan (eastern China): pressure-temperature-time-deformation path, composition of the fluid phase and fluid flow during exhumation of high-pressure rocks. *Contributions to Mineralogy and Petrology* **141**, 322-346.

Fu B., Touret J. L. R., and Zheng Y. (2001) Fluid inclusions in coesite-bearing eclogites and jadeite quartzites at Shuanghe, Dabie Shan. *China. J. Metamorphic Geol.* **19**, 531-548.

Fu B., Touret J. L. R., and Zheng Y. (2003) Remnants of premetamorphic fluid and oxygen isotopic signatures in eclogites and garnet clinopyroxenite from the Dabie-Sulu terranes, eastern China. *Journal of metamorphic Geology* **21**, 561-578.

Gao J., John T., Klemd R., and Xiong X. (2007) Mobilization of Ti-Nb-Ta during subduction: Evidence from rutile-bearing dehydration segregations and veins hosted in eclogite, Tianshan, NW China. *Geochimica et Cosmochimica Acta* **2007**, 4974-4996.

Green T. H. (1981) Experimental evidence for the role of accessory phases in magma genesis. *J. Volcanol. Geotherm. Res.* **10**, 405-422.

Green T. H. (1995) Significance of Nb/Ta as an indicator of geochemical processes in the crust-mantle system. *Chemical Geology* **120**, 347-359.

Green T. H. and Adam J. (2003) Experimentally-determined trace element characteristics of aquaous fluid from partially dehydrated oceanic crust at 3.0 GPa, 650-700°C. *Eur. J. Mineral.* **15**, 815-830.

Hacker B. R., Ratschbacher L., Webb L., Ireland T., Walker D., and Shuwen D. (1998) U/Pb zircon ages constrain the architecture of the ultrahigh-pressure Qinling-Dabie Orogen, China. *Earth and Planetary Science Letters* **161**, 215-230.

Hacker B. R., Wallis S. R., Ratschbacher L., Grove M., and Gehrels g. (2006) High-temperature geochronology constraints on the tectonic history and architecture of the ultrahigh-pressure Dabie-Sulu Orogen. *Tectonics* **25**, TC5006, doi:10.1029/2005TC001937.

Hacker B. R., Wang X., Eide E. A., and Ratschbacher L. (1996) The Qinling-Dabie ultra-high-pressure collisional orogen. In *The Tectonics of Asia* (ed. A. Yin and T. M. Harrison), pp. 345-370. Cambridge Univ. Press.

Hermann J., Spandler C., Hack A., and Korsakov A. V. (2006) Aqueous fluids and hydrous melts in high-pressure and ultra-high pressure rocks: implications for element transfer in subduction zones. *Lithos* **92**(3-4), 399-417.

Hickey R. L. and Frey F. A. (1982) Geochemical characteristics of boninite series volcanics: implications for their source. *Geochimica et Cosmochimica Acta* **46**, 2099-2115.

Hirajima T. and Nakamura D. (2003) Reviews of representative UHPM terranes: the Dabie Shan and Sulu region of China. In *Ultra-High Pressure Metamorphism*, Vol. 5 (ed. D. A.

Carswell and R. Compagnoni), pp. 105-144. European Mineralogical Union Notes in Mineralogy.

Hofmann A. W. (1988) Chemical differentiation of the Earth: the relationship between mantle, continental crust and oceanic crust. *Earth and Planetary Science Letters* **90**, 297-314.

Hofmann A. W. (1997) Mantle geochemistry: the message from oceanic volcanism. *Nature* **385**, 219-229.

Hofmann A. W., Jochum K. P., Seufert H. M., and White W. M. (1986) Nb and Pb in oceanic basalts: new constraints on mantle evolution. *Earth and Planetary Science Letters* **79**, 33-45.

Jagoutz E., Shatsky V. S., and Sobolev N. V. (1990) Sr-Nd-Pb isotopic study of ultrahigh PT rocks from Kotchetav massif. *EoS (Trans. Am. Geophy. Union)* **71**, 1707.

Jahn B. M., Cornichet J., Cong B.-L., and Yui T.-F. (1996) Ultrahigh-εNd eclogites from an ultrahigh-pressure metamorphic terrane of China. *Chemical Geology* **127**, 61-79.

Jahn B. M., Fan Q., Yang J. J., and Henin O. (2003) Petrogenesis of the Maowu pyroxenite-eclogite body from the UHP metamorphic terrane of Dabieshan: chemical and isotopic constraints. *Lithos* **70**, 243-267.

Jensen L. S. (1976) A new cation plot for classifying subalkaline volcanix rocks. *Ontario Div Mines Misc Pap*, pp66.

Jochum K. P., Hofmann A. W., and Stolz A. J. (1996) Nb and Ta in Ocean Island Basalts. *AGU Fall Meeting Abstracts. EOS* **77 (46) Suppl.**, 785.

Jochum K. P., Seufert H. M., Spettel B., and Palme H. (1986) The solar-system abundance of Nb, Ta and Y, and the relative abundance of refractory lithophile elements in differentiated planetary bodies. *Geochimica et Cosmochimica Acta* **50**, 1173-1183.

Jochum K. P., Stolz A. J., and McOrist G. (2000) Niobium and Tantalum in carbonaceous chondrites: constraints on the solar system and primitive mantle niobium/tantalum, zirconium/niobium and niobium/uranium ratios. *Meteorit. Planet. Sci.* **35**, 229-235.

John T., Klemd R., Gao J., and Garbe-Schönberg C.-D. (2007) Trace-element mobilization in slabs due to non steady-state fluid–rock interaction: Constraints from an eclogite-facies transport vein in blueschist (Tianshan, China). *Lithos* **doi:10.1016/j.lithos.2007.09.005**.

John T. and Schenk V. (2003) Partial eclogitisation of gabbroic rocks in a late Precambrian subduction zone (Zambia): prograde metamorphism triggered by fluid infiltration. *Contributions to Mineralogy and Petrology* **146**, 174-191.

John T., Scherer E. E., Haase K., and Schenk V. (2004) Trace element fractionation during fluid-induced eclogitization in a subducting slab: trace element and Lu-Hf-Sm-Nd isotope systematics. *Earth and Planetary Science Letters* **227**(3-4), 441-456.

Kalfoun K., Ionov D., and Merlet C. (2002) HFSE residence and Nb/Ta ratios in metasomatised, rutile-bearing mantle peridotites. *Earth and Planetary Science Letters* **199**, 49-65.

Kamber B. S. and Collerson K. D. (2000) Role of 'hidden' deeply subducted slabs in mantle depletion. *Chemical Geology* **166**, 241-254.

Klemme S., Prowatke S., Hametner K., and Günther D. (2005) Partitioning of trace elements between rutile and silicate melts: Implications for subduction zones. *Geochimica et Cosmochimica Acta* **69**(9), 2361-2371.

Lagos M., Scherer E. E., Tomaschek F., Münker C., Keiter M., Berndt J., and Ballhaus C. (2007) High Precision Lu-Hf geochronology of Eocene eclogite-facies rocks from Syros, Cyclades, Greece. *Chemical Geology* **243**(1-2), 16-35.

Lapen T. J. (2002) Lu-Hf geochronology of UHP metamorphism in the Zermatt-Saas Ophiolite, Lago di Cignana, Italy. *Geochimica et Cosmochimica Acta* **66**(15A), 431.

Lapen T. J., Johnson C. M., Baumgartner L. P., Mahlen N. J., Beard B. L., and Amato J. M. (2003) Burial rates during prograde metamorphism of an ultra-high-pressure terrane: an example from Lago di Cignana, western Alps, Italy. *Earth and Planetary Science Letters* **215**, 57-72.

Li Q., Li S., Zheng Y.-F., Li H., Massonne H. J., and Wang Q. (2003) A high precision U-Pb age of metamorphic rutile in coesite-bearing eclogite from the Dabie Mountains in central China: a new constraint on the cooling history. *Chemical Geology* **200**, 225-265.

Li S., Jagoutz E., Chen Y., and Li Q. (2000) Sm-Nd and Rb-Sr isotopic chronology and cooling history of ultrahigh pressure metamorphic rocks and their country rocks at Shuanghe in the Dabie Mountains, Central China. *Geochimica et Cosmochimica Acta* **62**(6), 1077-1093.

Li S., Xiao Y., Liou D., Chen Y., Ge N., Zhang Z., Sun S.-s., Cong B.-L., Zhang R. Y., Hart S. R., and Wang S. (1993) Collision of the North China and Yangtse Blocks and formation of coesite-bearing eclogites: Timing and processes. *Chemical Geology* **109**, 89-111.

Li X.-P., Zheng Y., Wu Y.-B., Chen F., Gong B., and Li Y.-L. (2004) Low-T eclogite in the Dabie terrane of China: petrological and isotopic constraints on fluid activity and radiometric dating. *Contributions to Mineralogy and Petrology* **148**, 443-470.

Liou J. G., Wang Q., Zhai M., Zhang R. Y., and Cong B.-L. (1995) Ultrahigh-P metamorphic rocks and their associated lithologies from the Dabie Mountains, central China: A field trip guide to the 3rd international eclogite field symposium. *Chinese Science Bulletin* **40**, 1-41.

Liu D., Jian P., Kröner A., and Xu S. (2006a) Dating of prograde metamorphic events deciphered from episodic zircon growth in rocks of the Dabie-Sulu UHP complex, China. *Earth and Planetary Science Letters* **250**(3-4), 650-666.

Liu F. L., Gerdes A., Liou J. G., Xue H., and Liang F. (2006b) SHRIMP U-Pb zircon dating from Sulu-Dabie dolomitic marble, eastern China: constraints on prograde, ultrahigh-pressure and retrograde metamorphic ages. *Journal of metamorphic Geology* **doi:10.111/j.1525-1314-2006.00655.x**.

Liu F. L., Liou J. G., and Xue H. (2006c) Identification of UHP and Non-UHP Orthogneisses in the Sulu Terrane, Eastern China: Evidence from SHRIMP U-Pb Dating of Mineral Inclusion-Bearing Zircons. *International Geology Review* **48**.

Liu Y.-C., Li S., and Xu S. T. (2007) Zircon SHRIMP U-Pb dating for gneisses in northern Dabie high T/P metamorphic zone, central China: Implications for decoupling within subducted continental crust. *Lithos* **96**(3-4), 170-185.

Mahlen N. J., Skora S., Johnson C. M., Baumgartner L. P., Lapen T. J., Beard B. L., and Pilet S. (2005) Lu-Hf geochronology of eclogites from Pfulwe, Zermatt-Saas ophiolite, western Alps, Switzerland. *Geochimica et Cosmochimica Acta Supplement - Goldschmidt Conference Abstracts* **69**(10), A305.

Maruyama S., Liou J. G., and Zhang R. (1994) Tectonic evolution of the ultrahigh-pressure (UHP) and high-pressure (HP) metamorphic belts from central China. *The Island Arc* **3**, 112-121.

McDonough W. F. (1991) Partial melting of subducted oceanic crust and isolation of its residual eclogitic lithology. *Phil. Trans. R. Soc. Lond.* **335**, 407-418.

McDonough W. F. and Sun S. (1995) The composition of the Earth. *Chemical Geology* **120**, 223-253.

Morris J. D. and Hart S. R. (1983) Isotopic and incompatible element constraints on the genesis of island arc volcanic from Cold Bay and Amak Island, Aleutians, and implications for mantle structure. *Geochimica et Cosmochimica Acta* **47**, 2015-2030.

Münker C. (1998) Nb/Ta fractionation in a Cambrian arc/back arc system, New Zealand: source constraints and application of refined ICPMS techniques. *Chemical Geology* **144**, 23-45.

Münker C., Paulick H., and König S. (2007) The geochemical behaviour of W, Nb-Ta, and Zr-Hf during mid ocean ridge melting. *Geochimica et Cosmochimica Acta* **71 - Supplement**, A696.

Münker C., Pfänder J. A., Weyer S., Büchl A., Kleine T., and Mezger K. (2003) Evolution of planetary cores and the Earth-Moon system from Nb/Ta systematics. *Science* **301**, 84-87.

Münker C., Weyer S., Scherer E. E., and Mezger K. (2001) Separation of High Field Strength Elements (Nb, Ta, Zr, Hf) and Lu from rock samples for MC-ICPMS measurements. *Geochemistry, Geophysics, Geosystems (G3) 2*, paper number 10.1029/2001GC000183.

Okay A. I., Sengör A. M. C., and Satir M. (1993) Tectonics of an ultrahigh-pressure metamorphic terrane: The Dabie Shan/Tongbai Shan orogen, China. *Tectonics* **12**(6), 1320-1334.

Okay A. I., Xu S. T., and Sengör A. M. C. (1989) Coesite from the Dabie Shan eclogites, central China. *Eur. J. Mineral.* **1**, 595-598.

Patchett P. J. and Tatsumoto M. (1980) A routine high-precision method for Lu-Hf isotope geochemistry and geochronology. *Contributions to Mineralogy and Petrology* **75**, 263-267.

Peate D. W., Pearce J. A., Hawkesworth C. J., Colley H., Edwards C. M. H., and Hirose K. (1997) Geochemical variations in Vanuatu Arc lavas: the role of subducted material and a variable mantle wedge composition. *Journal of Petrology* **38**, 1331-1358.

Pfänder J., Münker C., Stracke A., and Mezger K. (2007) Nb/Ta and Zr/Hf in ocean island basalts - Implications for crust-mantle differentiation and the fate of Niobium. *Earth and Planetary Science Letters* **254**, 158-172.

Pin C. and Zalduegui J. F. (1997) Sequential separation of light rare-earth elements, thorium and uranium by miniturized extraction chromatography: Application to isotopic analysis of silicate rocks. *Analytica Chimica Acta* **339**(1-2), 79-89.

Plank T. and White W. M. (1995) Nb and Ta in arc and mid-ocean basalts. *AGU Fall Meeting Abstracts. EOS* **76 (46) Suppl.**, 655.

Prouteau G., Maury R. C., Sajona F. G., Cotten J., and Joron J.-L. (2000) Behavior of Niobium, Tantalum and other high field strength elements in adakites and related lavas from The Philippines. *The Island Arc* **9**, 487-498.

Raimbourg H., Goffé B., and Jolivet L. (2007) Garnet reequilibration and growth in the eclogite facies and geodynamical evolution near peak metamorphic conditions. *Contributions to Mineralogy and Petrology* **153**, 1-28.

Rapp R. P., Shimizu N., and Norman M. D. (2003) Growth of early continental crust by partial melting of eclogite. *Nature* **425**, 605-609.

Ratschbacher L., Hacker B. R., Calvert A., Webb L., Grimmer J. C., McWilliams M. O., Ireland T., Dong S., and Hu J. (2003) Tectonics of the Qinling (Central China): tectonostratigraphy, geochronology, and deformation history. *Tectonophysics* **366**, 1-53.

Rowley D. B., Xue F., Tucker R. D., Peng Z. X., Baker J., and Davis A. (1997) Ages of ultrahigh pressure metamorphism and protolith orthogneisses from eastern Dabie Shan: U/Pb zircon geochronology. *Earth and Planetary Science Letters* **151**, 191-203.

Rudnick R. L., Barth M. G., Horn I., and McDonough W. F. (2000) Rutile-bearing refractory eclogites: Missing link between continents and depleted mantle. *Science* **287**, 278-281.

Rumble D. and Yui T. F. (1998) The Qinglongshan oxygen and hydrogen isotope anomaly near Donghai in Jiangsu Province, China. *Geochimica et Cosmochimica Acta* **62**, 3307-3321.

Ryerson F. J. and Watson E. B. (1987) Rutile saturation in magmas: implications for Ti-Nb-Ta depletion in island-arc basalts. *Earth and Planetary Science Letters* **86**, 225-239.

Saunders A. D., Tarney J., and Weaver S. D. (1980) Transverse geochemical variations across the Antarctic Peninsula: implications for the genesis of calc-alkaline magmas. *Earth and Planetary Science Letters* **46**, 344-360.

Scherer E. E., Cameron K. L., and Blichert-Toft J. (2000) Lu-Hf garnet geochronology: Closure temperature relative to the Sm-Nd system and the effects of trace mineral inclusions. *Geochimica et Cosmochimica Acta* **64**, 3413-3432.

Scherer E. E., Cameron K. L., Johnson C. M., Beard B. L., Barovich K. M., and Collerson K. D. (1997) Lu-Hf geochronology applied to dating Cenozoic events affecting lower crustal xenoliths from Kilbourne Hole, New Mexico. *Chemical Geology* **142**, 63-78.

Scherer E. E., Münker C., and Mezger K. (2001) Calibration of the Lutetium-Hafnium Clock. *Science* **293**, 683-687.

Scherer E. E., Münker C., and Mezger K. (2003) Advances in Lu-Hf garnet geochronology. *Berichte der Deutschen Mineralogischen Gesellschaft* **15**(1), 169.

Schertl H. P. and Okay A. I. (1994) Coesite inclusion in dolomite of Dabie Shan, China: Petrological and rheological significance. *Eur. J. Mineral.* **6**, 995-1000.

Schertl H. P., Schreyer W., and Chopin C. (1991) The pyrope-coesite rocks and their country rocks at Parigi, Dora Maira massif, western Alps: Detailed petrography, mineral chemistry and PT-path. *Contributions to Mineralogy and Petrology* **108**, 1-21.

Schmidt M. W., Dardon A., Chazot G., and Vannucci R. (2004) The dependence of Nb and Ta rutile-melt partitioning on melt composition and Nb/Ta fractionation during subduction processes. *Earth and Planetary Science Letters* **226**(3-4), 415-432.

Sims K. W. W. and DePaolo D. J. (1997) Inferences about mantle magma sources from incompatible element concentration ratios in oceanic basalts. *Geochimica et Cosmochimica Acta* **61**(4), 765-784.

Skora S., Baumgartner L. P., Mahlen N. J., Johnson C. M., Pilet S., and Hellebrand E. (2006) Diffusion-limited REE uptake by eclogite garnets and its consequences for Lu-Hf and Sm-Nd geochronology. *Contributions to Mineralogy and Petrology* **DOI 10.1007/s00410-006-0128-x**.

Spandler C., Hermann J., Arculus R. J., and Mavrogenes J. (2003) Redistribution of trace elements during prograde metamorphism from lawsonite blueschist to eclogite facies; implications for deep subduction-zone processes. *Contributions to Mineralogy and Petrology* **146**, 205-222.

Stalder R., Foley S. F., Brey G. P., and Horn I. (1998) Mineral-aqueous fluid partitioning of trace elements at 900-1200°C and 3.0-5.7 GPa: New experimental data for garnet,

clinopyroxene and rutile, and implications for mantle metasomatism. *Geochimica et Cosmochimica Acta* **62**(10), 1781-1801.

Stolper E. M. and Newman S. (1994) The role of water in the petrogenesis of Marianna trough magmas. *Earth and Planetary Science Letters* **121**, 293-325.

Stolz A. J., Jochum K. P., and Hofmann A. W. (1995) HFSE constraints on the nature of island arc and oceanic magma sources. *EUG abstracts, Terra Nova* **7**, 299.

Tang H.-F., Liu C.-Q., Nakai S. i., and Orihashi Y. (2007) Geochemistry of eclogites from the Dabie-Sulu terrane, eastern China: New insights into protoliths and trace element behaviour during UHP metamorphism. *Lithos* **95**(3-4), 441-457.

Tang J., Zheng Y., Wu Y.-B., and Gong B. (2006) Zircon SHRIMP U-Pb dating, C and O isotopes for impure marbles from the Jiaobei terrane in the Sulu orogen: Implications for tectonic affinity. *Precambrian Research* **144**(1-2), 1-18.

Taylor S. R. and McLennan S. M. (1985) *The continental crust: its composition and evolution.* Blackwell.

Vervoort J. D., Patchett P. J., Söderlund U., and Baker M. (2004) Isotopic composition of Yb and the determinations of Lu concentrations and Lu/Hf ratios by isotope dilution using MC-ICPMS. *Geochemistry, Geophysics, Geosystems (G3)* **5**(11), paper number: 10.1029/2004GC000721.

Wade J. and Wood B. J. (2001) The Earth´s "missing" niobium may be in the core. *Nature* **409**, 75-78.

Wain A. (1997) New evidence for coesite in eclogite and gneisses: Defining an ultrahigh-pressure province in the Western Gneiss region of Norway. *Geology* **25**(10), 927-930.

Wang X., Jing Y., Liou J. G., Pan G., Liang W., and Maruyama S. (1990) Field occurrences and petrology of eclogites from the Dabie Mountains, Anhui, central China. *Lithos* **25**, 119-131.

Wang X. and Liou J. G. (1991) Regional ultrahigh-pressure coesite-bearing eclogitic terrain in central China: Evidence from country rocks, gneiss, marble and metapelite. *Geology* **19**, 933-936.

Wawrzenitz N., Romer R., Oberhänsli R., and Dong S. (2006) Dating of subduction and different exhumation of UHP rocks from the Central Dabie Complex (E-China): Constraints from microfabrics, Rb-Sr and U-Pb isotope systems. *Lithos* **89**(1-2), 174-201.

Weyer S., Münker C., and Mezger K. (2003) Nb/Ta, Zr/Hf and REE in the depleted mantle: Implications for the differentiation history of the crust-mantle system. *Earth and Planetary Science Letters* **205**, 309-324.

Weyer S., Münker C., Rehkämper M., and Mezger K. (2002) Determination of ultra-low Nb, Ta, Zr and Hf concentrations and the chondritic Zr/Hf and Nb/Ta ratios by isotope dilution analyses with multiple collector ICP-MS. *Chemical Geology* **187**, 295-313.

Whitehouse M. J. and Platt J. P. (2003) Dating high-grade metamorphism - constraints from rare-earth elements in zircon and garnet. *Contributions to Mineralogy and Petrology* **145**, 61-74.

Wu Y.-B., Zheng Y., Zhao Z.-F., Gong B., Liu X., and Wu F. (2006) U-Pb, Hf and O isotope evidence for two episodes of a fluid-assisted zircon growth in marble-hosted eclogites from the Dabie orogen. *Geochimica et Cosmochimica Acta* **70**(14), 3743-3761.

Xiao Y. (2000) Fluid Histories During HP and UHP Metamorphism in Dabie Shan, China: Constraints from Trace Elements, Fluid Inclusions, and Stable Isotopes, University of Göttingen.

Xiao Y., Hoefs J., Van Den Kerkhof A. M., Fiebig J., and Zheng Y.-F. (2000) Fluid history of UHP metamorphism in Dabie Shan, China: a fluid inclusion and oxygen isotope study on the coesite-bearing eclogite from Bixiling. *Contributions to Mineralogy and Petrology* **139**, 1-16.

Xiao Y., Hoefs J., Van Den Kerkhof A. M., and Li S. G. (2001) Geochemical constraints of the eclogite and granulite facies metamorphism as recognized in the Raobazhai complex from North Dabie Shan, China. *Journal of metamorphic Geology* **19**, 3-19.

Xiao Y., Hoefs J., Van Den Kerkhof A. M., Simon K., Fiebig J., and Zheng Y.-F. (2002) Fluid Evolution during HP and UHP Metamorphism in Dabie Shan, China: Constraints from Mineral Chemistry, Fluid Inclusions and Stable Isotopes. *Journal of Petrology* **43**(8), 1505-1527.

Xiao Y., Zhang Z., Hoefs J., and van den Kerkhof A. (2006) Ultrahigh-pressure metamorphic rocks from the Chinese Continental Scientific Drilling Project: II Oxygen isotope and fluid inclusion distributions through vertical sections. *Contributions to Mineralogy and Petrology* **152**, 443-458.

Xie Z., Zheng Y.-F., Jahn B., Ballevre M., Chen J., Gautier P., Gao T., Gong B., and Zhou J. (2004) Sm-Nd and Rb-Sr dating of pyroxene-garnetite from North Dabie in east-central China: problem of isotope disequilibrium due to retrograde metamorphism. *Chemical Geology* **206**, 137-158.

Xiong X.-L., Adam J., and Green T. H. (2005) Rutile stability and rutile/melt HFSE partitioning during partial melting of hydrous basalt: Implications for TTG genesis. *Chemical Geology* **218**, 339-359.

Yang J. S., Wooden J. L., Wu C. L., Liu F. L., Xu Z. Q., Shi R. D., Katayama I., Liou J. G., and Maruyama S. (2003) SHRIMP U-Pb dating of coesite-bearing zircon from the ultrahigh-pressure metamorphic rocks, Sulu terrane, east China. *Journal of Metamorphic Geology* **21**, 551-560.

Zack T. and John T. (2007) An evaluation of reactive fluid flow and trace element mobility in subducting slabs. *Chemical Geology* **239**, 199-216.

Zack T., Kronz A., Foley S. F., and Rivers T. (2002) Trace element abundances in rutiles from eclogites and associated garnet mica schists. *Chemical Geology* **184**, 97-122.

Zhang R. Y., Liou J. G., and Tsai C.-H. (1996) Petrogenesis of a high-temperature metamorphic terrane: a new tectonic interpretation for the north Dabieshan, central China. *Journal of metamorphic Geology* **3**, 231-243.

Zhang R. Y., Yang J. S., Wooden J. L., Liou J. G., and Li T. F. (2005) U-Pb SHRIMP geochronology of zircon in garnet peridotite from Sulu UHP terrane, China: Implications for mantle metasomatism and subduction-zone UHP metamorphism. *Earth and Planetary Science Letters* **237**, 729-743.

Zhao Z.-F., Zheng Y., Gao T. S., Wu Y.-B., Chen B., Chen F., and Wu F. (2006) Isotopic constraints on age and duration of fluid-assisted high-pressure eclogite facies recrystallization during exhumation of deeply subducted continental crust in the Sulu orogen. *Journal of metamorphic Geology* **24**(8), 687-702.

Zheng Y., Fu B., Li Y.-L., Xiao Y., and Li S. (1998) Oxygen and hydrogen isotope geochemistry of ultrahigh-pressure eclogites from the Dabie Mountains and the Sulu terrane. *Earth and Planetary Science Letters* **155**, 113-129.

Zheng Y., Gong B., Zhao Z.-F., Fu B., and Li Y.-L. (2003) Two types of gneisses associated with eclogite at Shuanghe in the Dabie terrane: carbon isotope, zircon U-Pb dating and oxygen isotope. *Lithos* **70**, 321-343.

Zheng Y., Zhou J.-B., Wu Y.-B., and Xie Z. (2005) Low-grade metamorphic rocks in the Dabie-Sulu orogenic belt: a passive-margin accretionary wedge deformed during continent subduction. *International Geology Review* **47**, 851-871.

A Appendix - Supplementary data:

The appendix presents supplementary data to chapter one. This data describes the major element chemistry of garnets and clinopyroxenes in eclogites, blueshists and peridotites. Additionally the HFSE concentrations of garnets, clinopyroxenes and rutiles are shown in table A·3 and A·4. All HFSE budget calculations of table 1·2 are based on this data.

Major elements of the mineral phases garnet and clinopyroxene have been measured with a JEOL Superprobe JXA-8900. The major elements, especially Si and Ca, had to be determined for the LA-ICPMS to serve as the internal standard for normalization within the calculation of trace element and HFSE concentrations. Garnets e.g. have SiO_2-contents ranging from 38 wt-% to 40 wt-%, which is what has to be expected from stoechiometric balance in the general formula $X_3Y_2Si_3O_{12}$ for garnet (table A·1). Figure A·1 shows a classification of measured garnets from eclogites of different localities (based on data of table A·1). The localities shown here are extended compared to the samples presented in chapter one. In the course of this study a large pool of eclogites, blueshists and peridotites was collected. Most samples were analysed for multiple reasons, e.g. to establish measuring routines and to refine data evaluation, and only selected samples went into focus for the questions of chapter one. Some samples were also rejected because of alterations or very low abundances of rutile.

The classification in Fig. A·1 is based on the three major end members Grossular ($Ca_3Al_2Si_3O_{12}$), Pyrope ($Mg_3Al_2Si_3O_{12}$) and Almandine + Spessartine ($Fe_2^{+3}/Mn_3Al_2Si_3O_{12}$). The Grossular component varies between 5% and 50%, the Pyrope component between 5% and 60%, and the Almandine + Spessartine component varies between 25% and 70%. Most eclogitic garnet is rich in Almandine and Spessartine. Peridotites (here from the Dabie UHP terrane) instead compose mainly of Pyrope, the Mg end member. In general the garnets reflect changes in the compositions of the bulk rocks, that is, peridotites have higher Mg contents than basalts and distinctly lower Ca contents

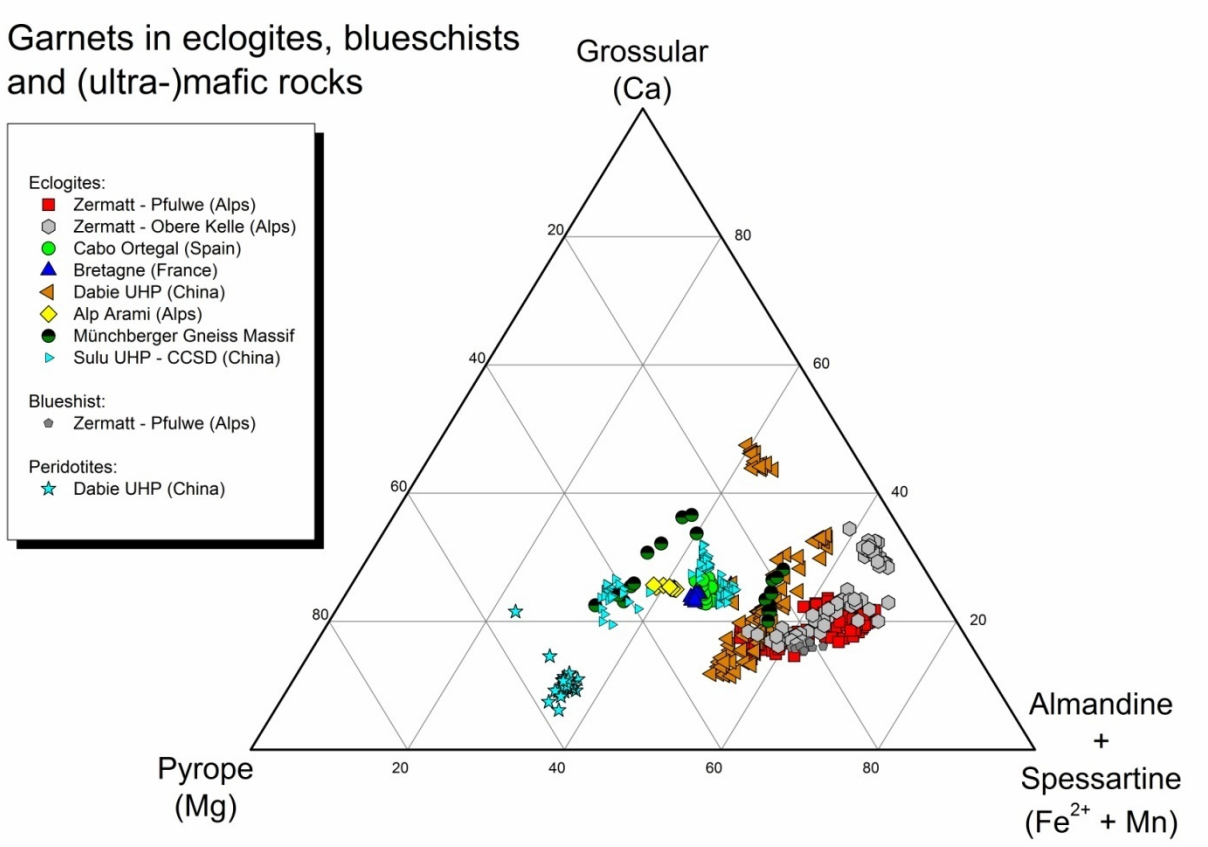

Figure A·1: Garnet classification based on three end member proportions grossular, pyrope and almandine + spessartine.

The second important mineral in eclogite is clinopyroxene. Major element compositions are shown in table A·2. In eclogites, clinopyroxenes are mainly omphacites which consist of jadeite, acmite and Ca-Mg-Fe pyroxene. A classification of Na-Ca-pyroxenes is shown in Fig. A·2. The majority of measured minerals are omphacites with 30% to 70% jadeite and a varying acmite component. Clinopyroxenes in the Dabie peridotites are mainly Ca-Mg-Fe pyroxenes with less than 10% Jd-component. Some samples also show occasional minerals which resemble a pure jadeite, others occasionally have more acmite-rich pyroxenes. The difference between eclogitic and basaltic pyroxenes (with mainly Ca, Mg and Fe) is that eclogitic pyroxenes have additionally a significant amount of a Na component, which comes from the breakdown of plagioclase (albite) to jadeite + quartz during metamorphism and increasing pressure ($NaAlSi_3O_8 \rightarrow NaAlSi_2O_6 + SiO_2$).

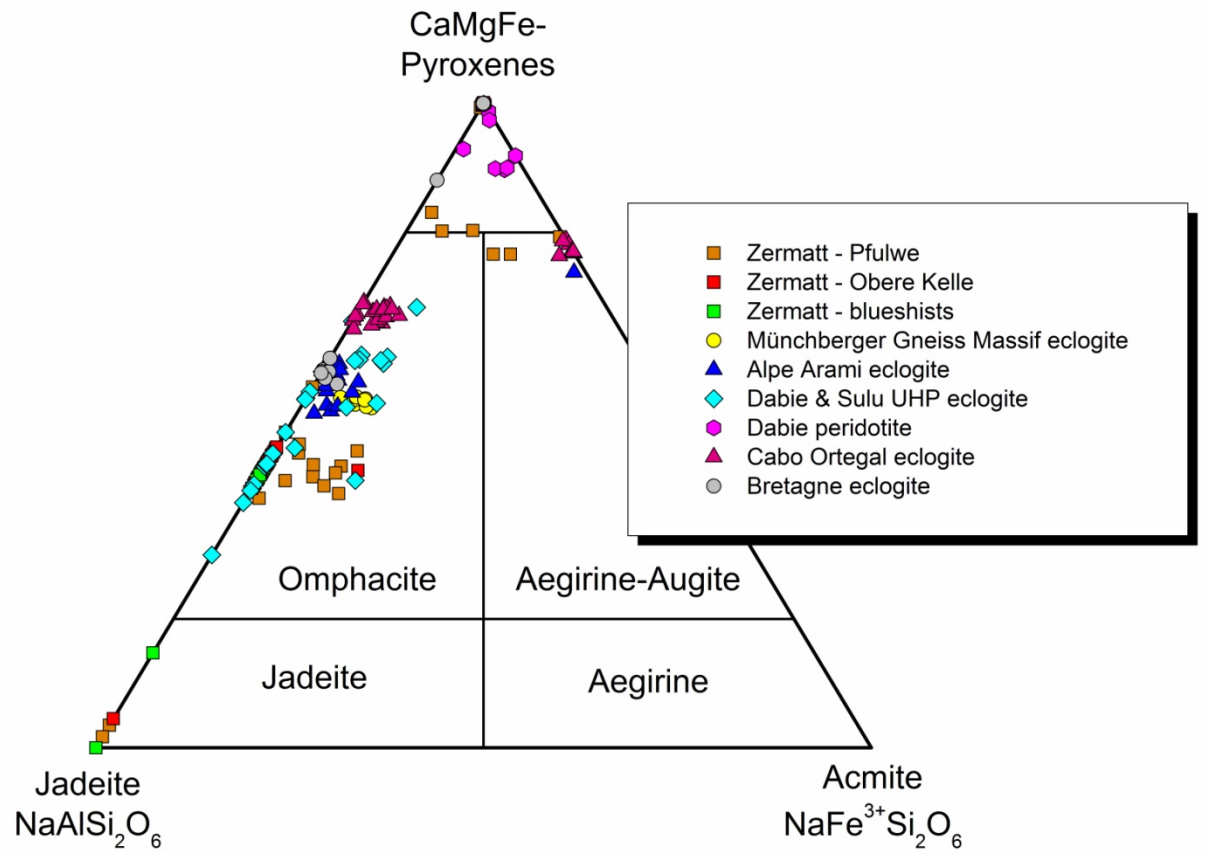

Fig. A·2: Classification of Na-Ca-pyroxenes in eclogites, blueshists and peridotites.

Table A·1: Major elements of garnets in eclogites, blueshists and peridotites (electron microprobe, values in wt-%)

Zermatt-Saas-Fee Ophiolite, Eclogites, Pfulwe												
	SiO_2	K_2O	Na_2O	CaO	MnO	MgO	TiO_2	P_2O_5	FeO	Al_2O_3	Cr_2O_3	NiO
PfL01 Grt	38.6	0.00	0.02	5.14	1.12	7.61	0.06	0.01	25.4	22.0	0.01	0.01
PfL01 Grt	38.9	0.02	0.05	6.57	0.64	7.52	0.05	0.02	24.4	21.8	0.04	0.00
PfL01 Grt	38.4	0.00	0.07	5.97	2.86	6.14	0.04	0.02	24.6	21.9	0.00	0.01
PfL01 Grt	38.6	0.01	0.06	6.78	0.67	7.41	0.04	0.03	24.2	22.1	0.00	0.02
PfL01 Grt	39.1	0.02	0.05	6.34	0.65	7.55	0.06	0.03	24.4	21.8	0.05	0.02
PfL01 Grt	38.5	0.00	0.06	5.85	2.56	6.31	0.06	0.04	24.7	21.8	0.01	0.06
PfL01 Grt	38.6	0.01	0.07	5.66	2.62	6.44	0.04	0.02	24.9	21.6	0.00	0.00
PfL01 Grt	38.6	0.00	0.04	5.75	1.26	7.27	0.01	0.00	25.0	22.1	0.01	0.00
PfL01 Grt	38.7	0.01	0.06	6.71	0.74	7.27	0.01	0.01	24.2	22.2	0.00	0.01
PfL01 Grt	38.6	0.01	0.04	5.92	1.43	7.06	0.07	0.00	25.0	21.9	0.00	0.05
	SiO_2	K_2O	Na_2O	CaO	MnO	MgO	TiO_2	P_2O_5	FeO	Al_2O_3	Cr_2O_3	NiO
PfL02 Grt	38.1	0.01	0.03	6.14	1.86	4.01	0.04	0.03	28.5	21.2	0.02	0.05
PfL02 Grt	38.3	0.00	0.05	6.22	1.44	4.41	0.03	0.03	28.4	21.2	0.02	0.00
PfL02 Grt	38.5	0.01	0.05	5.25	0.30	6.04	0.07	0.00	28.2	21.6	0.01	0.00
PfL02 Grt	38.0	0.01	0.03	6.66	4.17	3.41	0.04	0.03	26.5	21.1	0.02	0.00

Table A·1 cont.

	SiO_2	K_2O	Na_2O	CaO	MnO	MgO	TiO_2	P_2O_5	FeO	Al_2O_3	Cr_2O_3	NiO
PfL02 Grt	38.0	0.00	0.03	6.93	4.18	3.28	0.06	0.02	26.4	21.1	0.02	0.02
PfL02 Grt	38.0	0.00	0.02	7.42	6.04	2.88	0.05	0.00	24.5	21.0	0.05	0.04
PfL02 Grt	38.1	0.00	0.05	6.22	2.47	3.64	0.01	0.02	28.2	21.3	0.03	0.00
PfL02 Grt	38.0	0.00	0.06	5.98	1.84	4.26	0.06	0.00	28.5	21.3	0.04	0.00
PfL02 Grt	37.9	0.00	0.05	6.61	3.42	3.48	0.05	0.00	27.3	21.2	0.00	0.03
PfL02 Grt	37.9	0.01	0.02	6.61	2.95	3.63	0.04	0.01	27.6	21.2	0.00	0.04

	SiO_2	K_2O	Na_2O	CaO	MnO	MgO	TiO_2	P_2O_5	FeO	Al_2O_3	Cr_2O_3	NiO
Pf01 Grt	38.8	0.01	0.05	6.16	0.39	7.38	0.05	0.02	25.2	22.0	0.00	0.00
Pf01 Grt	39.1	0.01	0.03	6.37	0.32	7.51	0.03	0.00	24.8	21.9	0.00	0.01
Pf01 Grt	38.7	0.02	0.06	5.83	0.86	6.99	0.01	0.00	25.9	21.6	0.01	0.02
Pf01 Grt	38.6	0.01	0.06	6.04	0.44	7.47	0.02	0.00	25.4	21.9	0.05	0.02
Pf01 Grt	38.9	0.00	0.06	5.86	0.58	7.21	0.00	0.01	25.8	21.6	0.01	0.00
Pf01 Grt	38.5	0.00	0.08	6.61	2.48	5.43	0.08	0.00	25.4	21.4	0.00	0.00
Pf01 Grt	38.7	0.01	0.05	5.95	1.25	6.94	0.01	0.02	25.2	21.9	0.00	0.01
Pf01 Grt	38.4	0.01	0.04	5.68	0.67	7.11	0.04	0.01	26.2	21.9	0.00	0.00
Pf01 Grt	38.3	0.00	0.04	6.41	1.72	6.03	0.06	0.00	25.7	21.7	0.00	0.01
Pf01 Grt	38.8	0.00	0.05	6.12	0.78	6.77	0.00	0.00	25.7	21.8	0.00	0.03

	SiO_2	K_2O	Na_2O	CaO	MnO	MgO	TiO_2	P_2O_5	FeO	Al_2O_3	Cr_2O_3	NiO
Pf02 Grt	37.5	0.00	0.04	7.82	1.78	3.66	0.07	0.00	27.6	21.4	0.04	0.00
Pf02 Grt	37.6	0.02	0.07	8.26	1.20	4.32	0.03	0.01	27.0	21.5	0.01	0.00
Pf02 Grt	37.9	0.01	0.05	8.16	1.54	4.30	0.07	0.00	26.6	21.3	0.02	0.00
Pf02 Grt	37.6	0.01	0.04	7.11	3.78	3.67	0.02	0.00	26.5	21.2	0.01	0.00
Pf02 Grt	37.9	0.03	0.03	7.51	2.20	3.99	0.06	0.00	27.0	21.3	0.00	0.00
Pf02 Grt	37.9	0.01	0.07	7.92	3.04	3.44	0.06	0.02	26.3	21.1	0.04	0.00
Pf02 Grt	37.6	0.12	0.04	7.21	2.14	3.91	0.04	0.00	27.6	21.4	0.00	0.00
Pf02 Grt	38.0	0.04	0.05	8.18	3.08	3.43	0.10	0.02	26.0	21.1	0.02	0.03
Pf02 Grt	37.4	0.02	0.08	7.29	5.13	3.03	0.09	0.00	25.9	21.0	0.02	0.00
Pf02 Grt	37.6	0.03	0.05	7.84	2.24	3.83	0.07	0.00	27.1	21.2	0.04	0.03

	SiO_2	K_2O	Na_2O	CaO	MnO	MgO	TiO_2	P_2O_5	FeO	Al_2O_3	Cr_2O_3	NiO
Pf03 Grt	37.4	0.00	0.06	8.50	0.82	3.78	0.03	0.00	27.7	21.7	0.06	0.00
Pf03 Grt	37.7	0.00	0.04	7.50	0.84	3.86	0.05	0.04	28.4	21.5	0.00	0.05
Pf03 Grt	37.8	0.02	0.08	6.77	0.94	4.05	0.03	0.01	28.9	21.4	0.00	0.02
Pf03 Grt	37.6	0.00	0.07	8.27	0.83	3.82	0.10	0.00	27.6	21.7	0.02	0.00
Pf03 Grt	37.9	0.02	0.05	8.06	0.78	4.78	0.05	0.00	26.8	21.5	0.04	0.00
Pf03 Grt	37.9	0.00	0.06	7.13	0.85	4.56	0.03	0.00	28.0	21.5	0.01	0.05
Pf03 Grt	37.6	0.01	0.04	7.56	0.75	3.62	0.05	0.00	28.8	21.6	0.00	0.00
Pf03 Grt	37.7	0.01	0.07	7.98	0.81	3.70	0.03	0.00	28.2	21.5	0.02	0.00

	SiO_2	K_2O	Na_2O	CaO	MnO	MgO	TiO_2	P_2O_5	FeO	Al_2O_3	Cr_2O_3	NiO
Pf07 Grt	37.4	0.00	0.04	6.46	2.96	3.62	0.06	0.01	28.0	21.4	0.02	0.00
Pf07 Grt	37.2	0.01	0.03	7.00	4.80	2.96	0.09	0.03	26.5	21.4	0.02	0.00
Pf07 Grt	37.2	0.00	0.02	6.53	3.55	3.41	0.06	0.00	27.7	21.5	0.00	0.06
Pf07 Grt	36.4	0.00	0.01	6.87	4.43	3.19	0.06	0.01	27.0	21.9	0.03	0.07
Pf07 Grt	37.6	0.00	0.07	6.92	4.09	3.05	0.06	0.00	27.1	21.2	0.01	0.01
Pf07 Grt	38.3	0.04	0.04	6.05	1.06	5.26	0.05	0.00	27.7	21.5	0.01	0.00
Pf07 Grt	37.6	0.02	0.04	7.59	6.03	2.66	0.08	0.03	24.5	21.4	0.00	0.07
Pf07 Grt	38.5	0.00	0.04	6.35	0.15	6.98	0.03	0.04	26.0	21.9	0.01	0.00

Table A·1 cont.

	SiO_2	K_2O	Na_2O	CaO	MnO	MgO	TiO_2	P_2O_5	FeO	Al_2O_3	Cr_2O_3	NiO
Pf07 Grt	38.5	0.00	0.04	5.60	0.19	6.73	0.02	0.00	27.2	21.7	0.03	0.01

	SiO_2	K_2O	Na_2O	CaO	MnO	MgO	TiO_2	P_2O_5	FeO	Al_2O_3	Cr_2O_3	NiO
Pf05 Grt	37.6	0.00	0.04	7.75	4.43	2.87	0.08	0.00	25.9	21.2	0.00	0.00
Pf05 Grt	37.6	0.01	0.05	7.66	6.64	2.41	0.09	0.01	24.3	21.1	0.04	0.03
Pf05 Grt	38.4	0.01	0.05	7.11	1.37	3.82	0.02	0.08	28.3	21.3	0.03	0.00
Pf05 Grt	37.7	0.02	0.05	6.64	3.30	3.20	0.07	0.01	27.6	21.2	0.02	0.00
Pf05 Grt	37.5	0.02	0.07	6.31	1.20	4.60	0.02	0.00	28.3	21.6	0.00	0.02
Pf05 Grt	38.5	0.01	0.06	6.69	1.20	5.09	0.00	0.00	27.1	21.7	0.02	0.07
Pf05 Grt	37.4	0.01	0.04	7.48	4.34	2.87	0.08	0.01	26.0	21.3	0.02	0.03
Pf05 Grt	37.9	0.01	0.06	7.26	4.23	3.21	0.05	0.04	26.1	21.2	0.00	0.09
Pf05 Grt	38.2	0.01	0.05	7.21	4.31	2.99	0.06	0.00	26.4	21.0	0.02	0.00
Pf05 Grt	38.4	0.01	0.06	7.28	4.16	3.35	0.08	0.02	26.4	21.2	0.00	0.02

	SiO_2	K_2O	Na_2O	CaO	MnO	MgO	TiO_2	P_2O_5	FeO	Al_2O_3	Cr_2O_3	NiO
Pf04 Grt	37.1	0.00	0.03	7.01	7.08	2.85	0.03	0.00	24.0	21.3	0.02	0.00
Pf04 Grt	36.2	0.00	0.06	7.11	4.15	2.99	0.06	0.02	27.0	21.3	0.05	0.00
Pf04 Grt	37.7	0.04	0.04	7.67	1.28	4.23	0.01	0.00	27.4	21.4	0.00	0.01
Pf04 Grt	37.3	0.01	0.03	7.88	4.29	3.78	0.06	0.02	24.3	21.3	0.01	0.01
Pf04 Grt	37.8	0.02	0.05	7.01	2.51	3.72	0.08	0.02	28.3	21.4	0.00	0.00
Pf04 Grt	38.4	0.01	0.04	6.23	0.52	5.54	0.07	0.00	28.3	21.5	0.07	0.03
Pf04 Grt	37.0	0.02	0.05	7.37	2.77	3.79	0.06	0.00	27.1	21.4	0.06	0.00
Pf04 Grt	37.2	0.01	0.05	7.42	3.91	3.62	0.07	0.00	25.8	21.2	0.00	0.01
Pf04 Grt	37.4	0.01	0.05	7.70	5.83	2.58	0.11	0.01	24.9	21.2	0.04	0.00
Pf04 Grt	37.2	0.00	0.05	6.80	3.16	3.35	0.07	0.00	28.0	21.1	0.04	0.00

	SiO_2	K_2O	Na_2O	CaO	MnO	MgO	TiO_2	P_2O_5	FeO	Al_2O_3	Cr_2O_3	NiO
ZFUR-3 Grt	39.3	0.00	0.01	24.3	0.03	0.02	0.05	0.01	1.9	31.7	0.02	0.00
ZFUR-3 Grt	39.4	0.04	0.05	24.0	0.03	0.07	0.01	0.00	2.5	30.9	0.06	0.02
ZM-E1 Grt	38.3	0.02	0.08	8.12	1.00	3.18	0.03	0.02	29.4	21.2	0.01	0.00
ZM-E1 Grt	38.4	0.02	0.08	7.07	0.57	4.50	0.07	0.00	29.1	21.3	0.00	0.00
ZM-E1 Grt	38.0	0.03	0.15	8.37	1.19	2.70	0.10	0.00	29.2	20.9	0.04	0.01
ZM-E1 Grt	37.9	0.00	0.07	8.24	0.97	2.96	0.11	0.00	29.4	20.7	0.03	0.00
ZM-E1 Grt	38.1	0.00	0.02	8.44	1.03	2.92	0.09	0.00	29.1	21.1	0.06	0.00

Zermatt-Saas-Fee Ophiolite, Eclogites, Obere Kelle

	SiO_2	K_2O	Na_2O	CaO	MnO	MgO	TiO_2	P_2O_5	FeO	Al_2O_3	Cr_2O_3	NiO
ZOK-1 Grt	37.9	0.00	0.02	11.2	1.79	1.34	0.12	0.03	27.8	20.4	0.02	0.00
ZOK-1 Grt	37.9	0.00	0.02	10.8	1.68	1.38	0.09	0.00	28.0	20.7	0.01	0.01
ZOK-1 Grt	37.8	0.00	0.01	11.1	1.79	1.36	0.06	0.01	27.7	20.6	0.04	0.00
ZOK-1 Grt	37.8	0.00	0.03	11.8	1.70	1.30	0.08	0.01	27.3	20.4	0.02	0.01
ZOK-1 Grt	37.8	0.02	0.07	11.5	1.71	1.35	0.13	0.00	27.4	20.4	0.04	0.02
ZOK-1 Grt	37.6	0.00	0.02	10.3	1.93	1.41	0.12	0.00	28.2	20.3	0.02	0.02
ZOK-1 Grt	38.3	0.00	0.03	12.4	0.49	1.66	0.01	0.00	26.8	21.3	0.02	0.02
ZOK-1 Grt	37.9	0.00	0.01	11.3	1.25	1.58	0.05	0.00	27.4	20.8	0.05	0.00
ZOK-1 Grt	37.6	0.00	0.02	10.6	1.94	1.41	0.09	0.00	28.4	20.6	0.02	0.00
ZOK-1 Grt	37.7	0.00	0.02	11.2	0.41	1.41	0.06	0.03	28.4	21.2	0.02	0.04

Table A·1 cont.

	SiO_2	K_2O	Na_2O	CaO	MnO	MgO	TiO_2	P_2O_5	FeO	Al_2O_3	Cr_2O_3	NiO
ZOK-2 Grt	38.0	0.00	0.03	10.9	0.92	1.25	0.09	0.03	29.3	20.6	0.03	0.02
ZOK-2 Grt	37.6	0.00	0.05	11.3	0.34	1.43	0.08	0.01	29.0	20.7	0.03	0.02
ZOK-2 Grt	37.8	0.02	0.05	10.8	0.20	1.70	0.04	0.03	28.8	21.2	0.03	0.00

	SiO_2	K_2O	Na_2O	CaO	MnO	MgO	TiO_2	P_2O_5	FeO	Al_2O_3	Cr_2O_3	NiO
ZOK-2 Grt	37.8	0.01	0.06	7.17	1.17	2.56	0.07	0.00	30.9	20.9	0.09	0.00
ZOK-2 Grt	37.4	0.04	0.22	11.3	0.96	1.20	0.12	0.00	28.6	20.3	0.00	0.02
ZOK-2 Grt	37.8	0.01	0.04	11.5	0.28	1.33	0.09	0.00	29.0	20.8	0.03	0.03
ZOK-2 Grt	37.6	0.00	0.00	10.6	0.48	1.37	0.05	0.00	29.8	20.8	0.02	0.00
ZOK-2 Grt	37.5	0.01	0.04	10.5	0.97	1.16	0.08	0.01	29.8	20.3	0.01	0.00
ZOK-2 Grt	37.8	0.04	0.12	10.5	0.87	1.30	0.09	0.00	29.7	20.4	0.04	0.05
ZOK-2 Grt	38.0	0.01	0.03	8.25	0.86	1.86	0.10	0.00	31.3	21.0	0.00	0.02
ZOK-2 Grt	37.8	0.02	0.04	11.7	0.56	1.01	0.13	0.00	29.1	20.5	0.05	0.00
ZOK-2 Grt	37.6	0.00	0.05	10.5	1.00	1.21	0.12	0.00	29.8	20.3	0.02	0.00
ZOK-2 Grt	38.0	0.01	0.06	11.8	0.59	1.08	0.08	0.00	28.9	20.4	0.04	0.02
ZOK-2 Grt	37.9	0.01	0.03	11.1	0.21	1.50	0.05	0.00	28.7	21.2	0.03	0.01
ZOK-2 Grt	37.5	0.01	0.05	10.3	0.60	1.18	0.09	0.02	30.4	20.7	0.04	0.00

	SiO_2	K_2O	Na_2O	CaO	MnO	MgO	TiO_2	P_2O_5	FeO	Al_2O_3	Cr_2O_3	NiO
ZAR-1 Grt	38.1	0.00	0.03	7.49	0.24	4.23	0.06	0.00	29.3	21.7	0.00	0.02
ZAR-1 Grt	38.2	0.00	0.03	8.14	0.34	3.19	0.08	0.02	29.7	21.5	0.02	0.00
ZAR-1 Grt	38.4	0.00	0.03	7.99	0.30	3.68	0.01	0.03	29.1	21.2	0.00	0.02
ZAR-1 Grt	38.3	0.00	0.04	8.40	0.36	3.46	0.04	0.01	29.2	21.5	0.02	0.00
ZAR-1 Grt	38.5	0.00	0.03	8.21	0.38	3.23	0.06	0.04	29.7	21.5	0.01	0.00
ZAR-1 Grt	38.7	0.01	0.02	7.81	0.29	4.17	0.02	0.00	28.8	21.7	0.00	0.02
ZAR-1 Grt	38.4	0.01	0.01	8.96	0.34	2.97	0.07	0.02	29.0	21.4	0.01	0.00
ZAR-1 Grt	38.0	0.00	0.04	7.77	0.29	3.78	0.02	0.00	29.3	21.6	0.00	0.02
ZAR-1 Grt	38.4	0.01	0.02	8.40	0.35	3.35	0.00	0.00	29.1	21.6	0.01	0.00
ZAR-1 Grt	38.4	0.01	0.03	8.40	0.37	3.10	0.04	0.01	29.5	21.5	0.01	0.04
ZAR-1 Grt	38.2	0.00	0.03	8.24	0.30	3.60	0.05	0.01	29.0	21.6	0.02	0.04
ZAR-1 Grt	38.4	0.00	0.03	7.32	0.29	4.41	0.03	0.02	29.0	21.6	0.02	0.00
ZAR-1 Grt	38.4	0.01	0.06	7.29	0.33	4.67	0.03	0.00	28.4	21.7	0.01	0.00
ZAR-1 Grt	38.2	0.00	0.04	7.93	0.26	4.00	0.00	0.00	28.8	21.6	0.00	0.03
ZAR-1 Grt	38.6	0.00	0.02	7.67	0.29	4.70	0.05	0.00	28.4	21.8	0.00	0.02

	SiO_2	K_2O	Na_2O	CaO	MnO	MgO	TiO_2	P_2O_5	FeO	Al_2O_3	Cr_2O_3	NiO
ZAR-8 Grt	38.2	0.00	0.03	7.23	3.07	3.22	0.03	0.00	27.9	21.2	0.00	0.01
ZAR-8 Grt	39.1	0.00	0.03	6.26	0.72	6.70	0.05	0.02	26.7	21.8	0.04	0.00
ZAR-8 Grt	37.9	0.00	0.02	7.83	5.06	2.62	0.09	0.02	26.1	21.1	0.03	0.00
ZAR-8 Grt	39.0	0.00	0.05	6.56	0.80	5.89	0.02	0.00	27.4	21.8	0.01	0.01
ZAR-8 Grt	38.2	0.01	0.05	6.62	1.51	4.76	0.06	0.01	28.0	21.6	0.03	0.00
ZAR-8 Grt	38.7	0.01	0.02	6.23	0.76	6.30	0.03	0.02	27.2	21.9	0.00	0.04
ZAR-8 Grt	38.5	0.01	0.04	6.74	1.12	5.21	0.02	0.02	27.9	21.8	0.01	0.00
ZAR-8 Grt	38.4	0.00	0.06	6.63	0.95	5.49	0.04	0.01	27.6	21.8	0.02	0.00
ZAR-8 Grt	38.5	0.00	0.05	6.43	0.87	5.82	0.04	0.00	27.3	21.7	0.01	0.00
ZAR-8 Grt	38.7	0.03	0.08	6.60	0.83	5.84	0.03	0.00	27.3	21.7	0.00	0.02

	SiO_2	K_2O	Na_2O	CaO	MnO	MgO	TiO_2	P_2O_5	FeO	Al_2O_3	Cr_2O_3	NiO
ZAR-6 Grt	38.8	0.00	0.05	7.51	1.22	6.47	0.05	0.02	25.3	21.8	0.01	0.00
ZAR-6 Grt	38.3	0.00	0.05	6.98	2.27	6.04	0.02	0.00	25.2	21.6	0.01	0.00

Table A·1 cont.

	SiO_2	K_2O	Na_2O	CaO	MnO	MgO	TiO_2	P_2O_5	FeO	Al_2O_3	Cr_2O_3	NiO
ZAR-6 Grt	38.8	0.01	0.04	6.83	0.86	7.29	0.03	0.00	24.9	22.0	0.02	0.00
ZAR-6 Grt	39.0	0.02	0.04	6.66	0.90	7.05	0.05	0.03	25.6	22.0	0.00	0.00
ZAR-6 Grt	38.4	0.01	0.06	6.53	1.95	6.41	0.03	0.01	25.6	21.7	0.00	0.01

	SiO_2	K_2O	Na_2O	CaO	MnO	MgO	TiO_2	P_2O_5	FeO	Al_2O_3	Cr_2O_3	NiO
ZAR-5 Grt	38.4	0.00	0.02	6.55	1.08	5.73	0.04	0.00	27.5	21.7	0.02	0.00
ZAR-5 Grt	38.9	0.01	0.04	5.94	0.71	6.52	0.02	0.01	27.2	21.6	0.02	0.00
ZAR-5 Grt	38.8	0.00	0.04	6.50	1.16	5.68	0.02	0.02	27.3	21.4	0.04	0.01
ZAR-5 Grt	38.7	0.00	0.03	6.24	1.04	5.93	0.05	0.03	27.4	21.6	0.04	0.04
ZAR-5 Grt	38.5	0.00	0.04	6.20	1.16	5.61	0.02	0.02	28.0	21.5	0.04	0.02
ZAR-5 Grt	38.6	0.01	0.05	5.98	1.23	5.83	0.02	0.03	27.5	21.6	0.00	0.00

Zermatt-Saas-Fee Ophiolite, Blueshists

Pfulwe	SiO_2	K_2O	Na_2O	CaO	MnO	MgO	TiO_2	P_2O_5	FeO	Al_2O_3	Cr_2O_3	NiO
ZM-B2 Grt	38.7	0.00	0.05	5.82	0.75	5.42	0.01	0.02	29.0	21.4	0.02	0.02
ZM-B2 Grt	38.5	0.00	0.04	5.85	0.87	5.39	0.04	0.00	29.1	21.5	0.02	0.00
ZM-B2 Grt	38.4	0.00	0.03	5.91	1.33	5.02	0.05	0.01	29.3	21.5	0.00	0.01
ZM-B2 Grt	38.7	0.01	0.03	5.83	0.62	6.11	0.02	0.00	28.1	21.7	0.05	0.00
ZM-B2 Grt	38.6	0.00	0.02	6.23	0.87	5.38	0.04	0.00	28.7	21.3	0.01	0.02
ZM-B2 Grt	38.9	0.00	0.02	5.80	0.67	6.02	0.05	0.00	28.4	21.7	0.00	0.00
ZM-B2 Grt	38.7	0.00	0.04	5.92	0.54	5.79	0.04	0.01	28.7	21.5	0.04	0.01
ZM-B2 Grt	38.8	0.00	0.03	5.61	0.56	5.77	0.05	0.05	29.0	21.6	0.03	0.04
ZM-B2 Grt	38.7	0.00	0.06	5.66	0.53	5.72	0.02	0.00	29.0	21.6	0.03	0.00
ZM-B2 Grt	38.6	0.00	0.03	6.15	0.68	5.35	0.05	0.01	28.9	21.5	0.00	0.03

Vendée (Bretagne) eclogites

	SiO_2	K_2O	Na_2O	CaO	MnO	MgO	TiO_2	P_2O_5	FeO	Al_2O_3	Cr_2O_3	NiO
SBE3-1 Grt	39.4	0.00	0.05	9.08	0.50	8.26	0.19	0.04	20.7	21.9	0.10	0.00
SBE3-1 Grt	38.8	0.00	0.05	9.17	0.39	7.10	0.06	0.03	22.3	21.8	0.04	0.00
SBE3-1 Grt	39.2	0.00	0.02	8.56	0.36	8.52	0.03	0.02	20.7	22.2	0.03	0.00
SBE3-1 Grt	39.6	0.01	0.04	9.07	0.59	8.17	0.15	0.03	20.9	21.8	0.06	0.00
SBE3-1 Grt	39.2	0.00	0.03	8.82	0.34	8.52	0.10	0.00	20.7	22.2	0.02	0.00
SBE3-1 Grt	38.6	0.00	0.04	8.90	0.56	8.09	0.98	0.03	20.6	21.7	0.05	0.00
SBE3-1 Grt	39.4	0.00	0.05	9.44	0.51	6.84	0.19	0.02	22.3	21.5	0.09	0.00
SBE3-1 Grt	39.3	0.00	0.08	9.04	0.56	8.31	0.11	0.03	20.7	22.1	0.00	0.00
SBE3-1 Grt	39.3	0.01	0.03	8.53	0.51	8.50	0.05	0.05	21.0	22.1	0.06	0.00
SBE3-1 Grt	39.3	0.00	0.06	8.65	0.60	8.43	0.10	0.01	20.8	22.1	0.02	0.00

Cabo Ortegal eclogites

	SiO_2	K_2O	Na_2O	CaO	MnO	MgO	TiO_2	P_2O_5	FeO	Al_2O_3	Cr_2O_3	NiO
SCO16-1 Grt	38.3	0.00	0.04	8.60	0.43	8.35	0.07	0.03	21.7	22.2	0.00	0.00
SCO16-1 Grt	38.4	0.02	0.05	8.69	0.46	8.49	0.10	0.03	20.7	22.0	0.05	0.00
SCO16-1 Grt	38.6	0.01	0.04	9.04	0.47	7.83	0.11	0.04	21.5	22.1	0.06	0.00
SCO16-1 Grt	38.7	0.00	0.07	8.63	0.46	7.87	0.06	0.00	22.0	21.9	0.07	0.00
SCO16-1 Grt	37.9	0.02	0.04	8.46	0.49	8.16	0.02	0.00	21.7	21.9	0.02	0.00
SCO16-1 Grt	40.5	0.00	0.06	8.85	0.44	8.58	0.06	0.02	21.0	22.3	0.03	0.00
SCO16-1 Grt	40.4	0.00	0.06	9.11	0.56	8.17	0.14	0.04	20.9	21.9	0.00	0.00
SCO16-1 Grt	40.2	0.01	0.06	8.95	0.44	8.32	0.03	0.00	21.0	22.0	0.00	0.00
SCO16-1 Grt	39.8	0.02	0.07	9.10	0.56	8.21	0.11	0.00	20.9	21.9	0.02	0.00
SCO16-1 Grt	40.1	0.02	0.08	9.81	0.40	8.05	0.11	0.05	20.4	21.9	0.00	0.00

Table A·1 cont.

	SiO_2	K_2O	Na_2O	CaO	MnO	MgO	TiO_2	P_2O_5	FeO	Al_2O_3	Cr_2O_3	NiO
SCO12-5 Grt	39.9	0.01	0.05	9.20	0.43	7.89	0.18	0.04	21.2	22.0	0.00	0.00
SCO12-5 Grt	39.7	0.01	0.06	9.78	0.42	7.64	0.15	0.00	21.0	22.0	0.00	0.00
SCO12-5 Grt	39.1	0.00	0.03	9.38	0.48	7.42	0.08	0.02	21.9	22.0	0.00	0.00
SCO12-5 Grt	39.4	0.00	0.05	9.64	0.34	7.59	0.05	0.02	21.5	22.2	0.00	0.00
SCO12-5 Grt	39.2	0.00	0.07	9.98	0.37	7.58	0.16	0.04	21.1	22.1	0.06	0.00
SCO12-5 Grt	39.1	0.00	0.06	8.75	0.41	8.06	0.01	0.00	21.5	22.2	0.08	0.00

	SiO_2	K_2O	Na_2O	CaO	MnO	MgO	TiO_2	P_2O_5	FeO	Al_2O_3	Cr_2O_3	NiO
SCO12-5 Grt	39.6	0.01	0.07	9.47	0.35	7.67	0.10	0.03	21.7	22.1	0.02	0.00
SCO12-5 Grt	39.6	0.01	0.02	9.08	0.41	8.08	0.04	0.04	21.5	22.3	0.01	0.00
SCO12-5 Grt	39.8	0.00	0.06	9.55	0.37	7.96	0.10	0.02	21.0	22.0	0.00	0.00
SCO12-5 Grt	39.4	0.00	0.03	9.84	0.37	7.79	0.05	0.01	20.8	22.3	0.04	0.00

Münchberger Gneiss Massif eclogites

	SiO_2	K_2O	Na_2O	CaO	MnO	MgO	TiO_2	P_2O_5	FeO	Al_2O_3	Cr_2O_3	NiO
MB-1 Grt	38.7	0.00	0.03	8.99	0.42	5.61	0.09	0.02	24.9	21.1	0.04	0.00
MB-1 Grt	38.7	0.00	0.06	9.87	0.40	5.42	0.23	0.01	25.0	21.0	0.00	0.00
MB-1 Grt	39.0	0.00	0.04	8.26	0.43	5.97	0.04	0.01	25.5	21.7	0.01	0.01
MB-1 Grt	39.1	0.01	0.03	8.69	0.47	6.04	0.05	0.00	25.2	21.8	0.02	0.03
MB-1 Grt	38.8	0.00	0.03	7.99	0.43	6.17	0.05	0.00	25.7	21.8	0.00	0.01
MB-1 Grt	38.7	0.00	0.01	9.01	0.43	5.69	0.03	0.00	25.3	21.6	0.03	0.00
MB-1 Grt	38.8	0.00	0.10	10.5	0.71	4.84	0.37	0.00	25.0	20.7	0.03	0.00
MB-1 Grt	38.9	0.01	0.06	7.95	0.43	6.09	0.03	0.01	25.8	21.7	0.03	0.01
MB-1 Grt	38.9	0.00	0.03	7.40	0.38	6.36	0.02	0.00	26.1	21.8	0.00	0.02
MB-1 Grt	38.7	0.01	0.05	9.93	0.56	5.17	0.10	0.01	24.9	21.3	0.05	0.01

Alp Arami eclogites

	SiO_2	K_2O	Na_2O	CaO	MnO	MgO	TiO_2	P_2O_5	FeO	Al_2O_3	Cr_2O_3	NiO
AA-E1 Grt	39.6	0.00	0.02	9.54	0.42	9.14	0.02	0.00	19.9	22.5	0.02	0.00
AA-E1 Grt	40.0	0.00	0.06	9.67	0.40	9.77	0.01	0.02	18.7	22.3	0.04	0.00
AA-E1 Grt	40.0	0.00	0.02	9.71	0.37	9.43	0.01	0.00	19.0	22.3	0.02	0.03
AA-E1 Grt	39.6	0.02	0.02	9.56	0.40	9.12	0.02	0.03	19.7	22.2	0.07	0.00
AA-E1 Grt	39.7	0.01	0.02	9.56	0.39	9.17	0.03	0.01	19.8	22.3	0.03	0.01
AA-E1 Grt	39.9	0.01	0.03	9.78	0.38	9.80	0.05	0.01	18.4	22.3	0.05	0.02
AA-E1 Grt	39.7	0.00	0.03	9.50	0.44	9.09	0.08	0.02	19.9	22.4	0.05	0.01
AA-E1 Grt	39.7	0.02	0.05	9.48	0.44	9.15	0.03	0.02	19.3	22.1	0.00	0.01
AA-E1 Grt	39.7	0.00	0.03	9.52	0.41	9.18	0.06	0.03	19.6	22.2	0.02	0.01
AA-E1 Grt	39.5	0.02	0.11	9.67	0.41	9.27	0.06	0.01	19.5	22.4	0.00	0.00

	SiO_2	K_2O	Na_2O	CaO	MnO	MgO	TiO_2	P_2O_5	FeO	Al_2O_3	Cr_2O_3	NiO
AA-E2 Grt	40.1	0.01	0.01	10.6	0.38	9.85	0.04	0.00	17.5	22.3	0.02	0.02
AA-E2 Grt	39.6	0.01	0.04	10.3	0.39	9.27	0.05	0.03	18.4	22.4	0.06	0.01
AA-E2 Grt	39.6	0.00	0.04	10.1	0.42	9.69	0.04	0.03	18.5	22.6	0.03	0.01
AA-E2 Grt	39.8	0.00	0.02	10.5	0.36	9.87	0.03	0.01	17.3	22.5	0.04	0.02
AA-E2 Grt	39.8	0.01	0.04	10.7	0.39	9.74	0.05	0.00	17.6	22.5	0.07	0.06
AA-E2 Grt	39.6	0.01	0.04	11.0	0.36	9.77	0.05	0.01	17.2	22.6	0.05	0.03
AA-E2 Grt	39.7	0.00	0.06	10.2	0.36	9.70	0.05	0.03	18.2	22.5	0.06	0.00
AA-E2 Grt	39.9	0.02	0.04	10.3	0.39	9.68	0.06	0.00	18.1	22.7	0.07	0.00
AA-E2 Grt	39.8	0.01	0.04	10.2	0.37	9.64	0.03	0.00	18.5	22.4	0.03	0.01
AA-E2 Grt	39.7	0.00	0.03	10.8	0.36	9.65	0.04	0.03	17.4	22.5	0.06	0.00

Table A·1 cont.

Dabie UHP terrane, peridotite

	SiO_2	K_2O	Na_2O	CaO	MnO	MgO	TiO_2	P_2O_5	FeO	Al_2O_3	Cr_2O_3	NiO
DB10 Grt	41.0	0.00	0.02	4.01	0.46	15.4	0.02	0.03	17.1	21.8	0.51	0.03
DB10 Grt	40.7	0.01	0.03	3.69	0.45	15.7	0.03	0.04	17.1	21.6	0.65	0.00
DB10 Grt	40.9	0.01	0.04	3.74	0.45	15.1	0.02	0.04	17.6	21.4	0.84	0.00
DB10 Grt	40.6	0.01	0.06	3.97	0.47	14.9	0.02	0.03	17.3	20.7	1.82	0.02
DB10 Grt	41.0	0.02	0.08	4.15	0.52	15.1	0.02	0.01	16.4	22.5	0.05	0.06
DB10 Grt	40.9	0.02	0.09	4.22	0.50	15.1	0.02	0.00	17.0	21.8	0.50	0.01
	SiO_2	K_2O	Na_2O	CaO	MnO	MgO	TiO_2	P_2O_5	FeO	Al_2O_3	Cr_2O_3	NiO
DB10 Grt	41.1	0.01	0.02	4.54	0.51	14.9	0.01	0.03	16.7	22.5	0.14	0.01
DB10 Grt	41.1	0.01	0.05	3.60	0.45	15.7	0.03	0.03	16.9	21.6	0.60	0.00
DB10 Grt	41.1	0.01	0.07	3.56	0.48	15.8	0.01	0.00	16.5	22.6	0.03	0.00
DB10 Grt	41.1	0.02	0.07	4.57	0.55	14.7	0.01	0.01	16.5	22.2	0.40	0.00
DB10 Grt	41.0	0.02	0.09	4.13	0.49	15.2	0.01	0.02	16.6	22.3	0.27	0.03

Dabie UHP terrane, eclogite

	SiO_2	K_2O	Na_2O	CaO	MnO	MgO	TiO_2	P_2O_5	FeO	Al_2O_3	Cr_2O_3	NiO
DB44 Grt	39.6	0.00	0.04	6.55	0.55	7.49	0.04	0.01	24.9	21.8	0.03	0.01
DB44 Grt	39.0	0.01	0.04	9.83	0.63	4.82	0.08	0.00	24.9	21.4	0.00	0.00
DB44 Grt	39.1	0.00	0.04	8.45	0.52	5.58	0.06	0.01	25.4	21.3	0.01	0.00
DB44 Grt	38.8	0.01	0.05	11.7	3.48	2.72	0.13	0.00	22.8	21.2	0.08	0.01
DB44 Grt	39.6	0.01	0.03	5.73	0.45	7.84	0.03	0.01	25.5	21.9	0.04	0.00
DB44 Grt	39.2	0.00	0.05	10.8	1.33	4.70	0.08	0.00	23.2	21.5	0.03	0.00
DB44 Grt	39.4	0.01	0.05	7.40	0.64	6.46	0.04	0.01	25.4	21.7	0.03	0.00
DB44 Grt	39.5	0.01	0.04	6.15	0.62	7.16	0.04	0.01	26.0	21.8	0.03	0.00
DB44 Grt	39.5	0.01	0.04	7.57	0.45	6.24	0.05	0.01	25.6	21.7	0.03	0.01
DB44 Grt	39.5	0.00	0.05	7.48	0.44	6.77	0.07	0.02	24.9	21.7	0.00	0.01
	SiO_2	K_2O	Na_2O	CaO	MnO	MgO	TiO_2	P_2O_5	FeO	Al_2O_3	Cr_2O_3	NiO
DB05 Grt	39.3	0.01	0.04	7.38	0.39	6.52	0.04	0.02	25.5	21.6	0.01	0.00
DB05 Grt	39.4	0.00	0.04	7.95	0.38	6.24	0.04	0.02	25.3	21.4	0.03	0.00
DB05 Grt	39.3	0.00	0.05	6.66	0.40	6.78	0.03	0.00	25.8	21.6	0.01	0.01
DB05 Grt	39.4	0.00	0.06	7.90	0.38	6.42	0.06	0.02	25.1	21.3	0.03	0.00
DB05 Grt	39.3	0.01	0.05	7.88	0.38	6.32	0.05	0.02	25.4	21.3	0.03	0.00
	SiO_2	K_2O	Na_2O	CaO	MnO	MgO	TiO_2	P_2O_5	FeO	Al_2O_3	Cr_2O_3	NiO
DB63 Grt	39.2	0.01	0.07	17.1	0.39	3.36	0.19	0.01	18.7	20.7	0.01	0.00
DB63 Grt	39.4	0.00	0.06	16.3	0.42	3.29	0.14	0.02	19.7	21.0	0.01	0.01
DB63 Grt	39.2	0.01	0.08	16.4	0.40	3.46	0.17	0.01	19.2	20.9	0.03	0.00
DB63 Grt	39.4	0.01	0.07	16.1	0.41	3.39	0.14	0.02	19.7	21.1	0.01	0.00
DB63 Grt	39.4	0.01	0.07	16.3	0.41	3.47	0.13	0.01	19.0	21.1	0.02	0.00
	SiO_2	K_2O	Na_2O	CaO	MnO	MgO	TiO_2	P_2O_5	FeO	Al_2O_3	Cr_2O_3	NiO
DB48 Grt	39.6	0.00	0.03	5.62	0.61	7.37	0.02	0.00	25.9	21.9	0.01	0.01
DB48 Grt	40.0	0.00	0.03	5.06	0.60	8.89	0.03	0.01	24.5	22.1	0.01	0.00
DB48 Grt	38.9	0.00	0.04	11.8	2.47	2.77	0.14	0.00	23.4	21.3	0.07	0.00
DB48 Grt	39.8	0.00	0.03	4.48	0.73	8.51	0.04	0.01	25.6	21.9	0.04	0.01
DB48 Grt	39.9	0.00	0.04	5.07	0.54	8.71	0.02	0.02	24.9	22.1	0.02	0.00

Table A·1 cont.

Sulu UHP terrane, eclogite

	SiO_2	K_2O	Na_2O	CaO	MnO	MgO	TiO_2	P_2O_5	FeO	Al_2O_3	Cr_2O_3	NiO
PH10 Grt	41.0	0.01	0.02	8.83	0.46	11.7	0.02	0.02	16.5	22.1	0.05	0.01
PH10 Grt	40.9	0.01	0.03	9.77	0.43	11.3	0.02	0.02	15.8	22.2	0.06	0.01
PH10 Grt	40.7	0.00	0.02	8.71	0.48	10.6	0.02	0.01	18.2	22.2	0.03	0.00
PH10 Grt	40.8	0.00	0.02	8.91	0.44	11.2	0.01	0.01	16.9	22.2	0.04	0.00
PH10 Grt	40.8	0.00	0.02	8.24	0.45	11.6	0.03	0.02	17.3	22.1	0.05	0.00
PH10 Grt	41.0	0.00	0.03	8.78	0.48	11.8	0.02	0.02	16.4	22.2	0.05	0.01
PH10 Grt	40.8	0.00	0.03	8.88	0.46	11.5	0.01	0.02	16.7	22.1	0.05	0.01
PH10 Grt	40.8	0.00	0.02	8.79	0.43	11.5	0.02	0.02	16.8	22.1	0.04	0.00
PH10 Grt	40.8	0.00	0.03	8.30	0.47	11.5	0.02	0.03	17.4	22.1	0.04	0.00
PH10 Grt	40.8	0.01	0.03	8.83	0.46	11.4	0.02	0.02	16.6	22.1	0.04	0.01

Table A·2: Major element concentrations of clinopyroxenes in eclogites, peridotites and blueshists (electron microprobe, values in wt-%)

Zermatt - Pfulwe eclogite											
	SiO_2	K_2O	Na_2O	CaO	MnO	MgO	TiO_2	P_2O_5	FeO	Al_2O_3	Cr_2O_3	NiO
PfL02 Cpx	59.79	0.02	7.74	0.80	0.02	12.16	0.02	0.02	8.04	11.36	0.01	0.01
PfL02 Cpx	59.97	0.03	7.71	0.47	0.03	11.57	0.00	0.02	9.10	11.04	0.02	0.05
PfL02 Cpx	66.78	0.02	9.53	0.30	0.00	6.04	0.06	0.00	1.13	16.10	0.05	0.00
PfL02 Cpx	60.56	0.05	7.40	0.85	0.00	13.17	0.02	0.00	6.12	11.78	0.04	0.02
PfL02 Cpx	60.30	0.03	7.53	0.54	0.00	12.15	0.02	0.00	8.11	11.25	0.04	0.03
PfL02 Cpx	60.87	0.03	7.47	0.82	0.02	12.96	0.00	0.00	6.09	11.71	0.04	0.00
	SiO_2	K_2O	Na_2O	CaO	MnO	MgO	TiO_2	P_2O_5	FeO	Al_2O_3	Cr_2O_3	NiO
Pf03 Cpx	56.58	0.02	8.48	10.64	0.00	7.07	0.10	0.01	4.47	12.55	0.03	0.06
Pf03 Cpx	56.37	0.01	8.71	10.32	0.03	6.83	0.06	0.00	4.74	12.90	0.02	0.02
Pf03 Cpx	55.92	0.00	7.77	11.76	0.18	7.02	0.02	0.00	6.64	10.60	0.05	0.04
Pf03 Cpx	56.43	0.02	8.13	11.17	0.06	6.86	0.06	0.00	6.43	10.83	0.00	0.02
Pf03 Cpx	56.42	0.01	8.33	10.93	0.07	6.69	0.04	0.00	6.05	11.44	0.02	0.00
Pf03 Cpx	56.81	0.02	8.07	11.17	0.07	7.24	0.02	0.00	5.21	11.33	0.05	0.02
	SiO_2	K_2O	Na_2O	CaO	MnO	MgO	TiO_2	P_2O_5	FeO	Al_2O_3	Cr_2O_3	NiO
Pf07 Cpx	60.19	0.01	7.62	0.54	0.02	12.39	0.04	0.04	7.45	11.61	0.05	0.05
Pf07 Cpx	60.56	0.03	7.50	0.80	0.01	13.28	0.01	0.00	5.89	11.87	0.05	0.00
Pf07 Cpx	60.10	0.03	7.54	0.78	0.00	12.27	0.01	0.00	7.24	12.01	0.02	0.01
Pf07 Cpx	60.56	0.02	7.47	0.86	0.01	13.08	0.01	0.00	6.03	11.93	0.00	0.03
Pf07 Cpx	60.66	0.02	7.71	0.32	0.00	12.10	0.03	0.00	7.52	11.53	0.06	0.05
Pf07 Cpx	60.46	0.01	7.42	0.78	0.05	12.50	0.01	0.00	6.87	11.85	0.06	0.00
	SiO_2	K_2O	Na_2O	CaO	MnO	MgO	TiO_2	P_2O_5	FeO	Al_2O_3	Cr_2O_3	NiO
Pf02 Cpx	50.78	0.19	3.29	8.81	0.18	14.11	0.03	0.00	12.54	10.02	0.02	0.04
Pf02 Cpx	49.85	0.13	2.91	9.71	0.20	14.60	0.02	0.00	13.59	8.88	0.03	0.07
Pf02 Cpx	60.12	0.05	5.43	7.93	0.07	11.27	0.00	0.03	4.91	10.16	0.02	0.03
Pf02 Cpx	52.10	0.17	2.79	9.31	0.16	14.93	0.13	0.00	11.75	8.67	0.00	0.00
Pf02 Cpx	51.30	0.17	2.77	9.74	0.17	14.72	0.06	0.02	11.90	9.03	0.05	0.08
Pf02 Cpx	50.26	0.16	3.27	8.84	0.22	13.16	0.01	0.00	14.33	9.69	0.02	0.04
Pf02 Cpx	52.35	0.18	2.38	9.97	0.14	15.29	0.19	0.04	11.60	7.84	0.03	0.01
	SiO_2	K_2O	Na_2O	CaO	MnO	MgO	TiO_2	P_2O_5	FeO	Al_2O_3	Cr_2O_3	NiO
Pf05 Cpx	58.69	0.05	7.24	5.40	0.04	8.09	0.03	0.01	6.09	12.09	0.08	0.00
Pf05 Cpx	55.63	0.02	7.77	11.01	0.03	7.27	0.03	0.00	4.45	11.97	0.00	0.00
Pf05 Cpx	58.93	0.02	7.00	0.92	0.03	12.46	0.01	0.00	6.13	11.20	0.06	0.04
Pf05 Cpx	56.49	0.00	8.68	9.47	0.03	6.14	0.07	0.00	4.79	12.97	0.00	0.02
Pf05 Cpx	58.67	0.03	6.85	0.73	0.00	12.59	0.00	0.00	5.40	11.40	0.00	0.03
Pf05 Cpx	58.36	0.02	7.00	0.50	0.04	12.28	0.06	0.05	6.46	11.02	0.04	0.07
Pf05 Cpx	58.00	0.02	7.01	0.43	0.06	11.11	0.00	0.00	8.77	10.54	0.01	0.00
Pf05 Cpx	68.06	0.03	11.22	0.36	0.01	0.21	0.02	0.01	0.28	18.80	0.00	0.04
Pf05 Cpx	58.15	0.02	6.97	0.48	0.01	11.88	0.00	0.01	7.24	11.08	0.00	0.00
Pf05 Cpx	58.13	0.04	7.14	0.54	0.03	11.39	0.00	0.00	8.35	10.66	0.01	0.00
	SiO_2	K_2O	Na_2O	CaO	MnO	MgO	TiO_2	P_2O_5	FeO	Al_2O_3	Cr_2O_3	NiO
Pf04 Cpx	58.32	0.03	6.90	0.67	0.06	12.05	0.02	0.03	6.69	11.33	0.00	0.09
Pf04 Cpx	57.50	0.01	7.00	0.42	0.04	10.97	0.00	0.01	8.89	10.81	0.04	0.04
Pf04 Cpx	58.06	0.04	6.19	0.66	0.00	13.97	0.04	0.02	5.90	10.33	0.01	0.05
Pf04 Cpx	55.14	0.02	8.62	9.72	0.05	6.23	0.01	0.00	6.10	11.81	0.08	0.09
Pf04 Cpx	37.65	0.01	0.05	6.88	0.66	5.71	0.01	0.02	26.97	21.75	0.05	0.02
Pf04 Cpx	57.87	0.02	7.01	0.53	0.00	11.81	0.00	0.02	7.09	11.02	0.05	0.03
Pf04 Cpx	55.58	0.01	8.24	9.93	0.00	6.36	0.05	0.00	5.41	12.06	0.02	0.00

Table A·2 cont.

	SiO_2	K_2O	Na_2O	CaO	MnO	MgO	TiO_2	P_2O_5	FeO	Al_2O_3	Cr_2O_3	NiO
Pf04 Cpx	55.66	0.01	7.49	11.59	0.03	7.39	0.05	0.00	4.65	11.26	0.00	0.03
Pf04 Cpx	58.17	0.01	6.91	0.56	0.03	11.93	0.00	0.04	6.67	11.15	0.05	0.01

	SiO_2	K_2O	Na_2O	CaO	MnO	MgO	TiO_2	P_2O_5	FeO	Al_2O_3	Cr_2O_3	NiO
ZFUR-3 Cpx	39.38	0.01	0.03	24.10	0.00	0.04	0.00	0.00	1.39	31.85	0.04	0.02
ZFUR-3 Cpx	39.43	0.00	0.03	24.04	0.02	0.03	0.05	0.02	1.52	31.67	0.04	0.01
ZFUR-3 Cpx	39.30	0.00	0.05	24.01	0.00	0.06	0.05	0.00	2.41	31.00	0.14	0.02
ZFUR-3 Cpx	39.60	0.00	0.02	24.37	0.03	0.00	0.04	0.04	1.04	32.30	0.02	0.02
ZFUR-3 Cpx	39.16	0.01	0.03	24.14	0.08	0.06	0.04	0.02	2.59	31.24	0.05	0.01
ZFUR-3 Cpx	39.38	0.03	0.08	24.16	0.06	0.05	0.05	0.02	2.68	31.01	0.03	0.03
ZFUR-3 Cpx	39.32	0.01	0.11	24.08	0.09	0.07	0.10	0.02	2.99	30.80	0.04	0.03
ZFUR-3 Cpx	39.35	0.01	0.04	24.20	0.04	0.04	0.07	0.02	1.78	31.50	0.06	0.00

	SiO_2	K_2O	Na_2O	CaO	MnO	MgO	TiO_2	P_2O_5	FeO	Al_2O_3	Cr_2O_3	NiO
ZOK-2 Cpx	39.01	0.00	0.04	24.07	0.02	0.04	0.08	0.07	2.20	31.09	0.02	0.03
ZOK-2 Cpx	39.21	0.00	0.05	24.12	0.03	0.06	0.03	0.07	2.25	31.20	0.02	0.00
ZOK-2 Cpx	38.82	0.00	0.04	24.16	0.00	0.07	0.05	0.03	2.71	30.86	0.04	0.00
ZOK-2 Cpx	39.31	0.00	0.03	24.31	0.01	0.04	0.07	0.00	1.86	31.34	0.01	0.00
ZOK-2 Cpx	38.80	0.00	0.03	23.64	0.00	0.10	0.19	0.08	4.90	28.91	0.03	0.00
ZOK-2 Cpx	39.07	0.01	0.02	24.25	0.02	0.02	0.05	0.04	1.55	31.53	0.05	0.03
ZOK-2 Cpx	39.18	0.01	0.01	23.93	0.02	0.06	0.08	0.06	2.46	30.93	0.05	0.00
ZOK-2 Cpx	47.03	0.53	7.59	0.20	0.00	0.12	0.05	0.01	0.36	39.94	0.02	0.00

Zermatt - Obere Kelle eclogite

	SiO_2	K_2O	Na_2O	CaO	MnO	MgO	TiO_2	P_2O_5	FeO	Al_2O_3	Cr_2O_3	NiO
ZAR-1 Cpx	55.99	0.01	8.34	11.40	0.04	7.02	0.03	0.00	5.30	11.54	0.03	0.00
ZAR-8 Cpx	58.12	0.03	7.54	0.46	0.02	11.46	0.01	0.01	8.28	11.16	0.00	0.03
ZAR-8 Cpx	58.18	0.05	7.45	0.51	0.02	11.64	0.02	0.01	7.88	11.18	0.03	0.02
ZAR-8 Cpx	57.94	0.04	7.52	0.63	0.03	11.83	0.01	0.00	7.91	11.20	0.03	0.02
ZAR-8 Cpx	58.06	0.05	7.49	0.72	0.03	11.85	0.03	0.02	7.75	11.27	0.03	0.02
ZAR-8 Cpx	58.03	0.02	7.36	0.63	0.02	11.65	0.03	0.01	8.12	11.20	0.04	0.00
ZAR-8 Cpx	57.99	0.05	7.31	0.75	0.01	11.86	0.01	0.01	7.92	11.30	0.01	0.01
ZAR-8 Cpx	58.32	0.08	7.57	0.38	0.02	11.28	0.02	0.00	8.72	11.02	0.05	0.02
ZAR-8 Cpx	57.99	0.05	7.30	0.73	0.03	12.11	0.01	0.00	7.51	11.42	0.01	0.04
ZAR-8 Cpx	57.98	0.04	7.29	0.73	0.01	11.82	0.05	0.00	7.87	11.23	0.02	0.03
ZAR-8 Cpx	58.31	0.03	7.37	0.63	0.02	11.75	0.02	0.00	7.87	11.19	0.02	0.02

	SiO_2	K_2O	Na_2O	CaO	MnO	MgO	TiO_2	P_2O_5	FeO	Al_2O_3	Cr_2O_3	NiO
ZAR-5 Cpx	58.35	0.02	7.10	0.78	0.02	13.05	0.00	0.00	7.78	9.80	0.00	0.04
ZAR-5 Cpx	58.17	0.02	6.96	1.15	0.00	13.48	0.03	0.00	6.39	10.58	0.01	0.04
ZAR-5 Cpx	57.92	0.01	7.05	1.14	0.02	13.19	0.00	0.00	6.92	10.38	0.00	0.02
ZAR-5 Cpx	58.46	0.02	6.89	0.98	0.03	13.00	0.03	0.01	6.99	10.64	0.03	0.05
ZAR-5 Cpx	58.28	0.02	6.83	1.29	0.04	13.09	0.03	0.00	7.20	10.32	0.00	0.04
ZAR-5 Cpx	58.34	0.03	6.96	1.07	0.01	13.38	0.03	0.00	6.38	10.53	0.00	0.03
ZAR-5 Cpx	57.66	0.02	7.15	0.98	0.03	12.96	0.01	0.01	6.90	10.63	0.04	0.04
ZAR-5 Cpx	58.16	0.04	6.84	1.26	0.03	13.46	0.02	0.03	6.33	10.59	0.01	0.03
ZAR-5 Cpx	58.27	0.02	7.05	1.01	0.02	13.13	0.04	0.00	6.54	10.65	0.02	0.01

	SiO_2	K_2O	Na_2O	CaO	MnO	MgO	TiO_2	P_2O_5	FeO	Al_2O_3	Cr_2O_3	NiO
ZAR-6 Cpx	58.13	0.03	6.85	0.87	0.04	13.21	0.01	0.01	4.99	11.62	0.02	0.04
ZAR-6 Cpx	58.43	0.02	7.08	0.81	0.02	13.27	0.05	0.00	5.15	11.48	0.00	0.01
ZAR-6 Cpx	58.50	0.03	7.03	0.95	0.02	13.08	0.04	0.00	5.44	11.35	0.00	0.02
ZAR-6 Cpx	58.53	0.03	7.11	0.78	0.03	13.04	0.02	0.01	5.62	11.43	0.00	0.01
ZAR-6 Cpx	58.54	0.03	7.01	0.86	0.03	13.18	0.03	0.00	5.43	11.36	0.00	0.01
ZAR-6 Cpx	57.87	0.02	6.97	0.94	0.04	12.97	0.02	0.01	5.34	11.31	0.01	0.00
ZAR-6 Cpx	58.46	0.02	7.16	0.97	0.03	13.30	0.04	0.01	5.20	11.39	0.00	0.00

Table A·2 cont.

	SiO_2	K_2O	Na_2O	CaO	MnO	MgO	TiO_2	P_2O_5	FeO	Al_2O_3	Cr_2O_3	NiO
ZAR-6 Cpx	58.78	0.02	7.14	0.95	0.03	13.55	0.04	0.00	5.07	11.37	0.01	0.02
ZAR-6 Cpx	57.99	0.04	6.73	1.33	0.03	13.24	0.01	0.02	5.46	11.19	0.00	0.01
ZAR-6 Cpx	57.91	0.03	7.03	1.09	0.06	13.06	0.03	0.02	5.48	11.38	0.00	0.00

Zermatt - Pfulwe blueshists

	SiO_2	K_2O	Na_2O	CaO	MnO	MgO	TiO_2	P_2O_5	FeO	Al_2O_3	Cr_2O_3	NiO
ZM-B2 Cpx	58.97	0.01	7.33	0.48	0.02	12.69	0.03	0.02	6.61	10.97	0.04	0.00
ZM-B2 Cpx	58.52	0.01	7.29	0.89	0.00	12.90	0.03	0.00	6.29	11.11	0.00	0.06
ZM-B2 Cpx	58.80	0.03	7.41	0.63	0.02	12.66	0.00	0.00	6.67	11.00	0.00	0.04
ZM-B2 Cpx	58.61	0.02	7.51	0.61	0.03	12.72	0.03	0.00	6.65	11.01	0.03	0.03
ZM-B2 Cpx	59.00	0.02	7.30	0.67	0.02	12.60	0.00	0.00	6.68	11.00	0.04	0.00
ZM-B2 Cpx	58.68	0.02	7.13	0.80	0.05	12.88	0.00	0.00	6.20	11.08	0.04	0.04
ZM-B2 Cpx	58.85	0.00	7.41	0.63	0.02	12.58	0.02	0.00	6.62	11.04	0.03	0.01
ZM-B2 Cpx	58.66	0.02	7.38	0.65	0.02	12.56	0.00	0.00	6.60	10.93	0.04	0.03
ZM-B2 Cpx	58.54	0.02	7.25	0.60	0.02	12.48	0.03	0.01	6.78	11.01	0.04	0.02

Vendée (Bretagne) eclogites

	SiO_2	K_2O	Na_2O	CaO	MnO	MgO	TiO_2	P_2O_5	FeO	Al_2O_3	Cr_2O_3	NiO
SBE3-1 Cpx	54.41	0.01	6.23	13.97	0.03	8.59	0.19	0.00	4.01	11.15	0.10	0.00
SBE3-1 Cpx	54.38	0.02	5.86	13.74	0.05	8.55	0.18	0.01	4.14	11.21	0.02	0.01
SBE3-1 Cpx	53.02	0.00	5.80	13.90	0.01	8.60	0.13	0.01	3.67	11.04	0.06	0.04
SBE3-1 Cpx	54.27	0.01	5.90	13.95	0.02	8.54	0.17	0.03	3.74	11.16	0.00	0.04
SBE3-1 Cpx	54.31	0.01	6.05	13.91	0.08	8.34	0.19	0.02	4.47	11.10	0.05	0.00
SBE3-1 Cpx	53.89	0.00	5.91	14.03	0.03	8.58	0.15	0.00	4.15	11.21	0.00	0.00
SBE3-1 Cpx	37.85	0.00	0.01	23.47	0.05	0.16	0.10	0.00	5.75	27.83	0.07	0.00
SBE3-1 Cpx	54.79	0.01	5.93	13.81	0.00	8.66	0.12	0.01	3.60	10.81	0.05	0.06
SBE3-1 Cpx	54.34	0.00	5.61	14.52	0.00	9.43	0.12	0.02	3.31	10.38	0.04	0.06
SBE3-1 Cpx	53.87	0.00	6.04	13.85	0.03	8.59	0.14	0.00	3.74	11.22	0.06	0.00
SBE3-1 Cpx	52.59	1.56	1.51	17.07	0.05	11.23	0.21	0.01	5.00	7.47	0.06	0.00
SBE3-1 Cpx	55.35	0.00	6.00	13.80	0.05	8.63	0.12	0.00	3.85	11.29	0.05	0.06

	SiO_2	K_2O	Na_2O	CaO	MnO	MgO	TiO_2	P_2O_5	FeO	Al_2O_3	Cr_2O_3	NiO
SCO16-1 Cpx	54.95	0.00	4.76	16.47	0.04	10.09	0.20	0.03	4.65	9.20	0.13	0.04
SCO16-1 Cpx	55.41	0.03	4.83	16.28	0.03	10.16	0.12	0.00	4.27	8.77	0.09	0.04
SCO16-1 Cpx	54.68	0.02	4.68	16.46	0.04	10.22	0.19	0.00	4.44	9.12	0.05	0.05
SCO16-1 Cpx	53.79	0.02	4.86	16.28	0.05	9.98	0.22	0.00	4.52	9.21	0.07	0.00
SCO16-1 Cpx	53.85	0.00	4.83	16.32	0.06	10.02	0.21	0.02	4.38	9.30	0.06	0.04
SCO16-1 Cpx	55.22	0.01	5.03	16.19	0.03	10.24	0.09	0.00	3.98	8.86	0.03	0.00
SCO16-1 Cpx	54.37	0.02	4.72	16.32	0.02	9.89	0.20	0.00	4.62	9.25	0.04	0.09
SCO16-1 Cpx	54.59	0.01	4.95	16.36	0.04	9.98	0.19	0.00	4.59	9.23	0.00	0.04
SCO16-1 Cpx	53.84	0.02	4.77	16.35	0.01	9.98	0.16	0.01	4.62	9.13	0.05	0.02
SCO16-1 Cpx	53.16	0.01	4.68	16.21	0.04	10.08	0.21	0.05	4.56	9.27	0.03	0.07

Cabo Ortegal eclogites

	SiO_2	K_2O	Na_2O	CaO	MnO	MgO	TiO_2	P_2O_5	FeO	Al_2O_3	Cr_2O_3	NiO
SCO12-5 Cpx	54.28	0.00	4.61	16.65	0.02	10.33	0.12	0.00	4.50	8.60	0.00	0.03
SCO12-5 Cpx	53.83	0.00	4.53	16.66	0.05	10.06	0.15	0.02	4.89	8.70	0.05	0.06
SCO12-5 Cpx	53.47	0.01	4.46	16.76	0.04	10.09	0.22	0.02	5.12	8.82	0.06	0.00
SCO12-5 Cpx	54.42	0.00	4.40	16.61	0.03	10.25	0.21	0.04	4.78	8.68	0.09	0.03
SCO12-5 Cpx	54.15	0.01	4.42	16.63	0.03	10.22	0.14	0.00	4.62	8.57	0.07	0.05
SCO12-5 Cpx	53.68	0.00	4.51	16.60	0.04	10.13	0.19	0.00	5.07	9.17	0.07	0.00
SCO12-5 Cpx	53.73	0.02	4.52	16.59	0.06	10.25	0.20	0.04	4.93	8.78	0.00	0.04
SCO12-5 Cpx	53.59	0.01	4.68	16.71	0.02	10.19	0.17	0.02	4.73	8.81	0.08	0.04
SCO12-5 Cpx	53.30	0.01	4.51	16.49	0.02	10.14	0.24	0.02	4.77	8.78	0.06	0.00

Table A·2 cont.

	SiO_2	K_2O	Na_2O	CaO	MnO	MgO	TiO_2	P_2O_5	FeO	Al_2O_3	Cr_2O_3	NiO
SCO12-5 Cpx	53.55	0.02	4.53	16.56	0.05	10.27	0.20	0.03	4.94	8.82	0.00	0.01
SCO12-5 Cpx	45.14	0.38	3.17	9.92	0.01	13.99	0.66	0.02	8.87	13.65	0.11	0.05
SCO12-5 Cpx	45.11	0.30	2.89	10.16	0.07	14.10	0.81	0.00	9.08	13.28	0.04	0.03
SCO12-5 Cpx	44.25	0.27	2.99	10.20	0.04	13.78	0.64	0.00	9.22	14.26	0.06	0.04
SCO12-5 Cpx	45.99	0.36	3.25	9.83	0.01	13.48	0.63	0.01	9.61	13.55	0.02	0.05
SCO12-5 Cpx	44.79	0.30	3.13	10.31	0.07	13.48	0.61	0.00	9.59	14.32	0.08	0.00
SCO12-5 Cpx	44.82	0.48	3.14	9.99	0.04	14.04	0.71	0.01	8.81	13.86	0.07	0.00
SCO12-5 Cpx	45.56	0.26	2.95	10.07	0.05	14.07	0.74	0.02	9.29	13.77	0.09	0.03
SCO12-5 Cpx	45.18	0.62	3.15	9.88	0.02	13.78	0.69	0.00	9.02	14.10	0.07	0.03
SCO12-5 Cpx	44.70	0.52	3.13	9.93	0.03	13.86	0.66	0.00	8.98	14.04	0.03	0.04
SCO12-5 Cpx	45.07	0.49	3.14	10.01	0.02	13.85	0.67	0.00	8.85	14.23	0.10	0.04

Dabie UHP - peridotite

	SiO_2	K_2O	Na_2O	CaO	MnO	MgO	TiO_2	P_2O_5	FeO	Al_2O_3	Cr_2O_3	NiO
DB10 Cpx	50.47	0.18	1.44	11.15	0.16	19.85	0.15	0.01	5.95	7.25	0.18	0.05
DB10 Cpx	40.74	0.01	0.18	3.98	0.46	15.35	0.03	0.03	17.17	21.23	0.60	0.00
DB10 Cpx	50.66	0.14	1.42	11.13	0.15	20.13	0.21	0.00	5.57	6.75	0.32	0.06
DB10 Cpx	57.51	0.00	0.02	0.08	0.08	33.25	0.01	0.00	8.71	0.17	0.00	0.05
DB10 Cpx	45.71	0.01	0.38	9.95	0.32	15.76	0.02	0.02	12.41	14.89	0.43	0.01
DB10 Cpx	41.06	0.00	0.03	4.00	0.48	15.21	0.03	0.03	17.12	21.63	0.80	0.00
DB10 Cpx	40.14	0.00	0.01	0.01	0.10	45.94	0.00	0.00	13.81	0.01	0.00	0.27
DB10 Cpx	55.02	0.00	1.00	22.41	0.04	16.43	0.00	0.00	3.46	0.54	0.13	0.03
DB10 Cpx	50.07	0.21	1.38	11.84	0.17	18.90	0.18	0.01	6.54	6.89	0.09	0.04
DB10 Cpx	45.12	0.08	1.15	12.24	0.20	16.07	0.09	0.01	9.47	13.99	0.41	0.04

Dabie & Sulu UHP, eclogite

	SiO_2	K_2O	Na_2O	CaO	MnO	MgO	TiO_2	P_2O_5	FeO	Al_2O_3	Cr_2O_3	NiO
DB44 Cpx	56.46	0.03	8.03	9.32	0.02	6.97	0.06	0.00	4.92	13.21	0.03	0.02
DB44 Cpx	57.86	0.02	7.73	10.84	0.03	6.88	0.04	0.01	4.21	11.60	0.07	0.02
DB44 Cpx	59.13	0.03	7.52	8.69	0.04	5.42	0.04	0.00	3.65	14.86	0.03	0.01
DB44 Cpx	56.18	0.01	8.34	10.57	0.01	6.82	0.02	0.00	7.01	10.18	0.03	0.00
DB44 Cpx	58.95	0.01	8.20	9.85	0.02	6.36	0.03	0.01	3.34	12.93	0.07	0.01
DB44 Cpx	56.58	0.01	7.69	11.80	0.03	7.86	0.04	0.01	3.65	11.57	0.04	0.02
DB44 Cpx	60.69	0.09	7.61	8.45	0.02	6.03	0.06	0.01	3.33	13.83	0.07	0.02
DB44 Cpx	55.81	0.03	7.38	7.60	0.03	6.92	0.13	0.00	5.67	15.93	0.05	0.03
DB44 Cpx	54.06	0.11	4.45	14.19	0.08	10.90	0.07	0.01	8.37	7.01	0.02	0.01
DB44 Cpx	58.30	0.04	7.46	11.34	0.02	7.05	0.03	0.00	3.73	11.81	0.05	0.02
DB44 Cpx	55.51	0.02	6.58	10.70	0.05	8.52	0.07	0.00	5.58	12.24	0.06	0.02

	SiO_2	K_2O	Na_2O	CaO	MnO	MgO	TiO_2	P_2O_5	FeO	Al_2O_3	Cr_2O_3	NiO
DB05 Cpx	55.82	0.03	5.52	15.13	0.03	9.80	0.05	0.01	6.55	6.61	0.05	0.03
DB05 Cpx	55.94	0.03	5.65	14.89	0.03	9.80	0.05	0.00	6.43	6.62	0.04	0.02
DB05 Cpx	56.11	0.03	5.58	15.01	0.03	9.85	0.05	0.00	6.53	6.53	0.05	0.02

	SiO_2	K_2O	Na_2O	CaO	MnO	MgO	TiO_2	P_2O_5	FeO	Al_2O_3	Cr_2O_3	NiO
DB63 Cpx	56.04	0.05	5.51	15.43	0.02	9.73	0.05	0.01	5.46	7.46	0.02	0.02
DB63 Cpx	55.78	0.05	5.53	15.13	0.03	9.64	0.05	0.01	5.59	7.23	0.02	0.02
DB63 Cpx	56.11	0.04	5.65	15.24	0.02	9.63	0.04	0.00	5.24	7.74	0.04	0.02

	SiO_2	K_2O	Na_2O	CaO	MnO	MgO	TiO_2	P_2O_5	FeO	Al_2O_3	Cr_2O_3	NiO
DB48 Cpx	59.53	0.11	7.08	9.81	0.05	6.22	0.03	0.00	4.34	13.02	0.07	0.00
DB48 Cpx	60.19	0.12	7.03	9.62	0.03	6.11	0.03	0.00	3.84	13.81	0.06	0.01
DB48 Cpx	54.66	0.21	4.77	12.13	0.06	10.29	0.07	0.00	7.24	9.94	0.05	0.02
DB48 Cpx	61.69	0.19	8.41	5.82	0.03	4.45	0.05	0.00	2.81	17.06	0.03	0.01
DB48 Cpx	58.04	0.12	5.94	11.33	0.05	8.29	0.03	0.01	4.96	11.45	0.02	0.02
DB48 Cpx	59.50	0.05	6.03	12.83	0.05	7.48	0.02	0.00	3.29	11.40	0.04	0.01

Table A·2 cont.

	SiO_2	K_2O	Na_2O	CaO	MnO	MgO	TiO_2	P_2O_5	FeO	Al_2O_3	Cr_2O_3	NiO
DB48 Cpx	57.62	0.12	5.59	11.95	0.05	8.53	0.04	0.00	5.70	10.81	0.04	0.01

	SiO_2	K_2O	Na_2O	CaO	MnO	MgO	TiO_2	P_2O_5	FeO	Al_2O_3	Cr_2O_3	NiO
PH10 Cpx	56.48	0.01	6.76	13.11	0.02	8.67	0.05	0.01	5.87	9.14	0.06	0.03
PH10 Cpx	56.07	0.01	6.72	13.40	0.03	8.85	0.05	0.00	6.08	8.74	0.05	0.05

Alpe Aramai eclogite

	SiO_2	K_2O	Na_2O	CaO	MnO	MgO	TiO_2	P_2O_5	FeO	Al_2O_3	Cr_2O_3	NiO
AA-E1 Cpx	55.71	0.00	6.49	14.12	0.04	9.11	0.09	0.01	2.93	11.25	0.00	0.00
AA-E1 Cpx	55.47	0.02	6.80	13.64	0.01	8.78	0.09	0.00	2.74	11.77	0.02	0.02
AA-E1 Cpx	54.85	0.02	6.50	14.19	0.01	8.90	0.11	0.01	3.28	11.57	0.06	0.03
AA-E1 Cpx	54.09	0.01	6.24	14.51	0.02	8.78	0.25	0.00	3.51	11.73	0.23	0.02
AA-E1 Cpx	55.52	0.00	6.37	14.21	0.02	9.18	0.11	0.00	2.89	11.38	0.01	0.02
AA-E1 Cpx	55.39	0.00	6.97	13.13	0.05	8.40	0.08	0.00	2.87	12.27	0.03	0.01
AA-E1 Cpx	43.41	0.07	3.69	10.96	0.04	15.97	0.53	0.02	8.07	13.58	0.08	0.08
AA-E1 Cpx	54.70	0.01	5.82	14.75	0.04	9.29	0.10	0.00	3.51	11.14	0.01	0.01
AA-E1 Cpx	55.15	0.00	6.94	13.48	0.05	8.49	0.17	0.01	2.86	12.38	0.01	0.03
AA-E1 Cpx	55.23	0.00	6.83	13.66	0.03	8.80	0.12	0.00	2.82	11.89	0.02	0.04

	SiO_2	K_2O	Na_2O	CaO	MnO	MgO	TiO_2	P_2O_5	FeO	Al_2O_3	Cr_2O_3	NiO
AA-E2 Cpx	55.49	0.00	6.19	14.63	0.03	9.41	0.13	0.00	2.60	11.30	0.01	0.05
AA-E2 Cpx	55.11	0.01	6.23	14.52	0.01	9.40	0.11	0.00	2.65	11.24	0.00	0.05
AA-E2 Cpx	55.15	0.00	6.13	14.52	0.03	9.45	0.15	0.00	2.90	11.18	0.08	0.04
AA-E2 Cpx	55.35	0.00	5.89	15.00	0.00	9.78	0.10	0.00	2.75	10.63	0.02	0.03
AA-E2 Cpx	55.26	0.01	6.13	14.54	0.02	9.32	0.13	0.03	2.87	11.29	0.06	0.05
AA-E2 Cpx	55.47	0.00	6.00	14.74	0.03	9.60	0.07	0.00	2.49	10.69	0.01	0.06
AA-E2 Cpx	55.40	0.00	5.91	14.57	0.03	9.39	0.13	0.00	2.78	11.32	0.02	0.01
AA-E2 Cpx	55.12	0.01	5.98	14.64	0.01	9.36	0.11	0.01	2.66	11.26	0.00	0.01
AA-E2 Cpx	55.32	0.01	6.00	15.04	0.03	9.69	0.08	0.01	2.55	10.87	0.03	0.07

Münchberger Gneiss massif eclogite

	SiO_2	K_2O	Na_2O	CaO	MnO	MgO	TiO_2	P_2O_5	FeO	Al_2O_3	Cr_2O_3	NiO
MB-1 Cpx	55.75	0.01	6.66	13.44	0.02	8.27	0.12	0.00	5.78	10.05	0.02	0.01
MB-1 Cpx	55.45	0.00	6.73	13.26	0.04	8.18	0.12	0.01	5.85	10.11	0.01	0.01
MB-1 Cpx	54.94	0.00	6.57	13.39	0.02	8.17	0.14	0.01	5.74	9.95	0.00	0.00
MB-1 Cpx	55.08	0.00	6.78	13.32	0.03	8.18	0.12	0.00	5.90	9.88	0.01	0.02
MB-1 Cpx	54.30	0.01	6.44	13.27	0.02	8.14	0.13	0.04	5.72	9.74	0.05	0.00
MB-1 Cpx	55.70	0.01	6.57	13.39	0.04	8.18	0.11	0.00	5.88	9.98	0.03	0.00
MB-1 Cpx	55.11	0.01	6.76	13.18	0.03	8.25	0.11	0.00	5.79	10.02	0.02	0.01
MB-1 Cpx	54.92	0.00	6.57	13.52	0.05	8.21	0.13	0.00	5.87	9.99	0.06	0.00
MB-1 Cpx	54.91	0.00	6.60	13.49	0.00	8.20	0.09	0.00	5.79	10.01	0.00	0.00
MB-1 Cpx	55.32	0.00	6.69	13.34	0.04	8.30	0.10	0.01	5.85	9.99	0.01	0.00

Table A·3: HFSE concentrations in garnet and clinopyroxene of selected samples, as a basis for the HFSE budget calculations of table 1·2 (LA-ICPMS, values in ppm).

SCO12-5	Ti	Zr	Nb	Hf	Ta	**SCO15-1**	Ti	Zr	Nb	Hf	Ta
grt1	7966	11.2	1.39	0.268	0.034	grt1	776.0	7.80	<0.01	0.122	<0.01
grt2	800.6	6.16	<0.01	0.096	0.02	grt2	2587	21.4	0.20	0.498	<0.01
grt3	2480	4.62	0.37	0.086	<0.01	grt3	684.4	6.28	<0.01	0.096	<0.01
grt4	934.6	11.1	<0.01	0.138	<0.01	grt4	65.6	0.44	<0.01	0.006	<0.01
grt5	695.5	4.75	0.02	0.076	0.02	grt5	1318	7.07	0.07	0.122	<0.01
grt6	588.5	4.64	<0.01	0.073	<0.01	grt6	2859	18.5	0.249	0.516	<0.01
grt7	600.3	4.77	<0.01	0.082	<0.01	grt7	848.4	12.1	<0.01	0.190	<0.01
grt8	1043	5.67	0.07	0.097	0.03	grt8	1090	13.3	<0.01	0.211	<0.01
grt9	398.1	3.76	<0.01	0.050	<0.01	grt9	1697	9.16	0.09	0.168	<0.01
grt10	3208	6.01	0.613	0.129	0.03	grt10	1040	6.69	0.05	0.108	<0.01
cpx1	1021	12.9	<0.01	0.629	<0.01	cpx1	1415	12.6	0.1	0.663	<0.01
cpx2	1042	13.2	<0.01	0.644	<0.01	cpx2	810.6	9.78	<0.01	0.597	<0.01
cpx3	1034	13.3	<0.01	0.650	<0.01	cpx3	844.5	10.9	<0.01	0.631	<0.01
cpx4	1168	12.3	<0.01	0.563	<0.01	cpx4	924.0	11.8	<0.01	0.649	<0.01
cpx5	779.2	8.75	<0.01	0.435	<0.01	cpx5	857.7	9.67	<0.01	0.501	<0.01
cpx6	891.5	10.2	<0.01	0.491	<0.01	cpx6	818.0	9.50	<0.01	0.513	<0.01
cpx7	889.5	10.2	<0.01	0.504	<0.01	cpx7	980.5	12.1	<0.01	0.635	<0.01
cpx8	789.4	9.87	<0.01	0.538	<0.01	cpx8	953.3	12.7	<0.01	0.701	<0.01
cpx9	776.2	9.08	<0.01	0.510	<0.01	cpx9	841.4	10.4	<0.01	0.585	<0.01
cpx10	767.1	9.27	<0.01	0.516	<0.01	cpx10	858.1	10.5	<0.01	0.588	<0.01

table A·3 cont.

WGR1	Ti	Zr	Nb	Hf	Ta
grt1	124.1	1.58	<0.02	0.032	<0.01
grt2	416.0	4.20	<0.02	0.062	<0.01
grt3	136.0	2.28	<0.02	0.031	<0.01
grt4	150.7	1.04	<0.02	0.042	<0.01
grt5	253.2	3.47	<0.02	0.055	<0.01
grt6	269.1	2.78	<0.02	<0.02	<0.01
grt7	274.5	2.92	<0.02	0.055	<0.01
grt8	183.0	3.53	<0.02	0.057	<0.01
grt9	256.5	3.27	<0.02	0.071	<0.01
grt10	340.2	2.78	<0.02	0.046	<0.01
cpx1	5.61	<0.06	<0.02	<0.01	<0.01
cpx2	14.8	<0.06	<0.02	0.002	<0.01
cpx3	27.9	<0.05	<0.02	<0.03	<0.01
cpx4	197.9	0.45	<0.02	0.021	<0.01
cpx5	<5.14	<0.06	<0.02	<0.02	<0.01
cpx6	1380	2.32	0.210	0.171	<0.01
cpx7	368.0	1.31	0.033	0.100	<0.01
cpx8	188.3	1.04	<0.02	0.078	<0.01
cpx9	393.5	1.73	0.03	0.107	<0.01
cpx10	332.8	1.67	<0.02	0.104	<0.01

WGR4	Ti	Zr	Nb	Hf	Ta
grt1	124.4	0.748	<0.02	<0.01	<0.01
grt2	119.6	0.662	<0.02	<0.01	<0.01
grt3	218.7	1.20	<0.02	<0.01	<0.01
grt4	131.6	0.747	<0.02	<0.01	<0.01
grt5	135.2	0.900	<0.02	0.02	<0.01
grt6	121.6	0.524	<0.02	0.01	<0.01
grt7	102.3	0.669	<0.02	0.01	<0.01
grt8	148.4	0.929	<0.02	0.02	<0.01
grt9	163.6	0.895	<0.02	<0.01	<0.01
grt10	133.5	0.640	<0.02	0.01	<0.01
cpx1	259.2	3.96	<0.02	0.16	<0.01
cpx2	313.5	5.19	<0.02	0.18	<0.01
cpx3	341.7	5.45	<0.02	0.21	<0.01
cpx4	301.9	4.88	<0.02	0.22	<0.01
cpx5	438.6	7.41	<0.02	0.28	<0.01
cpx6	275.2	4.59	<0.02	0.17	<0.01
cpx7	251.4	3.96	<0.02	0.18	<0.01
cpx8	275.4	4.53	<0.02	0.20	<0.01
cpx9	321.0	5.12	<0.02	0.19	<0.01
cpx10	336.0	4.86	<0.02	0.19	<0.01

SCO13-1	Ti	Zr	Nb	Hf	Ta
grt1	515.7	6.20	<0.01	0.094	<0.02
grt2	1388	8.27	0.100	0.117	<0.01
grt3	3279	9.99	0.413	0.163	<0.02
grt4	717.7	6.48	<0.02	0.093	<0.02
grt5	568.2	5.90	<0.01	0.089	<0.02
grt6	1287	11.6	0.06	0.154	<0.01
grt7	631.4	5.91	<0.01	0.084	<0.02
grt8	917.6	10.2	<0.02	0.132	<0.02
grt9	470.6	3.72	<0.01	0.058	<0.02
grt10	568.6	4.17	<0.01	0.071	<0.02
cpx1	1576	12.9	0.104	0.614	<0.01
cpx2	964.1	13.4	<0.02	0.671	<0.02
cpx3	1055	14.3	<0.02	0.673	<0.02
cpx4	939.5	12.5	<0.02	0.615	<0.02
cpx5	680.9	8.20	<0.02	0.474	<0.02
cpx6	1177	15.6	<0.02	0.707	<0.02
cpx7	933.8	12.3	<0.02	0.603	<0.02
cpx8	1062	12.4	<0.02	0.562	<0.02
cpx9	988.5	12.3	<0.02	0.580	<0.02
cpx10	935.0	12.1	<0.02	0.597	<0.02

SCO11-1	Ti	Zr	Nb	Hf	Ta
grt1	975.8	7.98	0.07	0.127	0.004
grt2	2400	4.47	0.513	0.095	0.022
grt3	408.1	3.98	<0.01	0.066	<0.01
grt4	574.4	6.85	<0.01	0.121	<0.01
grt5	744.3	4.99	0.101	0.097	<0.01
grt6	800.8	5.94	0.116	0.099	<0.01
grt7	3170	4.89	0.670	0.123	0.03
grt8	357.4	2.65	<0.01	0.051	<0.01
grt9	580.2	6.54	<0.01	0.121	<0.01
grt10	627.1	7.03	0.02	0.130	<0.01
cpx1	950.8	13.8	<0.01	0.682	<0.01
cpx2	806.1	12.7	<0.01	0.690	<0.01
cpx3	644.9	8.63	<0.01	0.499	<0.01
cpx4	914.0	13	<0.01	0.720	<0.01
cpx5	891.1	12.8	<0.01	0.680	<0.01
cpx6	1009	14.1	<0.01	0.690	<0.01
cpx7	783.7	10.3	<0.01	0.578	<0.01
cpx8	1314	15.1	<0.01	0.770	<0.01
cpx9	770.5	11.8	<0.01	0.650	<0.01
cpx10	953.6	14.3	<0.01	0.740	<0.01

table A·3 cont.

SBE7-5	Ti	Zr	Nb	Hf	Ta	**SBE6-1**	Ti	Zr	Nb	Hf	Ta
grt1	1102	13.9	<0.01	0.178	<0.01	grt1	869.7	9.04	<0.01	0.136	<0.01
grt2	886.1	8.94	<0.01	0.123	<0.01	grt2	1125	13.2	<0.01	0.166	<0.01
grt3	2077	9.18	0.441	0.189	0.02	grt3	2788	6.61	0.333	0.131	0.016
grt4	251.0	1.66	0.023	0.031	<0.01	grt4	642.9	7.44	<0.01	0.121	<0.01
grt5	1195	11.9	0.131	0.158	<0.01	grt5	151.0	2.10	<0.01	0.035	<0.01
grt6	1443	13.8	0.149	0.186	<0.01	grt6	862.4	9.59	<0.01	0.140	<0.01
grt7	893.6	11.8	<0.01	0.173	<0.01	grt7	1155	6.08	0.109	0.112	<0.01
grt8	594.8	7.28	<0.01	0.089	<0.01	grt8	538.4	6.26	<0.01	0.089	<0.01
grt9	525.9	4.51	<0.01	0.067	<0.01	grt9	1175	14.1	0.017	0.171	<0.01
grt10	567.3	6.61	<0.01	0.091	<0.01	grt10	816.3	8.13	<0.01	0.122	<0.01
cpx1	3648	13.3	0.230	0.604	<0.01	cpx1	688.2	6.89	<0.01	0.435	<0.01
cpx2	5765	46.5	1.35	1.37	0.03	cpx2	897.1	9.85	<0.01	0.543	<0.01
cpx3	1824	14.2	0.129	0.594	<0.01	cpx3	851.3	9.46	<0.01	0.548	<0.01
cpx4	779.7	8.03	<0.01	0.436	<0.01	cpx4	3.9	0.080	<0.01	0.001	<0.01
cpx5	823.2	8.75	<0.01	0.498	<0.01	cpx5	626.3	5.91	<0.01	0.414	<0.01
cpx6	846.6	7.84	0.028	0.411	<0.01	cpx6	777.8	8.51	<0.01	0.462	<0.01
cpx7	805.4	8.72	<0.01	0.499	<0.01	cpx7	503.7	3.30	<0.01	0.135	<0.01
cpx8	306.6	3.22	<0.01	0.045	<0.01	cpx8	875.7	9.13	<0.01	0.518	<0.01
cpx9	187.9	2.81	<0.01	0.053	<0.01	cpx9	758.1	7.09	<0.01	0.350	<0.01
cpx10	913.5	10.2	<0.01	0.553	<0.01	cpx10	858.6	9.57	<0.01	0.543	<0.01

Table A·4: HFSE concentrations of rutiles in eclogites (and blueshist) by LA-ICPMS (values in ppm).

Zermatt, eclogite (ZM-Pf01)							**Zermatt, eclogite (ZM-Pf05)**						
	Zr	Nb	Hf	Ta	Nb/Ta	Zr/Hf		Zr	Nb	Hf	Ta	Nb/Ta	Zr/Hf
R1	92.2	359	2.42	23.2	15.5	38.1	R1	280	318	11.5	11.2	28.3	24.3
R2	329	337	7.32	23.1	14.6	45.0	R2	280	181	11.8	6.65	27.2	23.9
R3	180	323	4.32	19.4	16.6	41.7	R3	308	744	12.4	44.8	16.6	24.8
R4	154	351	4.09	23.3	15.1	37.5	R4	303	134	12.2	6.39	21.0	24.8
R5	246	342	5.74	21.0	16.3	42.9	R5	287	241	12.2	10.1	23.9	23.5
R6	180	343	4.68	19.3	17.7	38.5	R6	296	798	12.3	38.9	20.5	24.2
R7	728	328	14.2	19.9	16.5	51.2	R7	290	340	11.7	16.1	21.1	24.7
R8	484	328	10.7	19.2	17.1	45.2	R8	322	196	13.6	7.16	27.4	23.7
R9	3294	425	67.1	22.5	18.9	49.1	R9	319	175	13.0	6.05	28.9	24.6
R10	3239	336	67.0	22.1	15.2	48.3	R10	297	136	12.5	6.23	21.8	23.8

table A·4 cont.

	Zermatt, blueshist (ZM-B1)							Zermatt, blueshist (ZM-B2)					
	Zr	Nb	Hf	Ta	Nb/Ta	Zr/Hf		Zr	Nb	Hf	Ta	Nb/Ta	Zr/Hf
R1	45.9	350	1.63	19.5	18.0	28.2	R1	113	285	3.31	26.3	10.8	34.3
R2	198	345	4.49	18.2	19.0	44.2	R2	38.6	290	1.75	21.3	13.6	22.1
R3	63.9	321	2.12	14.3	22.6	30.1	R3	34.2	293	1.42	25.8	11.4	24.1
R4	50.9	347	1.85	18.6	18.6	27.5	R4	26.1	280	1.04	30.4	9.2	25.1
R5	60.4	328	1.35	16.8	19.5	44.8	R5	165	385	3.66	39.7	9.7	45.0
R6	465	326	10.2	16.5	19.7	45.4	R6	301	308	6.75	30.8	10.0	44.6
R7	79.5	338	2.47	20.0	16.9	32.2	R7	24.6	98.0	0.64	5.84	16.8	38.4
R8	37.4	318	1.48	17.6	18.1	25.3	R8	156	315	4.21	30.7	10.3	37.1
	Zermatt, eclogite (ZM-EB)							**Zermatt, eclogite (ZM-E1)**					
	Zr	Nb	Hf	Ta	Nb/Ta	Zr/Hf		Zr	Nb	Hf	Ta	Nb/Ta	Zr/Hf
R1	24.8	183	1.01	14.6	12.6	24.6	R1	69.9	382	2.20	22.9	16.7	31.8
R2	14.2	155	1.20	12.5	12.5	11.8	R2	37.8	343	1.48	18.0	19.0	25.5
R3	33.7	216	1.89	10.5	20.5	17.8	R3	38.6	418	1.67	22.3	18.8	23.1
R4	42.0	296	1.83	20.7	14.3	22.9	R4	117	354	2.61	19.5	18.2	44.7
R5	33.6	246	1.87	18.9	13.0	18.0	R5	39.2	381	1.54	19.4	19.6	25.5
R6	35.3	213	1.32	16.3	13.0	26.7	R6	55.2	389	1.96	20.3	19.1	28.1
R7	34.8	216	1.86	15.7	13.8	18.7	R7	40.4	452	1.50	23.5	19.2	27.0
R8	1342	245	32.9	17.4	14.1	40.8	R8	202	406	4.81	19.8	20.5	42.1
R9	45.9	220	1.70	15.5	14.2	27.0	R9	33.1	360	1.15	19.7	18.3	28.7
R10	36.7	252	1.68	16.1	15.7	21.8	R10	33.2	347	1.59	21.0	16.5	20.9
	Bretagne, eclogite (SBE3-1)							**Bretagne, eclogite (SBE6-3)**					
	Zr	Nb	Hf	Ta	Nb/Ta	Zr/Hf		Zr	Nb	Hf	Ta	Nb/Ta	Zr/Hf
R1	282	132	11.0	5.55	23.8	25.6	R1	336	70.9	16.3	4.81	14.7	20.6
R2	298	196	12.7	11.4	17.2	23.4	R2	336	65.0	13.8	3.70	17.6	24.3
R3	290	166	12.1	8.46	19.6	24.0	R3	367	70.5	16.5	4.50	15.7	22.3
R4	280	158	11.9	8.90	17.7	23.6	R4	347	75.7	15.1	4.44	17.0	23.0
R5	289	194	12.4	9.23	21.1	23.3	R5	349	71.0	15.1	3.78	18.8	23.1
R6	289	180	12.5	14.2	12.6	23.1	R6	390	80.0	18.1	4.88	16.4	21.6
R7	243	171	11.0	10.3	16.6	22.2	R7	335	70.9	16.6	4.59	15.4	20.2
R8	294	153	12.7	11.8	13.1	23.1	R8	379	75.4	18.2	5.44	13.9	20.8
R9	283	159	11.9	11.6	13.7	23.7	R9	347	90.4	18.0	5.09	17.8	19.2

table A·4 cont.

	Bretagne, eclogite (SBE3-1)							Bretagne, eclogite (SBE6-3)					
	Zr	Nb	Hf	Ta	Nb/Ta	Zr/Hf		Zr	Nb	Hf	Ta	Nb/Ta	Zr/Hf
R10	292	201	13.0	15.4	13.0	22.5	R10	371	82.0	18.7	5.57	14.7	19.9
R11	316	171	15.9	5.59	30.7	19.8	R11	320	57.5	13.9	4.33	13.3	23.0
R12	298	153	11.3	13.6	11.2	26.5	R12	316	73.1	14.7	4.36	16.8	21.6
R13	327	171	13.9	10.3	16.6	23.6	R13	359	61.9	14.7	5.78	10.7	24.4
R14	361	232	14.9	17.8	13.0	24.2	R14	285	50.2	12.9	2.25	22.3	22.1
R15	340	141	14.6	7.43	19.0	23.4	R15	383	69.4	16.5	4.42	15.7	23.2
R16	355	185	15.0	12.1	15.3	23.7	R16	311	61.3	13.4	3.63	16.9	23.3
R17	362	224	16.6	13.3	16.8	21.8	R17	285	69.6	13.0	4.48	15.5	21.9
R18	359	167	16.6	11.8	14.2	21.6	R18	313	79.9	13.8	4.02	19.9	22.7
R19	407	241	19.0	17.1	14.1	21.5	R19	254	69.4	11.7	3.61	19.2	21.8
R20	4538	166	189	10.4	15.9	24.0	R20	229	65.2	11.7	4.58	14.2	19.6
	Bretagne, eclogite (SBE6-1)							**Bretagne, eclogite (SBE7-5)**					
	Zr	Nb	Hf	Ta	Nb/Ta	Zr/Hf		Zr	Nb	Hf	Ta	Nb/Ta	Zr/Hf
R1	277	72.4	9.84	1.75	41.4	28.2	R1	344	746	12.3	54.4	13.7	27.9
R2	358	179	13.4	7.82	22.8	26.8	R2	295	201	11.8	8.50	23.7	25.1
R3	292	95.8	13.7	7.00	13.7	21.3	R3	292	608	11.8	42.6	14.3	24.8
R4	262	80.4	9.65	3.85	20.9	27.2	R4	295	250	12.5	11.1	22.5	23.5
R5	267	143	9.91	8.69	16.5	26.9	R5	302	606	11.9	32.3	18.8	25.4
R6	293	107	11.6	7.76	13.7	25.4	R6	303	193	13.2	8.86	21.8	22.9
R7	338	67.6	13.2	4.49	15.1	25.7	R7	306	440	13.5	25.7	17.1	22.7
R8	295	71.6	10.4	4.16	17.2	28.4	R8	327	581	13.4	35.9	16.2	24.4
R9	305	91.7	11.5	2.96	31.0	26.4	R9	288	285	11.7	14.6	19.5	24.6
R10	304	146	12.1	9.68	15.1	25.1	R10	279	116	10.9	1.97	58.7	25.7

table A·4 cont.

Cabo Ortegal, eclogite (SCO11-1)						
	Zr	Nb	Hf	Ta	Nb/Ta	Zr/Hf
R1	389	156	14.4	8.30	18.8	27.0
R2	355	124	13.5	7.48	16.6	26.3
R3	344	134	13.2	8.82	15.2	26.1
R4	356	123	13.2	5.35	22.9	27.1
R5	315	95	12.4	9.31	10.2	25.5
R6	353	182	14.3	10.7	16.9	24.6
R7	384	123	14.5	7.81	15.8	26.4
R8	446	210	17.6	12.9	16.2	25.4

Cabo Ortegal, eclogite (SCO16-1)						
	Zr	Nb	Hf	Ta	Nb/Ta	Zr/Hf
R1	402	84.0	20.7	4.40	19.1	19.4
R2	360	67.0	12.5	3.06	21.9	28.8
R3	427	68.1	16.6	3.53	19.3	25.8
R4	468	92.8	20.7	4.77	19.5	22.6
R5	377	69.3	16.9	4.29	16.2	22.3
R6	396	72.1	16.4	2.88	25.0	24.2
R7	412	81.5	19.0	4.77	17.1	21.7
R8	477	79.1	19.5	4.80	16.5	24.5
R9	472	78.6	21.2	4.66	16.9	22.3
R10	470	84.2	21.0	5.41	15.6	22.4

Cabo Ortegal, eclogite (SCO15-1)						
	Zr	Nb	Hf	Ta	Nb/Ta	Zr/Hf
R1	388	78.6	16.0	4.96	15.8	24.2
R2	435	82.6	17.1	4.05	20.4	25.4
R3	378	73.1	15.1	6.04	12.1	25.0
R4	353	52.2	14.2	3.18	16.4	24.8
R5	336	53.5	13.5	2.87	18.6	24.8
R6	363	73.8	15.3	3.97	18.6	23.8
R7	337	71.6	12.6	2.78	25.8	26.7
R8	368	68.0	15.2	3.52	19.3	24.2
R9	377	64.6	15.2	3.84	16.8	24.8
R10	377	86.1	15.9	3.96	21.7	23.7

Cabo Ortegal, eclogite (SCO13-1)						
	Zr	Nb	Hf	Ta	Nb/Ta	Zr/Hf
R1	380	142	14.7	7.64	18.5	25.9
R2	437	151	16.6	8.47	17.8	26.3
R3	319	98	12.3	5.02	19.5	25.9
R4	365	120	13.8	6.25	19.2	26.4
R5	397	127	14.8	7.63	16.7	26.8
R6	385	121	14.4	8.42	14.3	26.7
R7	400	127	15.8	7.24	17.5	25.3
R8	404	205	14.6	8.53	24.1	27.7
R9	368	101	13.6	3.14	32.0	27.1
R10	407	103	14.5	5.86	17.6	28.0

Cabo Ortegal, eclogite (SCO12-5)						
	Zr	Nb	Hf	Ta	Nb/Ta	Zr/Hf
R1	413	145	15.0	7.68	18.9	27.5
R2	335	138	13.2	7.57	18.2	25.3
R3	327	141	13.4	7.06	20.0	24.3
R4	390	139	15.6	8.31	16.7	25.0
R5	457	135	18.3	8.00	16.9	24.9
R6	461	127	17.3	9.52	13.4	26.6
R7	464	132	17.9	10.7	12.3	26.0

Cabo Ortegal, eclogite (SCO12-5)						
	Zr	Nb	Hf	Ta	Nb/Ta	Zr/Hf
R1	346	126	15.9	6.20	20.3	21.8
R2	359	110	11.9	5.52	19.9	30.0
R3	354	122	14.3	7.80	15.7	24.7
R4	365	152	15.1	8.77	17.3	24.2
R5	408	131	16.7	8.31	15.7	24.5
R6	395	126	16.7	7.01	18.0	23.6
R7	426	139	17.7	7.22	19.3	24.0

table A·4 cont.

Cabo Ortegal, eclogite (SCO12-5)							Cabo Ortegal, eclogite (SCO12-5)						
	Zr	Nb	Hf	Ta	Nb/Ta	Zr/Hf		Zr	Nb	Hf	Ta	Nb/Ta	Zr/Hf
R8	495	96.3	19.0	9.50	10.1	26.1	R8	421	134	18.6	8.24	16.2	22.6
R9	339	127	13.2	8.35	15.2	25.6	R9	390	150	16.4	10.48	14.3	23.8
R10	2260	134	54.4	9.77	13.8	41.5	R10	432	158	18.9	8.75	18.1	22.9
R11	346	170	13.2	6.33	26.9	26.3	R11	214	142	9.05	4.47	31.8	23.7
R12	308	118	11.9	8.07	14.6	25.8	R12	164	74.7	6.40	3.93	19.0	25.7
R13	304	119	12.3	9.30	12.8	24.8	R13	215	94.6	8.67	4.88	19.4	24.8
R14	328	156	12.3	9.69	16.1	26.8	R14	234	76.8	8.60	2.55	30.1	27.2
R15	363	183	13.7	8.77	20.8	26.4	R15	284	139	10.6	5.46	25.4	26.7
R16	321	157	12.5	6.01	26.2	25.6	R16	188	116	8.92	3.62	32.0	21.1
R17	321	168	12.4	7.32	22.9	25.9	R17	261	131	9.84	5.80	22.6	26.5
R18	336	146	12.3	7.74	18.8	27.3	R18	266	132	10.8	6.12	21.5	24.7
R19	336	138	13.1	6.01	22.9	25.6	R19	263	141	9.47	6.50	21.7	27.8
R20	320	141	12.6	7.44	18.9	25.5	R20	295	128	11.0	4.17	30.7	26.8
R21	319	153	11.5	8.43	18.1	27.8	R21	261	123	11.6	6.11	20.1	22.6
R22	333	136	13.0	5.65	24.0	25.6	R22	386	161	14.1	8.41	19.1	27.4
R23	362	141	13.5	8.49	16.6	26.8	R23	358	130	12.5	7.53	17.2	28.6
R24	350	148	13.3	8.35	17.7	26.2	R24	279	92	9.88	2.04	45.2	28.3
R25	304	155	12.6	10.42	14.9	24.1	R25	298	124	13.5	6.60	18.8	22.2
R26	315	133	11.7	8.33	16.0	26.8	R26	301	120	12.5	5.73	21.0	24.1
R27	288	109	11.7	8.67	12.5	24.6	R27	328	118	12.7	4.03	29.2	25.9
R28	335	114	13.2	5.11	22.3	25.3	R28	376	116	14.8	4.22	27.5	25.5
R29	343	125	12.8	6.85	18.2	26.7	R29	269	132	13.2	5.98	22.1	20.4
R30	338	126	12.6	8.48	14.9	26.9	R30	269	98	13.9	4.78	20.5	19.4
R31	302	246	13.7	14.03	17.5	22.0	R31	292	102	11.6	5.41	18.8	25.3
R32	279	105	10.1	8.34	12.6	27.6	R32	285	95	11.7	5.15	18.5	24.4
R33	305	140	12.0	4.81	29.0	25.3	R33	313	105	12.8	6.59	16.0	24.5
R34	362	382	16.3	17.2	22.2	22.3	R34	290	132	11.2	5.16	25.6	26.0
R35	347	130	13.5	7.31	17.7	25.6	R35	260	139	11.4	5.81	23.8	22.7
R36	332	116	12.5	6.76	17.2	26.6	R36	294	134	12.2	5.71	23.5	24.1
R37	388	132	14.4	8.33	15.8	27.0	R37	307	131	12.0	5.25	24.9	25.6
R38	300	105	12.7	3.29	31.9	23.6	R38	335	115	12.8	6.97	16.5	26.2
R39	371	119	13.8	6.84	17.4	26.9	R39	343	134	13.4	5.91	22.6	25.5
R40	338	143	12.6	7.68	18.6	26.7	R40	330	111	13.8	5.12	21.6	24.0

table A·4 cont.

Cabo Ortegal, eclogite (SCO12-5)							Cabo Ortegal, eclogite (SCO12-5)						
	Zr	Nb	Hf	Ta	Nb/Ta	Zr/Hf		Zr	Nb	Hf	Ta	Nb/Ta	Zr/Hf
R41	342	135	12.9	8.18	16.6	26.4	R41	384	167	14.1	9.17	18.2	27.1
R42	324	145	13.1	7.09	20.4	24.8	R42	371	127	12.9	7.43	17.1	28.9
R43	289	126	11.6	7.69	16.4	24.8	R43	385	167	13.7	9.11	18.3	28.2
R44	351	119	13.0	8.34	14.3	26.9	R44	340	125	13.0	5.79	21.6	26.2
R45	348	140	12.9	8.88	15.8	27.0	R45	308	122	11.4	7.69	15.9	27.2
R46	347	150	12.8	5.60	26.7	27.1	R46	337	126	12.2	5.51	22.8	27.5
R47	214	111	9.09	4.71	23.6	23.6	R47	322	128	12.3	7.06	18.1	26.1
R48	307	148	11.4	8.00	18.6	27.0	R48	346	151	12.8	6.24	24.2	27.0
R49	324	126	9.96	9.44	13.4	32.5	R49	326	122	12.4	6.83	17.9	26.4
R50	305	133	12.2	6.08	21.8	25.0	R50	402	129	15.0	8.56	15.1	26.9
R51	317	133	12.3	7.39	18.0	25.9	R51	336	150	14.0	6.26	24.0	23.9
R52	266	147	11.3	6.83	21.6	23.5	R52	386	154	14.7	7.33	21.0	26.3
R53	296	120	11.8	7.19	16.7	25.1	R53	343	114	13.7	7.71	14.8	24.9
R54	304	89.7	11.8	3.05	29.4	25.9	R54	292	179	13.7	9.47	18.8	21.4
R55	336	145	13.5	8.32	17.4	24.8	R55	314	122	11.7	8.63	14.1	26.9
R56	368	150	13.6	5.89	25.5	27.0	R56	339	141	11.8	8.74	16.1	28.8
R57	295	76.5	8.70	3.10	24.7	34.0	R57	373	160	13.0	8.41	19.0	28.6
R58	260	118	10.8	7.98	14.8	24.0	R58	305	71.3	10.1	2.36	30.2	30.1
R59	356	159	12.9	10.3	15.4	27.5	R59	238	110	9.0	6.15	17.9	26.4
R60	299	135	11.8	5.66	23.8	25.3	R60	366	161	15.3	8.88	18.1	23.9
Western Gneiss Region, eclogite (WGR1)							**Western Gneiss Region, eclogite (WGR2)**						
	Zr	Nb	Hf	Ta	Nb/Ta	Zr/Hf		Zr	Nb	Hf	Ta	Nb/Ta	Zr/Hf
R1	125	82.7	4.26	6.84	12.1	29.3	R1	106	101	3.80	6.27	16.1	28.0
R2	150	78.9	5.63	6.00	13.2	26.7	R2	166	102	7.19	6.55	15.6	23.1
R3	154	88.0	5.95	6.27	14.0	25.9	R3	166	111	7.11	6.34	17.5	23.3
R4	123	83.7	4.45	6.23	13.4	27.6	R4	114	107	4.03	6.27	17.1	28.3
R5	165	73.7	5.34	8.14	9.1	30.9	R5	114	108	4.23	6.59	16.4	26.9
R6	158	77.7	5.78	5.53	14.0	27.3	R6	114	104	5.23	6.43	16.2	21.9
R7	208	88.6	7.10	7.27	12.2	29.2	R7	130	107	5.41	6.39	16.7	24.1
R8	109	83.9	4.17	7.35	11.4	26.2	R8	130	129	5.23	7.88	16.3	24.9
R9	136	94.3	5.27	4.68	20.2	25.8	R9	167	108	7.13	6.48	16.7	23.4
R10	94.1	79.0	3.02	7.11	11.1	31.2	R10	121	100	4.91	5.78	17.3	24.6

table A·4 cont.

Western Gneiss Region, eclogite (WGR1)						
	Zr	Nb	Hf	Ta	Nb/Ta	Zr/Hf
R11	97.8	92.2	3.95	5.17	17.8	24.8
R12	100	89.8	3.10	9.54	9.4	32.3
R13	97.6	71.0	3.85	4.41	16.1	25.4
R14	142	98.1	5.58	9.23	10.6	25.5
R15	110	80.2	3.77	5.64	14.2	29.1
R16	95.0	86.0	3.33	5.61	15.3	28.5
R17	127	85.6	4.77	4.71	18.2	26.5

Western Gneiss Region, eclogite (WGR2)						
	Zr	Nb	Hf	Ta	Nb/Ta	Zr/Hf
R11	163	105	7.13	6.47	16.3	22.9
R12	145	103	5.77	6.69	15.4	25.2
R13	154	108	6.45	7.89	13.7	23.9
R14	144	101	6.10	6.70	15.1	23.6
R15	124	99	5.21	6.63	14.9	23.8
R16	119	104	4.89	6.30	16.4	24.4

Western Gneiss Region, eclogite (WGR3)						
	Zr	Nb	Hf	Ta	Nb/Ta	Zr/Hf
R1	210	101	8.30	7.16	14.1	25.3
R2	198	107	7.04	5.86	18.3	28.1
R3	209	90.7	6.62	5.78	15.7	31.6
R4	205	95.7	7.80	7.04	13.6	26.3
R5	184	95.3	6.07	6.11	15.6	30.2
R6	155	92.7	5.87	5.47	16.9	26.3
R7	176	88.6	7.14	5.61	15.8	24.7
R8	191	91.8	6.83	6.01	15.3	28.0
R9	105	93.4	3.97	6.57	14.2	26.4

Western Gneiss Region, eclogite (WGR5)						
	Zr	Nb	Hf	Ta	Nb/Ta	Zr/Hf
R1	306	649	9.19	41.8	15.5	33.3
R2	263	945	7.89	43.1	22.0	33.3
R3	238	756	6.93	40.6	18.6	34.3
R4	249	720	7.67	40.9	17.6	32.5
R5	296	875	8.95	48.6	18.0	33.1
R6	221	662	6.73	33.6	19.7	32.8
R7	274	828	8.07	49.9	16.6	34.0
R8	161	623	5.42	38.2	16.3	29.7
R9	224	646	6.20	35.1	18.4	36.0

Dabie UHP terrane, eclogite (DB63)						
	Zr	Nb	Hf	Ta	Nb/Ta	Zr/Hf
R1	86.0	291	4.04	15.1	19.2	21.3
R2	1146	265	25.7	10.9	24.3	44.7
R3	110	283	4.90	12.1	23.3	22.5
R4	103	307	4.43	13.8	22.3	23.2
R5	116	299	4.88	11.6	25.8	23.8

Dabie UHP terrane, eclogite (DB05)						
	Zr	Nb	Hf	Ta	Nb/Ta	Zr/Hf
R1	96.7	34.3	4.29	1.67	20.5	22.5
R2	136	30.6	5.99	1.49	20.5	22.7
R3	115	31.5	5.10	1.50	21.0	22.6

Alpe Arami, eclogite (AA-E1)						
	Zr	Nb	Hf	Ta	Nb/Ta	Zr/Hf
R1	404	258	19.1	51.9	5.0	21.2
R2	100	210	9.72	42.1	5.0	10.3
R3	231	158	8.96	20.3	7.8	25.8
R4	252	170	11.5	25.9	6.6	22.0
R5	256	159	10.7	16.3	9.8	23.9
R6	453	203	14.6	20.4	10.0	31.1
R7	310	203	11.5	14.8	13.7	27.1
R8	181	88.0	10.0	12.8	6.9	18.1
R9	382	177	16.3	14.8	11.9	23.4
R10	242	174	11.5	14.3	12.2	21.0
R11	354	316	19.0	45.0	7.0	18.6

table A·4 cont.

Dabie UHP terrane, eclogite (DB05)							Alpe Arami, eclogite (AA-E1)						
	Zr	Nb	Hf	Ta	Nb/Ta	Zr/Hf		Zr	Nb	Hf	Ta	Nb/Ta	Zr/Hf
R4	94.4	28.7	4.62	1.42	20.2	20.4	R12	344	361	12.6	28.1	12.9	27.2
R5	70.8	32.7	3.24	1.58	20.7	21.8	R13	262	337	11.8	34.7	9.7	22.2
R6	106	28.6	4.90	1.39	20.5	21.6	R14	14.1	4.46	0.94	0.90	5.0	15.0
R7	88.2	27.9	4.49	1.34	20.8	19.6	R15	286	296	14.7	44.6	6.6	19.5
R8	89.1	29.4	4.14	1.38	21.3	21.5	R16	22.5	12.2	2.14	3.00	4.1	10.5
R9	89.9	28.5	4.57	1.34	21.2	19.7	R17	264	358	13.6	61.3	5.8	19.5
R10	88.0	28.9	4.27	1.29	22.4	20.6	R18	5.88	3.58	0.67	0.44	8.1	8.8
							R19	238	326	9.65	23.3	14.0	24.6
							R20	275	328	13.4	22.9	14.3	20.5

Curriculum Vitae

Persönliche Daten

Name	Alexander Schmidt
Geburtsdatum	22.08.1974
Geburtsort	Gütersloh
Staatsangehörigkeit	deutsch

Schulbildung:

1981 - 1995	Grundschule und Gymnasium in Gütersloh, Abitur im Juni 1995

Zivildienst:

Okt. 1995 - Sept. 1996	Zivildienst im Städtischen Krankenhaus Gütersloh

Studium und Anstellungen

Nov. 1991 - Okt. 1995	Freier Mitarbeiter beim lokalen Radiosender „Radio Gütersloh“
Okt. 1996 - Sept. 2003	Studium Geologie/Paläontologie an der Westfälischen Wilhelms-Universität Münster (WWU)
Jan. 1999 - März 2001	Studentische Hilfskraft am Institut für Planetologie der WWU
Jan. 2002 - Sept. 2003	Studentische Hilfskraft am Institut für Mineralogie der WWU
Jun. 2001 - Okt. 2001	Praktikum im Westfälischen Museum für Naturkunde in Münster
Feb. 2002 - Apr. 2002	Diplomkartierung im Hutti-Maski Grünsteingürtel, Indien (Auslandsaufenthalt gefördert durch DAAD)
Okt. 2002	Diplomsprüfungen Geologie/Paläontologie an der WWU

Feb. 2002 - Sept. 2003	Diplomarbeit am Institut für Mineralogie der WWU. Thema: Geochemie und Geochronologie des archaischen Hutti-Maski Grünsteingürtels, Eastern Dharwar Craton, Karnataka, Süd-Indien. Kombinierte Sr-Nd-Pb Isotopenstudie und Rb-Sr und Pb-Pb Geochronologie an Biotiten und Feldspäten.
Dez. 2003 - Feb. 2008	Doktorand am Institut für Mineralogie der Johann Wolfgang Goethe-Universität Frankfurt. Thema: High Field Strength Element systematics and Lu-Hf & Sm-Nd garnet geochronology of orogenic eclogites.